

SPECTRUM SHARING OPPORTUNITY FOR LTE AND AIRCRAFT RADAR  
IN THE 4.2 - 4.4 GHZ BAND

BY  
ROHIT SINGH

Submitted in partial fulfillment of the  
requirements for the degree of  
Master of Science in Computer Science  
in the Graduate College of the  
Illinois Institute of Technology

Approved \_\_\_\_\_  
Advisor

Chicago, Illinois  
July 2017



## ACKNOWLEDGMENT

I would first like to thank my advisor, Dr. Cynthia Hood, without who's experience and expertise this thesis would not have been possible. She provided me with the insight to Wireless Networks and Spectrum Sharing. I would like to thank her for asking me the hard questions which encouraged me to widen my research from various perspectives. I would also like to thank Dr. Boris Glavic, the second member of my Masters Thesis Committee, for his great advice and support.

I would like to express my gratitude to Dr. Roger Peterson for providing me insight to Information Theory and Telecommunications domain. I would like to thank him for his continuing support and especially his assistance in reviewing this thesis.

I would like to thank Professor Dennis A. Roberson for being a great mentor, and giving me the opportunity to do real research in the telecommunications space. Professor Roberson experience, feedback and advice have helped me greatly in honing my knowledge. He is truly an amazing individual, and I am blessed to have had the chance to closely work with him.

I would also like to thank my various student colleagues and professors at the Wireless Network and Communications Research Center (WiNCom) at IIT for their advice and assistance over the last few years, including Vaishali Nagpure, Dr. Roger Bacchus, Ali Riaz and Philip Felber.

I also express my appreciation to the National Science Foundation (NSF) who have provided funding for this work under the “EARS: Modeling and Analysis of Radar/Communication Spectrum Sharing Opportunities” grant.

Finally, I would like to express my gratitude to my mother Suparna Singh and father Pashupati Singh for their support and encouragement in my studies. I congratulate them for this thesis; in reality, this work is partly theirs as well.

## TABLE OF CONTENTS

	Page
ACKNOWLEDGEMENT . . . . .	iii
LIST OF TABLES . . . . .	vi
LIST OF FIGURES . . . . .	xi
ABSTRACT . . . . .	xii
CHAPTER	
1. INTRODUCTION . . . . .	1
1.1. Spectrum Sharing . . . . .	4
1.2. Related Work . . . . .	6
1.3. Motivation for the Altimeter Radar Band . . . . .	8
1.4. Radar Altimeter . . . . .	9
1.5. Candidate Secondary User . . . . .	10
1.6. Challenges . . . . .	12
1.7. Goal and Approach . . . . .	12
2. ADS-B DATA ANALYSIS . . . . .	15
2.1. Overview of ADS-B Data . . . . .	16
2.2. FAA Airspace Division . . . . .	17
2.3. General Analysis of the Area . . . . .	18
2.4. Flight Count . . . . .	23
2.5. Geographic and Temporal Analysis . . . . .	25
2.6. Likelihood of Occupancy . . . . .	39
2.7. Discussion . . . . .	41
3. CO-EXISTENCE STUDY . . . . .	43
3.1. Altimeter System Model . . . . .	43
3.2. LTE System . . . . .	47
3.3. LTE to Radar (LTR) Study . . . . .	57
3.4. Radar to LTE (RTL) Study . . . . .	67
3.5. Discussion . . . . .	73
4. SHARING APPROACH . . . . .	75
4.1. Interference Likelihood . . . . .	75
4.2. Exclusion and Coordination Zone Formation . . . . .	81
4.3. Approach . . . . .	82
4.4. L2 Analysis . . . . .	85

4.5. L3 Analysis . . . . .	92
4.6. L2 and L3 Comparison . . . . .	95
4.7. Discussion . . . . .	97
5. CONCLUSION AND FUTURE WORK . . . . .	98
5.1. Summary . . . . .	98
5.2. Future Work . . . . .	100
APPENDIX . . . . .	102
A. EMPIRICAL LIKELIHOOD . . . . .	102
A.1. Kernel Distribution . . . . .	103
B. PDF AND CDF OF FIGHT OCCUPANCY FOR CELLS . . . . .	105
B.1. Zone 1 . . . . .	106
B.2. Zone 2 . . . . .	107
B.3. Zone 3 . . . . .	108
B.4. Zone 4 . . . . .	110
C. PDF AND CDF OF LTR INTERFERENCE FROM CELLS . . . . .	113
C.1. Zone 1 . . . . .	114
C.2. Zone 2 . . . . .	115
C.3. Zone 3 . . . . .	116
C.4. Zone 4 . . . . .	118
D. PDF AND CDF OF RTL UE INTERFERENCE . . . . .	121
D.1. Zone 1 . . . . .	122
D.2. Zone 2 . . . . .	123
D.3. Zone 3 . . . . .	124
D.4. Zone 4 . . . . .	126
E. PDF AND CDF OF RTL BS INTERFERENCE . . . . .	129
E.1. Zone 1 . . . . .	130
E.2. Zone 2 . . . . .	131
E.3. Zone 3 . . . . .	132
E.4. Zone 4 . . . . .	134
BIBLIOGRAPHY . . . . .	136

## LIST OF TABLES

Table	Page
3.1 Altimeter Model Parameters . . . . .	47
3.2 LTE Model Parameters for BS . . . . .	56
3.3 LTE Model Parameters for UE . . . . .	57
3.4 LTE Toolbox Parameters . . . . .	69
4.1 Zone deployment levels . . . . .	85

## LIST OF FIGURES

Figure	Page
1.1 Global Mobile Devices and Connection Growth from 2016 - 2021 [3]	1
1.2 Spectrum allocation $3GHz - 6GHz$	4
1.3 Average of the Maximum Power over one year in the 4.2-4.4 GHz Radar Altimeter band	10
2.1 Area considered for the work	18
2.2 Area considered for the work	19
2.3 1 Day Scatter Matrix Data	21
2.4 A 90 Day overlay of flight for the locations used by the flights in the given area	22
2.5 90 Day Overlay of Altitude Data	23
2.6 Area considered for the work	24
2.7 Heat-map for Chicagoland 9 Month Average Air Traffic	26
2.8 Surface Plot for Chicagoland 9 Month Average Air Traffic	27
2.9 The popular Flight Paths considered on an average by at least 10 flights on a daily basis	28
2.10 Zone division for the given area	29
2.11 Average Traffic Count for 9 months on the space domain for Zone 1	30
2.12 Traffic Count for 9 months on the time domain for Zone 1	31
2.13 Average Traffic Count for 9 months on the space domain for Zone 2	32
2.14 Traffic Count for 9 months on the time domain for Zone 2	33
2.15 Traffic Count for 9 months on the space domain for Zone 3	34
2.16 Average Traffic Count for 9 months on the time domain for Zone 3	34
2.17 Traffic Count for 9 months on the space domain for Zone 4	35
2.18 Traffic Count for 9 months on the time domain for Zone 4	36
2.19 Cell analysis on the time domain for Zone 1 (a) (63,23) (b) (65,23)	37
2.20 Cell analysis on the time domain for Zone 2 (a) (61,4) (b) (61,7)	38

2.21	Cell analysis on the time domain for Zone 3 (a) (12,16) (b) (14,15)	38
2.22	Cell analysis on the time domain for Zone 4 (a) (31,38) (b) (59,35)	39
2.23	Flight occupancy PDF plot for Cell (63,23) in Zone 1 . . . . .	40
2.24	Flight occupancy CDF plot for Cell (63,23) in Zone 1 . . . . .	41
3.1	Conceptual illustration of FMCW Altimeter . . . . .	44
3.2	Altimeter Transmit and Receive Frequencies as Function of Time .	45
3.3	Altimeter to LTE Interference Scenario . . . . .	47
3.4	LTE BS Azimuth Antenna Pattern . . . . .	50
3.5	The IIT Tower has direct line-of-sight to downtown Chicago and is the tallest building in the vicinity . . . . .	54
3.6	Waterfall for 746-756 MHz . . . . .	55
3.7	LTE Profile for 746-756 MHz . . . . .	56
3.8	Scenario with Aircraft positions and BS antenna direction . . . .	62
3.9	Same scenario as Figure 3.8 with 5 BSs . . . . .	63
3.10	Received Power at the radio altimeter from the BSs through (a) FSPL and (b) LPL . . . . .	64
3.11	Received Power at the radio altimeter from 10,000 UEs through (a) FSPL and (b) LPL . . . . .	65
3.12	Magnified version of Figure 3.11 . . . . .	66
3.13	Received Power at the radio altimeter from 100 UEs through (a) FSPL and (b) LPL . . . . .	66
3.14	Received Power at the radio altimeter from 5 BSs and 100 UEs through (a) FSPL and (b) LPL . . . . .	67
3.15	Throughput Measurement at the UE for different SINR with 1 and 3 Radars Altimeters . . . . .	70
3.16	Aircraft Flight Path and LTE User Equipment Locations Scenario	70
3.17	UE Throughput vs Time for 3 Radar . . . . .	71
3.18	Scenario for Uplink Analysis . . . . .	72

3.19	Power Received at the BS from the Radar Altimeter through (a) FSPL (b) LPL . . . . .	73
4.1	Existing Base Station Antenna Heat Map for Chicagoland . . . . .	76
4.2	LTR Interference PDF plot for Cell (63,23) in Zone 1 . . . . .	77
4.3	LTR Interference CDF plot for Cell (63,23) in Zone 1 . . . . .	78
4.4	RTL UE Throughput PDF plot for Cell (63,23) in Zone 1 at 5 pm-6 pm . . . . .	79
4.5	RTL UE Throughput CDF plot for Cell (63,23) in Zone 1 at 5 pm-6 pm . . . . .	79
4.6	RTL BS Interference PDF plot for Cell (63,23) in Zone 1 . . . . .	80
4.7	RTL BS Interference CDF plot for Cell (63,23) in Zone 1 . . . . .	81
4.8	Probability distribution for 3pm to 6pm for all days of week . . . . .	87
4.9	L2 implementation for Cell (63,23) in Zone 1 with $Pr_{LTR}^{w,t} < \mu - \sigma$	91
4.10	L2 implementation for Cell (63,23) in Zone 1 with $Pr_{LTR}^{w,t} < \mu$ . . .	91
4.11	L2 implementation for Cell (63,23) in Zone 1 with $Pr_{LTR}^{w,t} < \mu + \sigma$	92
4.12	L2 implementation for Cell (63,23) in Zone 1 with $Pr_{LTR}^{w,t} < 1$ . . .	92
4.13	L3 average BS usage for Cell (63,23) in Zone 1 . . . . .	95
4.14	Average spectrum usage for Cell (63,23) in Zone 1 . . . . .	96
4.15	Average Number of BS Handoff for Cell (63,23) in Zone 1 . . . . .	97
B.1	Fight Occupancy PDF plot for Cell (65,23) in Zone 1 . . . . .	106
B.2	Fight Occupancy CDF plot for Cell (65,23) in Zone 1 . . . . .	106
B.3	Fight Occupancy PDF plot for Cell (61,4) in Zone 2 . . . . .	107
B.4	Fight Occupancy CDF plot for Cell (61,4) in Zone 2 . . . . .	107
B.5	Fight Occupancy PDF plot for Cell (61,7) in Zone 2 . . . . .	108
B.6	Fight Occupancy CDF plot for Cell (61,7) in Zone 2 . . . . .	108
B.7	Fight Occupancy PDF plot for Cell (12,16) in Zone 3 . . . . .	109
B.8	Fight Occupancy CDF plot for Cell (12,16) in Zone 3 . . . . .	109
B.9	Fight Occupancy PDF plot for Cell (14,15) in Zone 3 . . . . .	110

B.10	Fight Occupancy CDF plot for Cell (14,15) in Zone 3 . . . . .	110
B.11	Fight Occupancy PDF plot for Cell (31,38) in Zone 4 . . . . .	111
B.12	Fight Occupancy CDF plot for Cell (31,38) in Zone 4 . . . . .	111
B.13	Fight Occupancy PDF plot for Cell (59,35) in Zone 4 . . . . .	112
B.14	Fight Occupancy CDF plot for Cell (59,35) in Zone 4 . . . . .	112
C.1	LTR Interference PDF plot for Cell (65,23) in Zone 1 . . . . .	114
C.2	LTR Interference CDF plot for Cell (65,23) in Zone 1 . . . . .	114
C.3	LTR Interference PDF plot for Cell (61,4) in Zone 2 . . . . .	115
C.4	LTR Interference CDF plot for Cell (61,4) in Zone 2 . . . . .	115
C.5	LTR Interference PDF plot for Cell (61,7) in Zone 2 . . . . .	116
C.6	LTR Interference CDF plot for Cell (61,7) in Zone 2 . . . . .	116
C.7	LTR Interference PDF plot for Cell (12,16) in Zone 3 . . . . .	117
C.8	LTR Interference CDF plot for Cell (12,16) in Zone 3 . . . . .	117
C.9	LTR Interference PDF plot for Cell (14,15) in Zone 3 . . . . .	118
C.10	LTR Interference CDF plot for Cell (14,15) in Zone 3 . . . . .	118
C.11	LTR Interference PDF plot for Cell (31,38) in Zone 4 . . . . .	119
C.12	LTR Interference CDF plot for Cell (31,38) in Zone 4 . . . . .	119
C.13	LTR Interference PDF plot for Cell (59,35) in Zone 4 . . . . .	120
C.14	LTR Interference CDF plot for Cell (59,35) in Zone 4 . . . . .	120
D.1	RTL UE Interference PDF plot for Cell (65,23) in Zone 1 . . . . .	122
D.2	RTL UE Interference CDF plot for Cell (65,23) in Zone 1 . . . . .	122
D.3	RTL UE Interference PDF plot for Cell (61,4) in Zone 2 . . . . .	123
D.4	RTL UE Interference CDF plot for Cell (61,4) in Zone 2 . . . . .	123
D.5	RTL UE Interference PDF plot for Cell (61,7) in Zone 2 . . . . .	124
D.6	RTL UE Interference CDF plot for Cell (61,7) in Zone 2 . . . . .	124
D.7	RTL UE Interference PDF plot for Cell (12,16) in Zone 3 . . . . .	125
D.8	RTL UE Interference CDF plot for Cell (12,16) in Zone 3 . . . . .	125

D.9	RTL UE Interference PDF plot for Cell (14,15) in Zone 3 . . . . .	126
D.10	RTL UE Interference CDF plot for Cell (14,15) in Zone 3 . . . . .	126
D.11	RTL UE Interference PDF plot for Cell (31,38) in Zone 4 . . . . .	127
D.12	RTL UE Interference CDF plot for Cell (31,38) in Zone 4 . . . . .	127
D.13	RTL UE Interference PDF plot for Cell (59,35) in Zone 4 . . . . .	128
D.14	RTL UE Interference CDF plot for Cell (59,35) in Zone 4 . . . . .	128
E.1	RTL BS Interference PDF plot for Cell (65,23) in Zone 1 . . . . .	130
E.2	RTL BS Interference CDF plot for Cell (65,23) in Zone 1 . . . . .	130
E.3	RTL BS Interference PDF plot for Cell (61,4) in Zone 2 . . . . .	131
E.4	RTL BS Interference CDF plot for Cell (61,4) in Zone 2 . . . . .	131
E.5	RTL BS Interference PDF plot for Cell (61,7) in Zone 2 . . . . .	132
E.6	RTL BS Interference CDF plot for Cell (61,7) in Zone 2 . . . . .	132
E.7	RTL BS Interference PDF plot for Cell (12,16) in Zone 3 . . . . .	133
E.8	RTL BS Interference CDF plot for Cell (12,16) in Zone 3 . . . . .	133
E.9	RTL BS Interference PDF plot for Cell (14,15) in Zone 3 . . . . .	134
E.10	RTL BS Interference CDF plot for Cell (14,15) in Zone 3 . . . . .	134
E.11	RTL BS Interference PDF plot for Cell (31,38) in Zone 4 . . . . .	135
E.12	RTL BS Interference CDF plot for Cell (31,38) in Zone 4 . . . . .	135
E.13	RTL BS Interference PDF plot for Cell (59,35) in Zone 4 . . . . .	136
E.14	RTL BS Interference CDF plot for Cell (59,35) in Zone 4 . . . . .	136

## ABSTRACT

The Federal Communications Commission (FCC) states that America is facing a spectrum crunch and there is no easy way to meet this increasing demand, hence spectrum sensing and sharing has gotten significant attention in the Spectrum Community. Spectrum is an increasingly scarce natural resource which needs to be used to the fullest. Using modern techniques, spectrum bands can be reused such that they do not interfere with the current users in a band. There are many bands in the RF Spectrum which are underutilized and can be reused in the space-time domain. A number of bands have been recognized as candidates for spectrum sharing. In this dissertation, we consider the  $4.2 - 4.4\text{GHz}$  band which is dedicated for used by the radar altimeter fixed on aircraft to measure their elevation above the earth's surface.

This spectrum is currently underutilized and with care can be shared with other technologies. This thesis examines the current use of this spectrum as a function of time and location and presents a methodology for assessing whether harmful interference is experienced by either the incumbent radar usage or by a proposed wireless secondary broadband user. However, this band is a potential "safety of life" spectrum which is used by aircraft during landing and takeoff. Improper sharing of this band could cause interference at the radar, which would result in false attitude detection by the radar. Because of its advance technology, LTE should can be a good sharing candidate for this sensitive band. We propose sharing of this band with small cells (perhaps inside buildings) in urban and/or suburban areas, where there is a high demand for LTE and the attenuation from the environment is high enough to cause less interference at the radar altimeters.

In this thesis, we propose to detect the aircraft (i.e. the altimeter radars) using the Automatic Dependent Surveillance Broadcast (ADS-B) data which is broadcasted by an aircraft. This aircraft detection mechanism helps us to take intelligent

sharing approaches with LTE using the space-time domain. Since the performance of the radar altimeter is safety-of-life critical, a deep understanding of co-existence between these systems is necessary to evaluate whether sharing is feasible. Given the availability of historical ADS-B data, what we believe is an appropriate analysis of Chicagoland has been done to propose implementation of a mix of Exclusion and Coordination zones in this area in the space-time domain. The novelty of this work is to develop spectrum sharing opportunities with radars which are highly transient and their locations are unpredictable due to emergency or traffic or weather. This thesis presents a method for evaluation of the potential for spectrum sharing between the ground-based LTE systems and commercial radar altimeters.

## CHAPTER 1

### INTRODUCTION

In the past two decades, the wireless communication industry has seen an explosive growth in smart devices and data traffic. This is mainly due to the enthusiasm for mobile and web applications services (e.g. YouTube, Facebook, Facetime, etc.) and the new technologies that enable these services (e.g. 4G/LTE and ever improving versions of WiFi). Data usage over mobile networks is rapidly increasing, and will continue to show an upward trend over the next decade [1][2]. Moreover with the advent of the Internet of Things (IoT) it is expected that there will be an even higher demand for more wireless network capacity at even higher performance levels. The Cisco Visual Networking (CVN) Index forecast report, shows that, by 2019, mobile and WiFi devices will account for 81% of Internet Traffic [3]. Figure 1.1 shows that by the year 2021 the device count could reach 12 billion, further increasing the demand for more wireless link capacity.

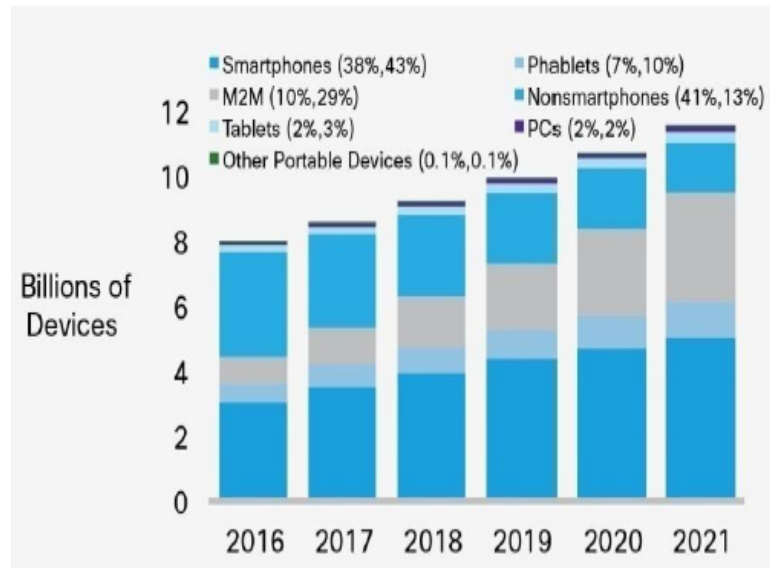


Figure 1.1. Global Mobile Devices and Connection Growth from 2016 - 2021 [3]

Link capacity is the maximum rate at which data can be transmitted over a link or a channel. Here, channel is the medium through which the electromagnetic signals can travel. The medium can be a physical wire or a wireless channel; in this work we are concerned with the wireless medium. From information theory, we know that in a non-idle case the channel capacity is related to the signal-to-noise ratio (SNR) and bandwidth (Shannon's Limits Theorem). Noise is something which distorts or corrupts the signal; SNR is the ratio of the level of desired signal to the level of background noise. Bandwidth is a range of frequencies within a given band; which is derived from the radio spectrum. The Shannon's result as shown in Equation 1.1 is that the maximum channel capacity in bits per second; where C is the channel capacity in bits per second and B is the bandwidth of the channel in Hertz. The SNR is important in the transmission of digital data because it sets the upper bound on the achievable data rate. Note that because noise is assumed to be white the wider the B, the more noise is admitted to the system. Hence, as B increases, SNR decreases.

$$C = B \log_2(1 + SNR) \quad (1.1)$$

Radio spectrum is a range of frequencies ranging from  $3kHz$  to  $300GHz$ . This wide range of frequency is divided into bands which support many different applications like national defense, cellular communication, personal communication, space exploration, federal (state and local) law enforcement and other vital government services; hence making the spectrum a valuable national asset. To prevent interference between these different types of application and users, the spectrum is highly regulated and is coordinated by an international body, namely, the International Telecommunication Union (ITU). Moreover, the actual use of spectrum in each country is overseen by the government or by a designated regulatory body [5]. In the USA, the use of radio spectrum is jointly managed by the National Telecommunication and

Information Administration (NTIA) and the Federal Communications Commission (FCC). The spectrum used by the federal agencies is managed by the NTIA while the spectrum used by the private sector (cellular operators, industries and broadcast) is managed by the FCC. In the case of sharing between government and commercial bands both the NTIA and the FCC have to agree.

Over the years, spectrum has been highly partitioned into different frequency bands with a specific application or set of applications assigned to each partition. This section is called Spectrum Allocation [6]. The spectrum is divided based on the services and class of users (licensed or unlicensed). Figure 1.2 shows an example for the spectrum allocation in the  $3GHz - 6GHz$  band. The vertical bar on the left is either colored red (Government Exclusive) or green (Non-Government Exclusive) or black (Government/Non-Government Shared). Each layer is then divided into compartments which signify the services that are permitted to operate in the band. The primary services are written in all capitals, while the secondary services are written in lower case. The primary services are the services to whom the band is allocated and the secondary services are those who use this same band without causing any harmful interference to the former service. As shown in Figure 1.2 and detailed in [6], the radio spectrum has been fully allocated. Since spectrum is a finite resource, to meet the increasing demand increased sharing is necessary. Hence, spectrum sharing technology (and specifically dynamic spectrum sharing technology) is required which will allow different users or services to share the band in a more fine grained space and time sliced manner such that they do not interfere with each other.

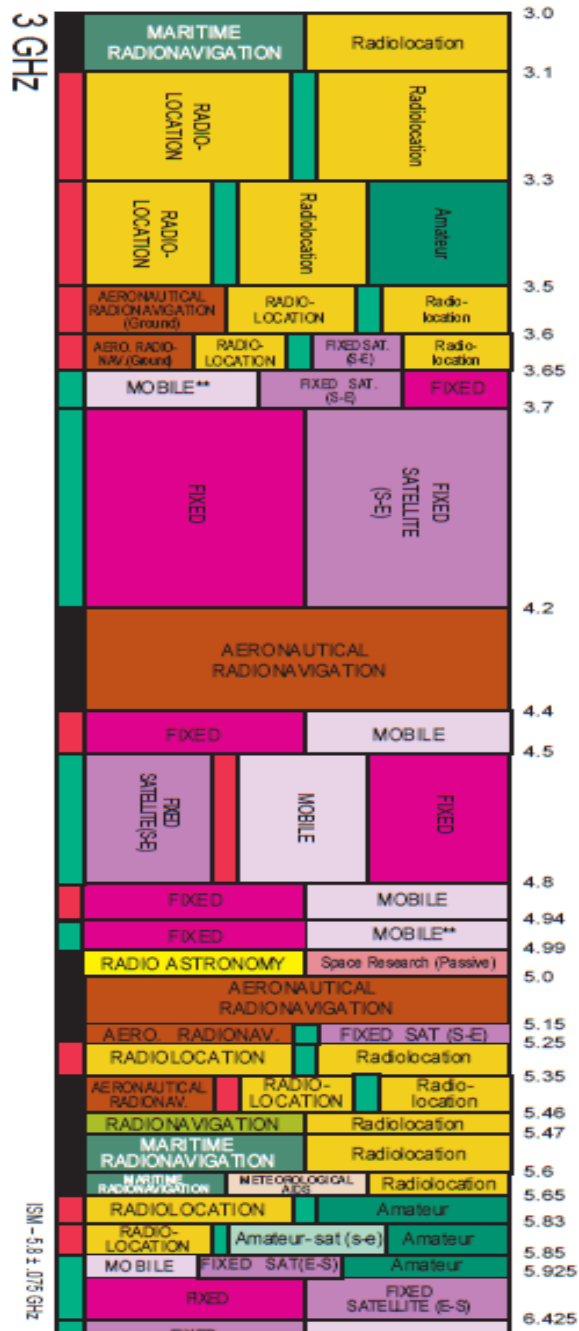


Figure 1.2. Spectrum allocation  $3GHz - 6GHz$

## 1.1 Spectrum Sharing

With the increasing growth of wireless communications and its role in economic, social and public safety domains; it is critical that the spectrum is used effectively.

ficiently. To satisfy the large need for spectrum, a number of spectrum bands are being considered for sharing with other applications (eg. Cellular and Public Safety) [8]. There are some frequency bands which are being shared based on the separation in the geographic location and/or by limiting the operational power. This is how television and radio stations share the spectrum. Another good example would be sharing between satellites and fixed links.

In response to the increasing demand for spectrum, on March 16, 2010 the U.S.National Broadband Plan (NBP) proposed to free up  $500MHz$  of frequency within ten years; of which  $300MHz$  was to be made available for mobile use within five years [7]. Following the plan on June 28, 2010, a U.S. Presidential Memorandum was released which ordered the NTIA and FCC to collaborate in the goal of NBP [10]. In 2012, the Presidents Council of Advisors on Science and Technology (PCAST) [9] reported that it would not be feasible to recover unused or consolidate enough spectrum to meet the ever increasing demand for spectrum. The report suggested that the under-utilized spectrum must be shared to the maximum degree possible to meet demand. Hence spectrum sensing and sharing has gotten significant attention in the spectrum community [7].

Spectrum sharing normally involves a Primary User (PU), to whom the band is allocated and a Secondary User (SU) who uses this same band without causing any harmful interference to the PU (or PUs) [11]. Work has been done on spectrum sensing [12] which allows a SU to keep sensing for a PU and use the band in the absence of the PU in space and time. However, spectrum sharing is limited by the resolution and quality of available sensing [18][19]. Spectrum monitoring is a key enabler for spectrum sharing. Monitoring data can be used in real time to impact sharing and network management decisions, or can be stored for offline analysis. This data can inform spectrum policy and management decisions, thereby facilitating

more efficient spectrum usage. There have been many spectrum studies, typically employing a spectrum analyzer to repeatedly measure and record the electromagnetic power spectrum density [13] [14] [15]. In this thesis, we describe our efforts to measure and record the whereabouts of the PUs and predict their trajectory so that SUs can effectively take measures to prevent harmful interference.

## 1.2 Related Work

There has been significant research on spectrum sharing in recent years [20][26]. This research has been motivated by DARPA (Defense Advanced Research Projects Agency) through their SSPARC (Shared Spectrum Access for Radar and Communications) program and the NSF(National Science Foundation) through the EARS (Enhancing Access to the Radio Spectrum) program. LTE used to work exclusively in licensed spectrum bands which was not enough for LTE to maintain a high Quality of Service (QoS) [16].With T-Mobile recent deployment of LTE in unlicensed spectrum (LTE-U), they have opened a direction for spectrum sharing within the context of LTE. LTE sharing in the unlicensed band, which is lightly regulated, points to the potential for LTE sharing opportunities in licensed bands too. Currently the major spectrum resources being considered for additional LTE deployments are TV White Space (TVWS) channels, Weather Radars, 3.5 GHz Citizens Broadband Radio Service (CBRS) spectrum and the unlicensed 5 GHz Unlicensed National Information Infrastructure (U-NII) bands [17]. The status of sharing in each of these bands is summarized below

White Space refers to the unused broadcasting frequency in the spectrum with television or TV White Space (TVWS) being a particularly popular embodiment. The TV band signals have high penetration power and hence can be used to provide good coverage for the television signal [21]. The TVWS has been shared in the Very High Frequency (VHF) and Ultra High Frequency (UHF) bands. Broadcast TV leaves large

portions of white spaces between channels particularly after the Digital Switchover (DSO). These white spaces can be reused by low powered devices at a particular geographic location and time. TVWS databases [21] are used to manage sharing. In U.S. the TVWS database is maintained by a third party WSDBA, like Neustar and Google; which collect data from regulatory agencies to get information on the location of the protected systems.

The CBRS band consists of the 3550-3700 MHz spectrum. This band is primarily used by the U.S. Navy (uses it for SPN-43 non-combat, aircraft carrier landing radar) and some Fixed Satellite Service earth stations. However, these users are heavily location and time dependent; which makes the spectrum vacant most time in most of the places. It has been proposed that the PU and the CBRS users share the spectrum via dynamic Spectrum Access System (SAS), with the Navy PUs at the first tier and the CBRS users as second tier or third tier [22]. The Navy has to be provided with absolute priority over anyone else, so priority levels have to be set up. The PUs operate in the Federal Primary Access with the highest priority while the SUs on the Priority Access; often known as Primary Access License (PAL). There are another layer of users called the opportunistic users which operate in the General Authorized Access(GAA) where they are provided with different levels of priorities [22]. Compared to TVWS database SAS is more accurate in providing the geo-location, since SAS has interacts directly with the users to implement the spectrum access.

The 5 GHz band is an unlicensed band which ranges from  $5.150 - 5.925\text{GHz}$  and is utilized by IEEE 802.11 WiFi as well other technologies complies. This band has low penetration capability thereby allowing more geographic reuse of the spectrum. The U-NII band is ideal for sharing with LTE due to the large amount of spectrum available. This band is subdivided into U-NII-1,U-NII-2,U-NII-2 Extended and U-NII-3 ranges. The U-NII-2 and U-NII-2 Extended sub-bands requires Dy-

namic Frequency Selection (DFS) to avoid interfering with the radars operating in this particular range. This band is already being used indirectly by the internet and mobile service providers through WiFi operations. Now, however, there is work on LTE-WLAN Aggregation (LWA) [23].

While these are interesting activities pointing to the intense interest in this space, in this thesis we try to draw focus onto a 200 MHz radar band that is not being used to its fullest nor has received the significant attention that the above spectrum has garnered. In the next Section we will discuss the reason for choosing this band followed by sharing schemes to do so in the later Chapters.

### **1.3 Motivation for the Altimeter Radar Band**

This work considers the  $4200 - 4400\text{MHz}$  band which is currently allocated to the Aeronautical Radio Navigation Service (ARNS). It is reserved exclusively for radio altimeters installed on board aircraft and for the associated transponders on the ground.

Compared to the other three popular candidates for spectrum sharing as discussed above, the unique nature of this spectrum is that it supports a “safety of life” application and the challenge is that these radars are transient at high rates of speed. Generally very few radars are stationary and/or rotate around an axis like the Weather Radars in S-band and C-band. Even though the naval radars in the  $3.5\text{GHz}$  are mobile, however they are slower compared to the radar altimeters on the aircraft. The naval radars movement is restricted to in and around the water bodies this allows spectrum sharing in the space domain. However, this is not the case for the aircraft radar. These radars are generally used in case of landing and take-offs. The aircraft radar needs to be analyzed both in time and in space domain to provide efficient and safe spectrum sharing.

In 1998 an industry-wide cooperative to study transformative technologies in aerospace was formed named the Aerospace Vehicle Systems Institute (AVSI), with member companies Boeing, United Technologies Aerospace Systems, Honeywell, Rockwell Collins and Moog. They researched how to make the aerospace vehicles advance using the current technology. One of their initiative was Wireless Avionics Intra-Communications (WAIC) [25]. WAIC tried allocating dedicated frequency for Aircraft Onboard Wireless Systems. WAIC's goal was to reduce the overall weight of the aircraft system. They found that the total wiring in an aircraft amounts to around  $5700Kg$ ; out of which about 30% of electrical wires are potential candidates for a wireless substitute. For this purpose, they chose the 4200-4400 MHz band. In 2015, the World Radiocommunication Conference approved a resolution to identify WAIC systems that can operate in the 4200-4400 MHz band; since they will not cause any harmful interference to the radar altimeter [24]. This shows that a world body is providing recommendations for sharing this band.

#### 1.4 Radar Altimeter

The radar altimeter is used to perform the safety critical task of providing guidance during takeoff and landing of aircraft [27]. The altitude is computed by the time taken for a transmitted Continuous Wave (CW) signal to travel from the aircraft to the ground and then return to the aircraft. The radar is active throughout the flight. Altimeter data is input to Ground Proximity Warning Systems (GPWS) which give a warning to the pilot at a particular altitude and closure rate to the ground. These systems have a required accuracy of 0.9 meters (3 feet), hence the implications of sharing of this band must be analyzed very carefully.

The radar altimeter system on a commercial aircraft consists of up to three identical but independently operating radar altimeters [27]. These radar altimeters use swept Frequency Modulated Continuous Wave (FMCW) technology with a sweep

bandwidth of approximately 100 MHz and a saw tooth sweep repetition rate of approximately 100 Hz. Additional description of the operation of the altimeter is contained in Chapter 3.

Spectrum measurements illustrating the variation in received power as a function of time of day and day of week are shown in Figure 1.3. This figure illustrates measurements at a single location approximately 13km from the nearest airport, and shows variations over time that might be exploited for spectrum sharing. Aircraft flight patterns are carefully controlled and monitored. Thus, interference to a ground-based LTE system from aircraft altimeters and interference to the altimeter from an LTE system will be a function of location and time. Measured power levels are expected to be greater during periods of high airline activity and near airports. A much lower level of power is expected at locations distant from airports and distant from established flight paths.

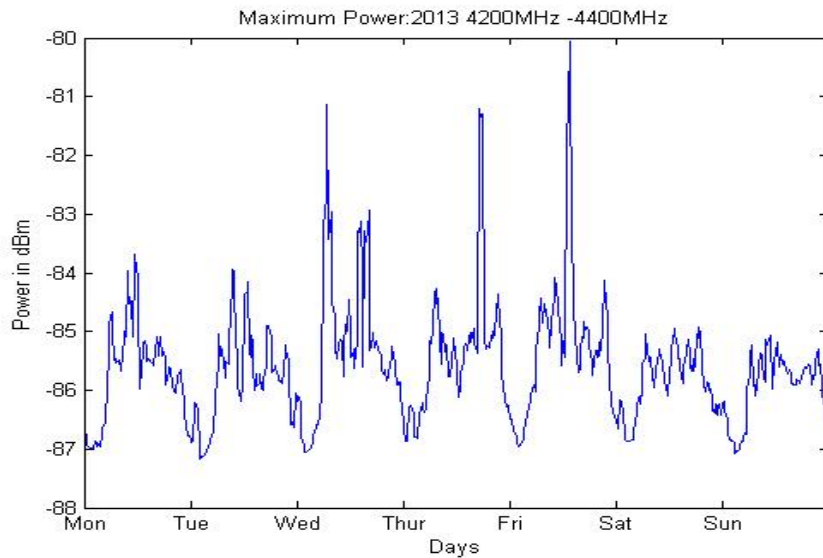


Figure 1.3. Average of the Maximum Power over one year in the 4.2-4.4 GHz Radar Altimeter band

## 1.5 Candidate Secondary User

The FCC and NTIA envision sharing the 4.2 to 4.4 GHz spectrum between the altimeters as primary users and small-cell systems as secondary users. Although other options are possible, we have presumed that the small-cell systems use Long Term Evolution (LTE) technology as defined in the 3GPP standards. LTE technology is widely used for cellular systems. An overview of the LTE physical layer is found in the overview paper by Larimo et al. [28]. The LTE physical layer employs Orthogonal Frequency Division Multiplexing (OFDM) in a highly complex time-frequency division design. Powerful error correction codes and hybrid automatic repeat request (HARQ) is employed as well as Multiple Input Multiple Output (MIMO) technology. The time space is partitioned into 10 msec frames each containing multiple OFDM symbols. OFDM subcarriers are spaced 15 kHz apart. Each OFDM symbol also includes the cyclic prefix designed to mitigate multipath transmission. LTE designs are available for bandwidths up to 20 MHz. In this research, results for a 10 MHz LTE bandwidth are presented.

Simulation analysis of LTE and altimeter coexistence is greatly facilitated by the Matlab LTE Toolbox. This Toolbox includes all details of the LTE standard and has the capability of modeling precisely the 3GPP standard or to modify any parameter of the standard for evaluation purposes. LTE may be deployed in large-cell configurations or in small-cell configurations. In this research, we consider small-cell systems with the option of limiting to in-building pico-cell deployments [29]. That is, the system level analysis may be configured for the deployment of interest. We note that cell-splitting, also referred to as cell densification, is a well-known means of enhancing overall spectrum utilization. The use of in-building deployments may be used to further mitigate interference to altimeter systems because the transmission powers for very small cells is reduced and also because of the transmission path loss as a signal exits a building.

## 1.6 Challenges

Sharing the radar altimeter band with LTE comes with challenges, as it is used for safety critical task of providing guidance. However, with deep understanding of the problem we can easily see opportunities for sharing this band without crossing the safety line. Nevertheless, there are challenges which need to dealt and can be classified as technical challenges, administrative challenges and psychological challenges.

In our proposal for sharing we suggest sensing the trajectory of the aircraft to trigger the SUs to leave the band in case a interference threshold is reached. In Chapter 2 we discuss about the challenges associated with sensing. Furthermore there are technical issues with LTE as well discussed in Chapter 3.

Administrative issues can be a key hurdle in solving this problem. The question is how much can we rely on the mobile providers for the safety of the aircraft? What if even after sensing the presence of the aircraft the SUs do not leave the band? This requires proper and clear policy implementation between the government and the mobile providers.

Public impression on the safety of the aircraft also becomes a hurdle. For a common person safety comes first, and even if all the problems mentioned above are avoided; there may still be concern in the minds of the public. This kind of strong impression might lead to panic causing politicians to question any decisions related to sanctioning policies related to radar altimeter spectrum sharing.

## 1.7 Goal and Approach

There have been many debates within the International Civil Aviation Organization (ICAO) as to how crucial this band and radar is for the safety of the passengers. An obvious conclusion is that the likelihood of harmful interference to the altimeter must be extremely low. It is noted, however, that the criticality of the

altimeters accuracy is high during take offs and landings and relatively low during the majority of a flight. It is further noted that (Global Positioning System) GPS and barometric altimeters are used in conjunction with the radar altimeter so it does not represent a single point of failure system element. The conjecture is that spectrum sharing opportunities may exist in the 4.2-4.4 GHz band over large geographic areas that are sufficiently distant from airport approach and take off flight paths. In addition, spatial and temporal information about flight paths and real-time locations as communicated with Automatic Dependent Surveillance Broadcast (ADS-B) system can provide detailed information that can enhance sharing opportunities.

The FCC and the NTIA have been jointly running tests to identify the issues an aircraft would face when subjected to interference from LTE signals from base-stations (BS) and from user equipment (UE). Papers from the ICAO and the International Telecommunications Union (ITU) have also addressed the coexistence problem. ICAO has prepared a recommendation [33] [8] [35]. This recommendation defines maximum interference levels for receiver desensitization, for front-end overload and for false altitude prevention. The recommendation does not, however, analyze the sharing problem at the system level as is provided in this work. ICAO has also studied adjacent band compatibility [34] wherein they studied the interference received at the altimeter from outdoor LTE access points and handsets for a single very specific flight path geometry. This interesting result leads to the conclusion that there are system scenarios where coexistence will not be possible. The current work will extend such results to consider different scenarios and to determine limits to constrain spectrum sharing.

In Chapter 2 we discuss a method for sensing the aircraft in real-time followed by analyzing the 9 month worth of extracted aircraft data. In Chapter 3 we consider the co-existence of Aircraft Radar and LTE, thereafter analyzing scenarios which can

help in finding threshold values for interference to both systems. In this chapter we discuss the aircraft radar and LTE system in detail. In Chapter 4 we combine our results from the previous two chapters to predict area or time periods where there is less likelihood of interference. We propose few approaches to deploy the band in space-time domain. Finally, we end with Chapter 5 where we summarize our finding and state if sharing in this band is beneficial or not and suggest future work.

## CHAPTER 2

### ADS-B DATA ANALYSIS

To find out prospects for sharing between the Aircraft Radar and LTE a detailed spatio-temporal analysis needs to be done. To do so we use the Automatic Dependent Surveillance Broadcast (ADS-B) a surveillance-based system that determines and broadcasts an aircraft's position, airspeed and other data [30]. The ADS-B is a reporting technology which allows the Federal Aviation Administration (FAA) to track the aircraft. The data is received by the ground stations for tracking the aircraft and it can also be used by other aircraft to allow them to have self-separation.

ADS-B is an integral part of the US Next Generation Air Transportation System (NextGen) [32] and Airports Authority of India (AAI) in line with ICAO for fixing the shortcomings of the present air-travel. ADS-B will help in managing air traffic, improving visibility, receiving weather information and easily broadcasting flight information. ADS-B equipment is currently mandatory in Indian and Australian airspace, and will become mandatory for all aircraft in United States by 2020 [30]. It is also deployed and used in Europe and Canada. Hence, ADS-B is a technology on which we can depend for real-time aircraft information.

The ADS-B technology uses the 978 MHz and 1090 MHz to broadcast the aircraft information. This data is currently not encrypted, i.e., anyone can access it using basic Software Define Radios (SDR). Currently it is used by many sites like FlightAware.com and FlightRadar24.com, who receive the data from their feeders spread across the world. These websites commercially sell this data for the users who want to use it for their APIs. We have collected nearly 10 months of data from ADSBexchange.com which publishes it free for non-commercial use.

The goals of this chapter are as follows:

- Extensively analyze the ADS-B data to figure out Times and Areas which have the least or no aircraft influence.
- To analyze the degree to which the aircraft traffic is predictable.
- To determine the impact of potentially frequent changes in aircraft flight paths.
- Ultimately to determine the likelihood of the aircraft occupancy for a given location and time.

## 2.1 Overview of ADS-B Data

In this Section we describe the properties associated with the data published in ADSBexchange.com. This website provides historical data starting from 20th June 2016. Every 60 sec it collects data from all its feeders around the world and combines them into a file, this results in 1440 JSON<sup>1</sup> files per day. The files contains many parameters; we have used the following for our work:

- ICAO.Id - The unique identifier of the aircraft. This is a six-digit hexadecimal identifier broadcast by the aircraft over the air in order to identify itself.
- Lat - The aircraft's latitude.
- Long- The aircraft's longitude.
- Alt- The altitude in feet at standard pressure. This measurement is above the Mean Sea Level (MSL).
- PosTime- The time (at UTC in JavaScript ticks) that the position was last reported by the aircraft.

---

<sup>1</sup>JavaScript Object Notation(JSON) is an open-standard file format that uses human-readable text to transmit data objects consisting of attribute and value pairs and array data types

- MLAT- True if the latitude and longitude appear to have been calculated by an MLAT server and were not transmitted by the aircraft itself. As it was mentioned that many aircraft do not broadcast ADS-B data, so to identify these kind of aircraft we can uses Multilateration (MLAT).
- Species - It is an integer value that signifies what kind of a flying object the data is for. The ADS-B data is broadcast by many other flying objects like helicopters, Gyrocopter, Tiltwing, Land Plane, Sea Plane and Amphibian.

## 2.2 FAA Airspace Division

Before we move on to analyzing the data we need to understand the US Airspace which is highly regulated and categorized. The ICAO divides airspace into seven classes from A through G (with class F not used in the US). Class A through E are called controlled airspace, which means that within the defined area Air Traffic Control (ATC) services will be provided. Whereas Class G is uncontrolled airspace, which means that ATC doesn't have any authority and it is out of the domain of the FAA.

In controlled airspace, the level of ATC control on the aircraft depends on the class of the airspace. Controlled airspaces are mainly deployed for areas with a high volume of air traffic, and/or for flights to fly under Instrument Flight Rules(IFR) with ATC guidance and security. Class A is generally 18,000 ft above Mean Sea Level (MSL) or more. In class A only IFR flights are allowed, and flights under Visual Flight Rules (VFR) are not allowed, except for failure of radio communication or emergency. The classes B through D are the airspaces surrounding the nation's busiest airports. The airspace represents an inverted wedding cake as shown in Figure 2.1. An airport is designated a particular class based on the traffic at that airport. Class B is the busiest and Class D is the least busy, and hence the size of the airspace. Generally

the elevation of the airspace from the surface for Class B, C and D are 10,000 ft MSL, 4,000 ft MSL and 2,500 ft MSL respectively. However, the area surrounding the airport is tailored based on the airport. Airspaces which is not labeled class A,B,C or D are generally labeled as class E. In United States Class E begins from 14,500 ft MSL to the base of Class A [31].

The uncontrolled airspace (i.e. Class G) extends from the surface till the base of the overlying Class E. ATC doesn't have control in this area, however there are some VFR minimums which apply to Class G.

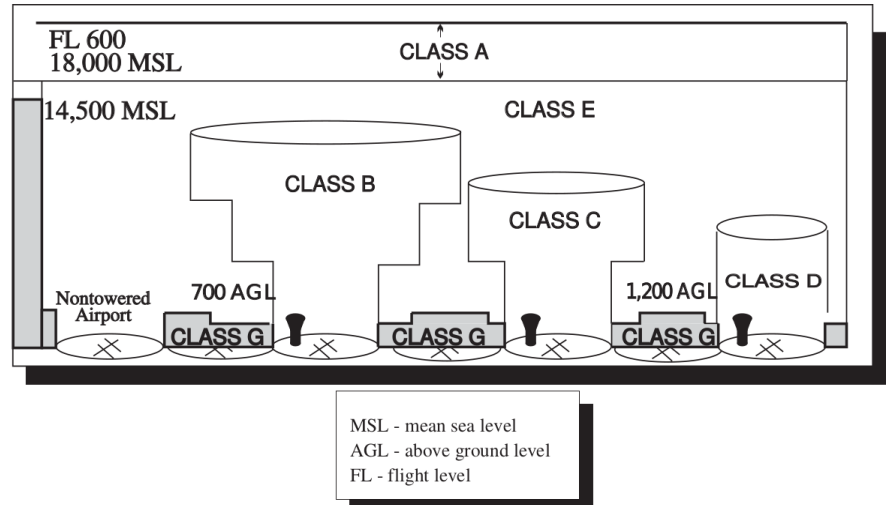


Figure 2.1. Area considered for the work

### 2.3 General Analysis of the Area

The data present in ADSBexchange.com has flight information from all over the world, however for the thesis we have considered a small area which concerns Chicago and its surrounding area as shown in Figure 2.2. The area is between 41.600700 and 42.104991 Latitude, and -88.403735 and -87.408099 Longitude. The reason for considering this area is because of its 2 busy airports O'Hare International

(ORD) and Midway International (MDW) Airports, which are 17 miles and 8 miles away from Downtown Chicago respectively. This close proximity of airports to the downtown provides us with a perfect example where there is high demand for spectrum and it is quite busy with aircraft. Moreover, O'Hare and Midway Airports are Class B and Class C airports respectively. There are also many Class D airports in this region, like Chicago Executive Airport formerly Palwaukee Municipal Airport (PWK), DuPage Airport (DPA), Schaumburg Airport (06C), Mill Rose Farm RLA Airport (IL68), Lewis University Airport (LOT), Bolingbrook's Clow International Airport (1C5) and Brookridge Airpark (LL22). Note that the abbreviations associated with each airport name is known as the Location Identifier (LID) for an airport. From this point we will refer to the airports with their respective LID.

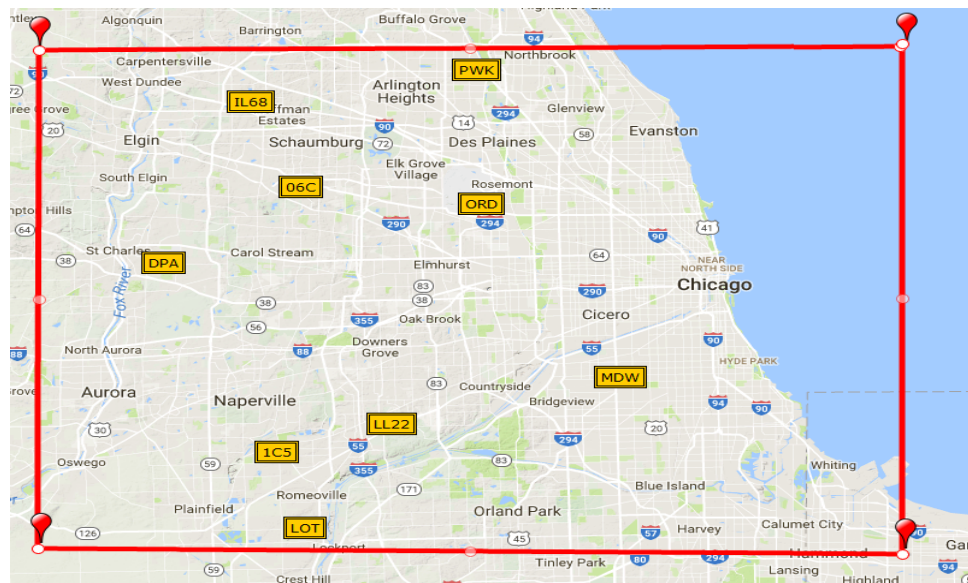


Figure 2.2. Area considered for the work

To understand the deployment strategy of this area or any area one needs to analyze its deployment of transmitters and receivers. In this case there are two participants the aircraft and the LTE system. The LTE system is in turn divided into Base stations (BSs) and User Equipment (UEs). We will analyze the BS deployment

in Chicagoland in Section 4.1. In this chapter we need to observe how the radars are deployed. As explained in Chapter 1, the radars in this problem are more transient in nature compared to weather radars and Navy radars, therefore we need to do both a geographical and temporal analysis of the area.

To efficiently share this spectrum, detailed information about the aircraft is required. This information is the X coordinate, Y coordinate, Altitude, Time, Velocity, Pitch, Roll and Yaw. These parameters have a correlation with each other and they need to be analyzed pair wise. Figure 2.3 visualizes a pairwise relationship of the parameters which are important for analyzing the flights using a 2D Scatter Plot Matrix. The figure has 16 subplots arranged in 4 rows and 4 columns. The 4 rows and 4 columns are labeled in the order of latitude, longitude, altitude and time. The 4 subplots on the diagonal are histogram plots for the variable labeled in the order mentioned, whereas the rest of the 12 subplots are scatter plots. The X and Y axes for the subplots are represented by the respective column and row label. Let us consider a sub-plot on the third row and fourth column. For this plot the X axis is time and the Y axis is altitude. From this subplot we can observe that there is a rush in flight traffic after 5 am till late night. However, most of the traffic is concentrated below the 15,000 ft mark. Again, for the sub-plot in the second row and first column, it gives us an insight to the spatial distribution of the flights and the usual traffic pattern. The histogram plots gives us an insight to the distribution of the data.

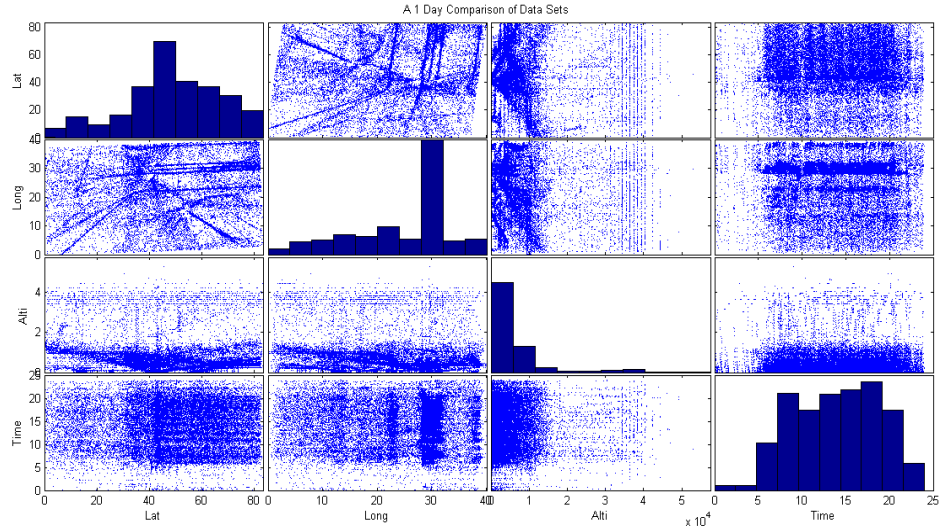


Figure 2.3. 1 Day Scatter Matrix Data

Since the aircraft is transient in nature, the aircraft's parameters can change based on the air traffic, weather and human response. Even the flight pattern may change based on the demand for that flight, company proprietary algorithms or city rules. Given this it is difficult to predict the flight pattern as a function of all the above parameters. To even find patterns in this complex data, a few months of data analysis is required. However, after analyzing the data carefully and not considering the outliers, there are some specific flight paths which are used by most of the aircraft on a regular basis. The majority of the paths taken by the aircraft remain the same for a given airport location, time of the day or aircraft ID. These paths may change for a temporary time period when there is a lot of traffic, or bad weather or in case of security purpose. However, analyzing 10 months of data would compensate for the effect of these changes in flight paths.

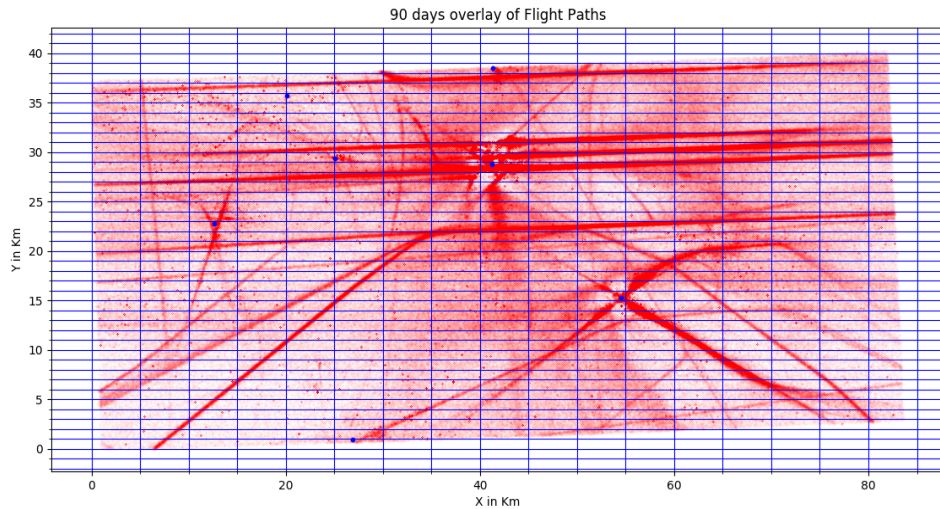


Figure 2.4. A 90 Day overlay of flight for the locations used by the flights in the given area

Figure 2.4 illustrates aircraft location data overlay over a 3-month period. It is evident from the plot that there are some distinct paths which are used by the major commercial aircraft while trying to landing or taking from O'Hare and Midway Airports. However, there are flights which have used paths other than the popular ones, but they are not so periodic. Moreover these flights might be heading out/towards the Class D airports mentioned earlier, and because their reduced frequency, they do not seem to look like popular flight paths. From this kind of overlay analysis we can easily draw some rudimentary conclusions as to which places on the grid are likely to expect more traffic.

Again we need to observe that merely being present at a particular location on the X-Y plane will not result in harmful interference. We would also need to consider the altitude of the aircraft. The interference experienced by an aircraft at  $1000\text{ft}$  would be much higher than that experienced at  $12,000\text{ft}$ . Figure 2.5 shows 3 months of aircraft altitude data overlay with respect to time of the day. A

prominent observation from the figure is that there are a lot of aircraft that are above the 18,000ft mark of Class A. Based on this one can get an intuition that many flights can be neglected based on their altitude, however before we can conclude on an altitude threshold we need to do a coexistence study as explained in Chapter 3.

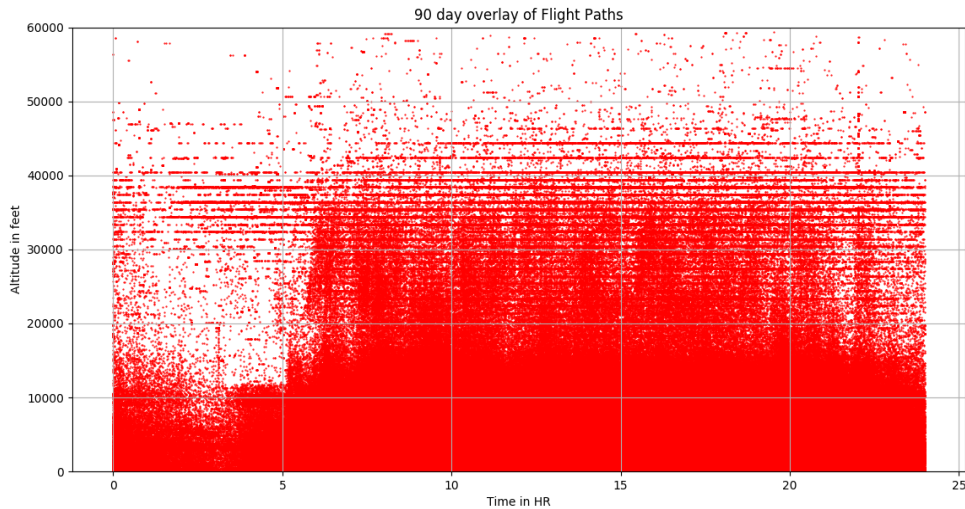


Figure 2.5. 90 Day Overlay of Altitude Data

In the next few sections we analyze the data and try to build an intuition regarding sharing opportunities.

## 2.4 Flight Count

Before we can count the flights which repeat on a daily basis, we need to define what a flight is. An *aircraft* is one with a unique ICAO ID. For our study we have considered the ICAO ID which is a unique ID for an aircraft. Blocks of these codes are assigned to countries by the ICAO, after which each country assigns individual codes to aircraft registered in that country. This hex code generally remains the same as long as the aircraft's Registration number remains the same. If the registration number changes, which can happen sometimes when an aircraft is sold to an owner in

another country, the ICAO hex code will also change. Now these flights might enter and exit the grid shown in Figure 2.2. We identify the single occurrence of an aircraft in the grid within a particular time interval (to avoid aircraft circling in and out of the grid) as a *flight*. Figure 2.6 shows the aircraft count and flight count for a 90 day period. It is evident from the figure that there are many aircraft which journey into and from the grid more than once a day.

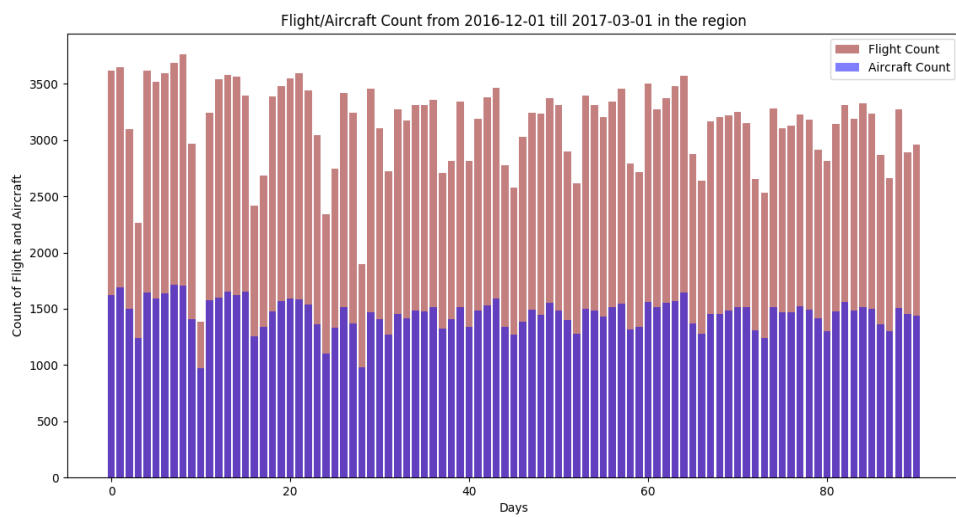


Figure 2.6. Area considered for the work

If we look closely at 11th of Dec 2016 in Figure 2.6, we would see a drastic fall in aircraft and flight count, this is because of winter storm [38]. Due to the winter storms many flights were canceled on that day; the flight count on that day decreased to less than 1500. This shows that bad weather allows for more spectrum sharing opportunities.

Weather is a key factor for flight paths and even whether a flight will take off or land at an airport. In case of bad weather many flights get canceled. This leads to passengers waiting at the airport which compels them to use their smart devices and

hence an increased demand in capacity. This a good example when this  $200MHz$  of band can be used because of its increased white space coinciding with a high demand for LTE.

Temperature and humidity combined play an important role in providing thrust, increased climb rate and more lift to the wings. As temperature and altitude change the performance of an aircraft decreases. On a hot sunny day an aircraft needs more runway and has a slower climb rate. The power of the engine is affected by high humidity, since there will be less fuel-air mixture (high water vapor level in air). An aircraft performs optimally in cold weather, as the cold air is denser compared to warm air. There would be a larger mass of fuel-air mixture, which leads to more power and thrust. However, in case of ice, snow and frost the aircraft performance decreases upto 30%, due to increased drag and aircraft weight.

Even, wind direction is important for an aircraft since it is used to determine the runway and which end of that runway the plane will use to take off. Sometimes the wind direction is opposite to the aircrafts destination. In that case they use the runway in the opposite direction, however after a climb out they circle around to the needed course direction to reach their destination. Wind direction can heavily change the usual flight path, and hence an intelligent sharing algorithm is required which takes into consideration these factors. Analyzing the weather can act as triggers for these sharing algorithms and sharing can be done extensively.

## 2.5 Geographic and Temporal Analysis

As we have seen in the previous section, the area under consideration is typically visited on average by 2500-3000 flights daily. However, these flights are distributed in space (X,Y and Z) and in time. In this section, we analyze the Chicagoland grid in detail by dividing the area into small  $1Km^2$  boxes (which we name *cells*); fol-

lowed by counting the traffic in each box. We define traffic as the occurrence of a flight in each and every box with respect to time. We normalize the traffic count by calculating the daily average for each box. We observe the grid for 10 months so that we can consider the change in flight paths and traffic irregularities. Figure 2.7 is a heat-map for Chicagoland for 10 months. One can observe that there are two major concentrations of traffic in the waterfall chart, the upper one is ORD and lower one is MDW. On an average there are certain distinct paths used by the 2 airports for take offs and landing, the trenches for the flight path are prominent in the Figure 2.8.

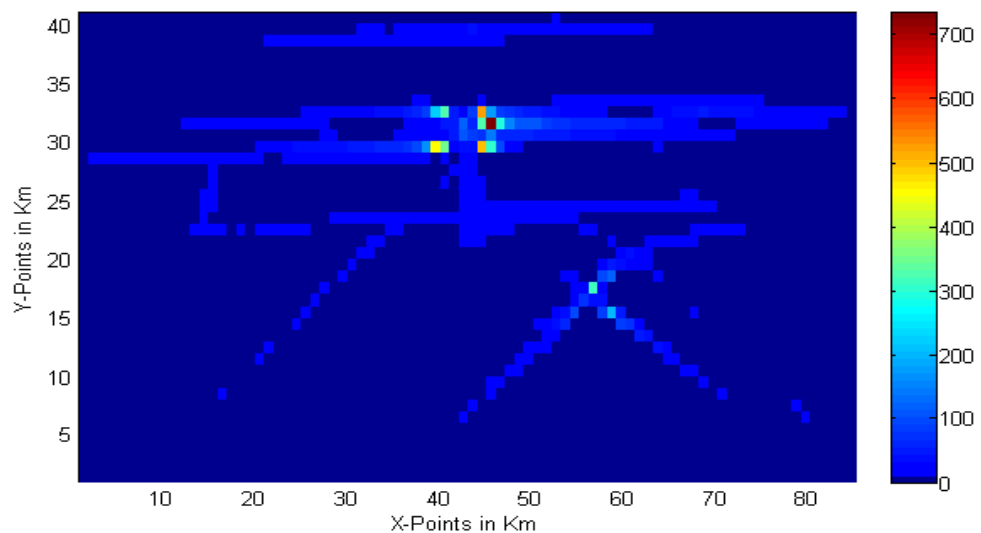


Figure 2.7. Heat-map for Chicagoland 9 Month Average Air Traffic

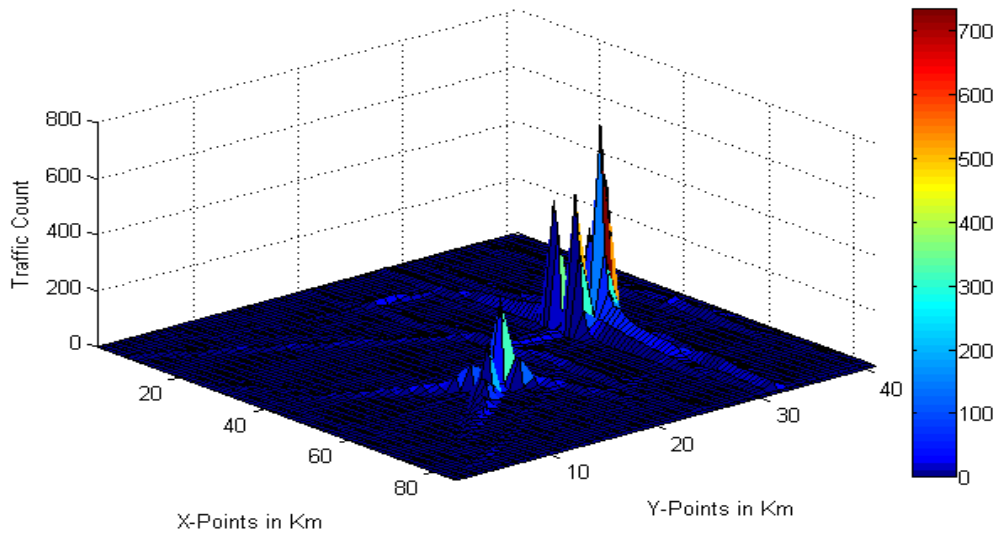


Figure 2.8. Surface Plot for Chicagoland 9 Month Average Air Traffic

The occupancy of the boxes will vary from the proximity to the airport location. To figure out the usual routes taken by aircraft, let us consider the boxes which are on an average visited by at least 10 flights per day. Figure 2.9 shows the boxes colored red as the popular/most used flight paths on an average. This figure helps us give an intuition for the candidate areas for sharing of this band.

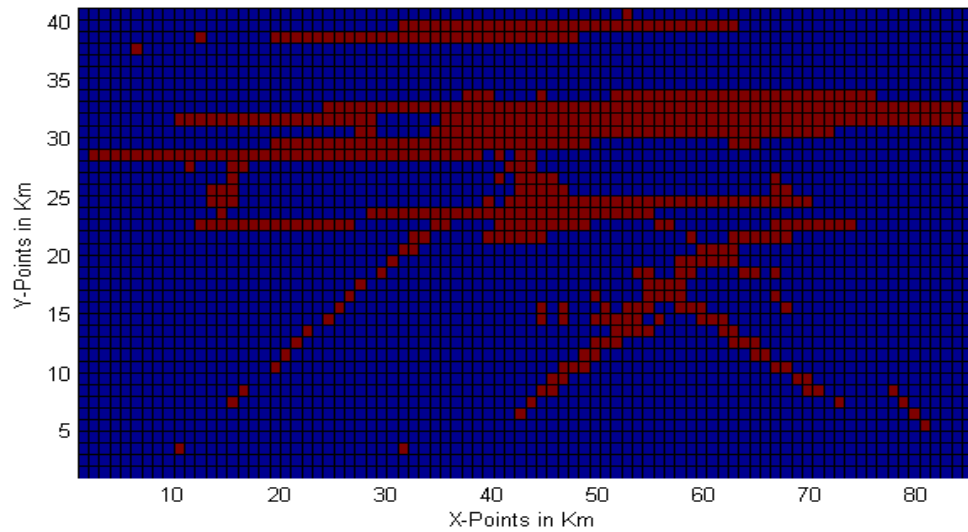


Figure 2.9. The popular Flight Paths considered on an average by at least 10 flights on a daily basis

To analyze the flight patterns in detail let us divide the area into zones based on the boxes which fall under the most used path as shown in Figure 2.9. Let us divide the grid into 4 Zones namely Zone 1, Zone 2, Zone 3 and Zone 4 as shown in Figure 2.10.

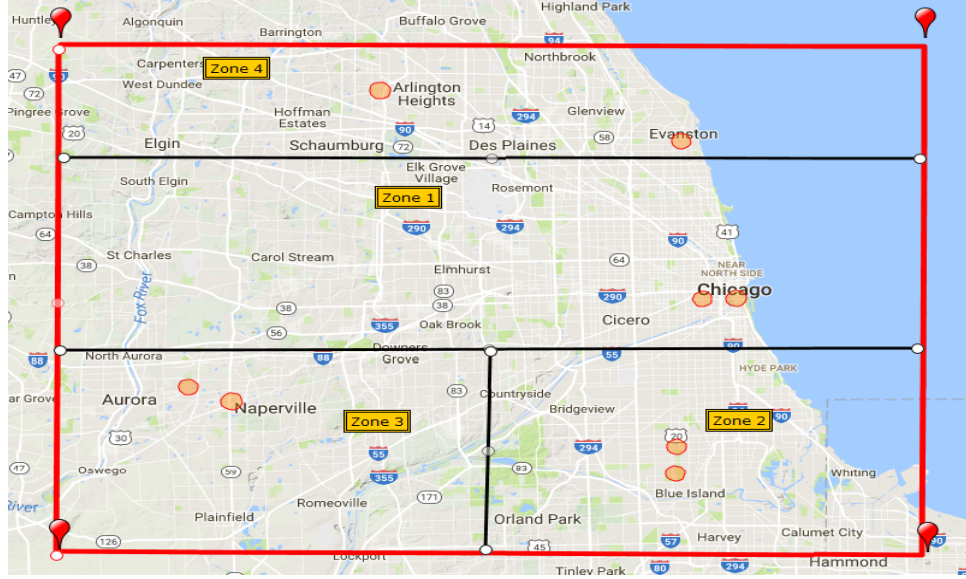


Figure 2.10. Zone division for the given area

**2.5.1 Zone 1.** In this zone we have considered the busiest airport ORD (Class A airport) and hence it has the majority of the traffic. We demarcated it based on the flights paths quite prominent from the waterfall chart shown in Figure 2.9. The flights can approach ORD from either the West or East side of the grid. Other than the ORD traffic this zone also has the DPA and 06C traffic (Class D airports). This area also has the Chicago Downtown area, which makes it a very important zone for our analysis. This zone is good blend of demand and flight occupancy in the band.

In Figure 2.11 we analyze the geography of the zone. The subplots on the  $X$  and  $Y$  axis show the histogram plots for the  $X$  and  $Y$  co-ordinates respectively. All figures in the next few sections have a similar construction as explained. The space analysis shows that there are 2 prominent flight paths in this region that are used to access ORD and MDW in Zone 2. It seems the lower flight path is for landing at DPA.

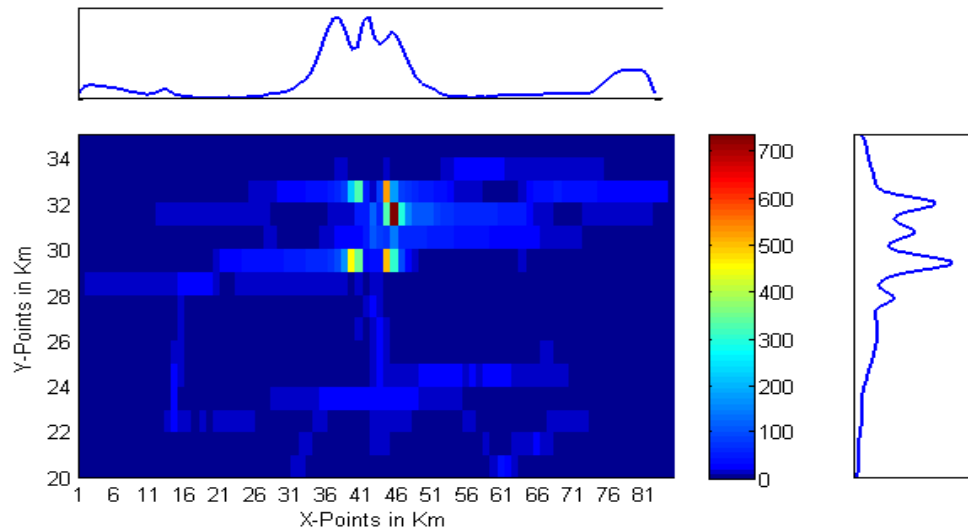


Figure 2.11. Average Traffic Count for 9 months on the space domain for Zone 1

In Figure 2.12 we analyze the time distribution of the traffic. The subplots on the y axis show the histogram plots for the time of the day. It is quite prominent from this waterfall chart that the busy hours are very cyclical. Though this zone is busy, sharing opportunities can be developed around these periodic busy hours. The major traffic is from 9 am till 7 pm, and shows small vacillation in this time period.

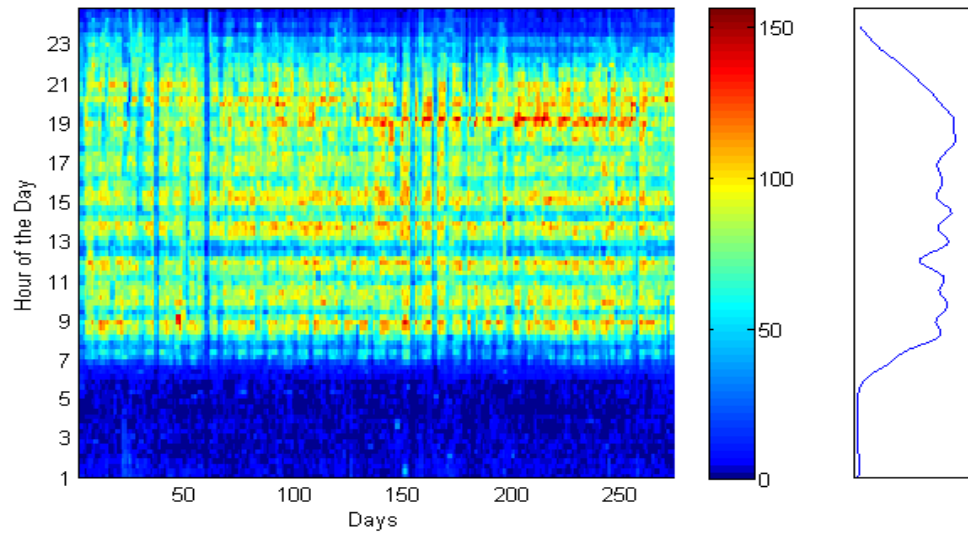


Figure 2.12. Traffic Count for 9 months on the time domain for Zone 1

**2.5.2 Zone 2.** In this zone we have considered the MDW (Class B airport). It is a smaller airport as compared to ORD, however there is a prominent flight paths from the airport representing a big 'X', which correlates well with the X shaped runway configuration at MDW. Figure 2.13 shows how extensively the area is being used. The scale for the waterfall chart has been lowered to 200 flight count for visual clarity. It seems that the maximum traffic is located in the direction of the runways. The area is residential and hence has demand for more spectrum.

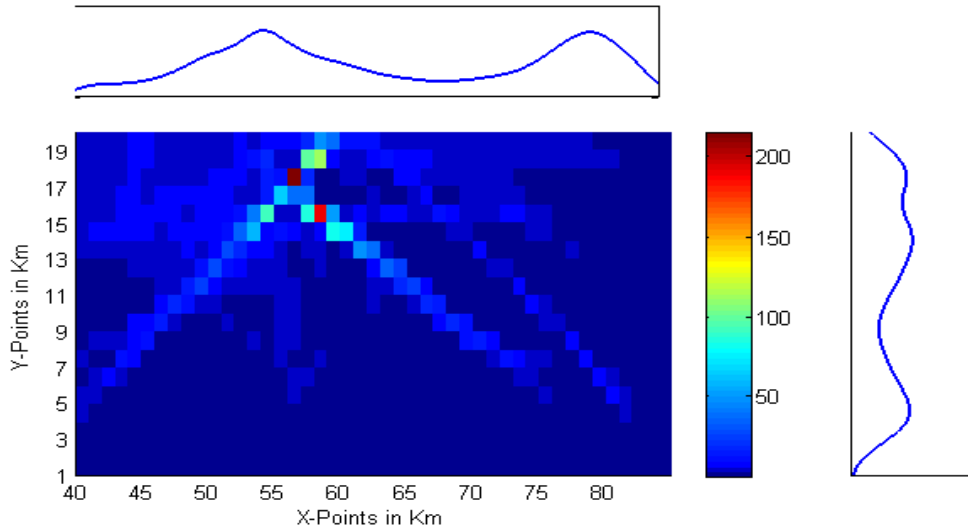


Figure 2.13. Average Traffic Count for 9 months on the space domain for Zone 2

The time analysis for this zone in Figure 2.14 shows that there are some periodic busy hours, however as would be expected these are less busy than ORD, since it is a smaller airport with fewer runways and less traffic. Note that the scale for the waterfall chart has been decreased for clarity. As we move from left to right in the graph, we see that the occupancy of flight has decreased. It seems that there was a significant change in flight timing and that the busy hours have been more evenly distributed. Compared to Zone 1, the air traffic in this zone starts late at 7am. (Please note that there is an outlier in the data at Days 101 and 102)

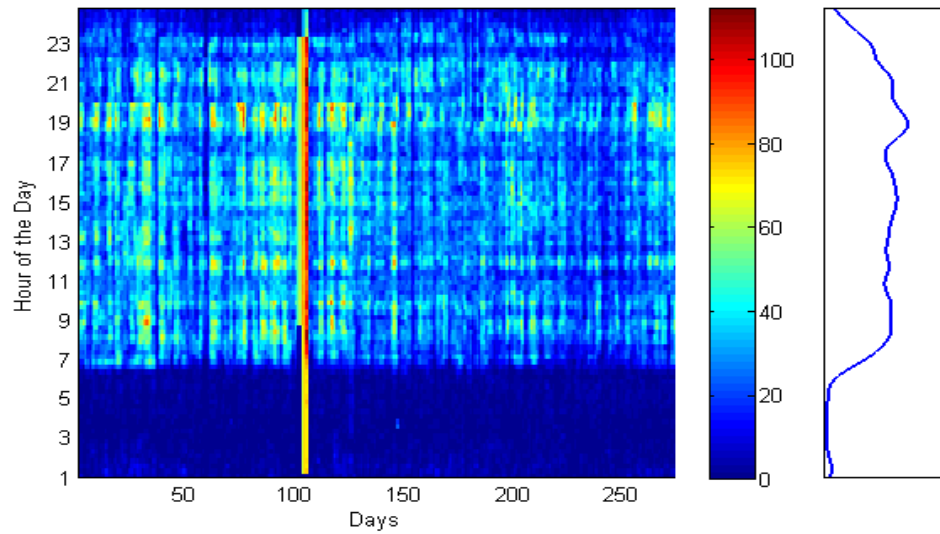


Figure 2.14. Traffic Count for 9 months on the time domain for Zone 2

**2.5.3 Zone 3.** This zone doesn't have major airports like the first two zones, however it is close to local airports like 1C5, LOT and LL22. These airports are used by recreational pilots, trainees and for skydiving. This area is mostly Class G airspace. That is the reason why the maximum average flight count in this region goes upto 12, as shown in Figure 2.15. Even the histograms for the respective axes show less occupancy of flights.

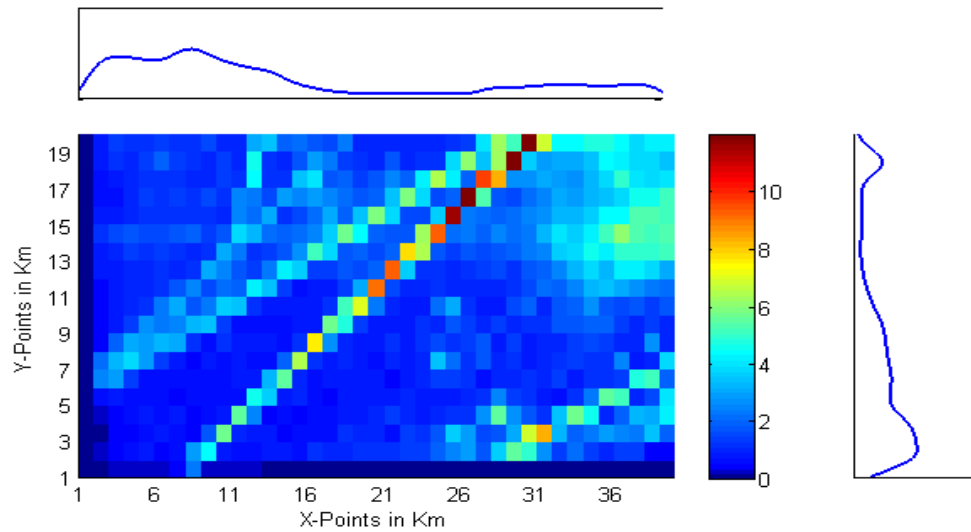


Figure 2.15. Traffic Count for 9 months on the space domain for Zone 3

In Figure 2.16 we see cyclic busy hours which steadily increases through the day and descends after evening time. Note that the scale for the water chart has been decreased for clarity.

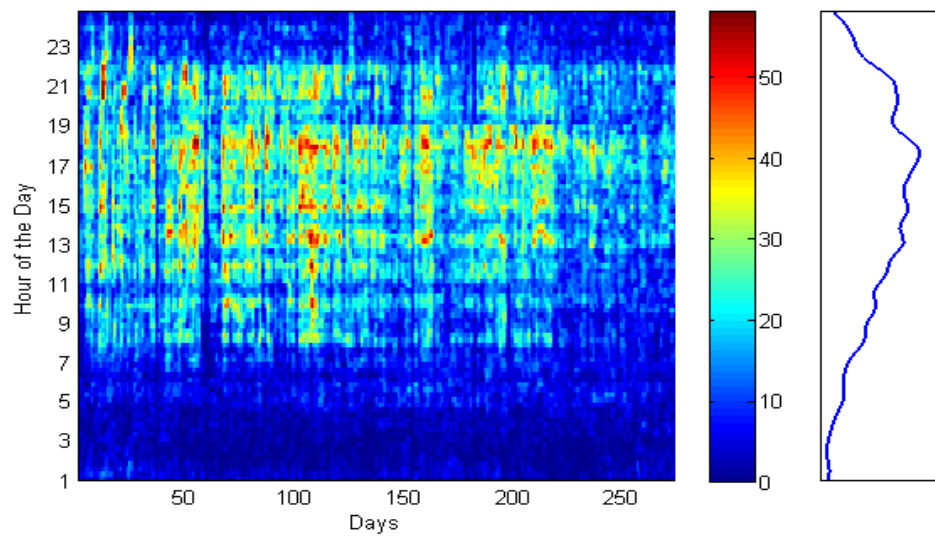


Figure 2.16. Average Traffic Count for 9 months on the time domain for Zone 3

Our major concerns are commercial flights, however radar altimeter are also used by these small private aircraft. The small aircraft approach and landing speeds are lower than commercial aircraft, and the pilots generally operate in visual estimation for landing and take-off. Nevertheless, altimeter radars are important for these pilots at night time and do prevent unforeseen accidents [39]. The count of these aircraft are small compared to the other 3 zones and should be easily managed using spectrum sharing algorithms. This area is a rural area with 2 major cities Aurora and Naperville and it has a reasonably large population that could use this spectral band to meet their broadband needs.

**2.5.4 Zone 4.** In this zone we have considered PWK (Class D airport) and a small local airport IL68. From Figure 2.17 it is quite prominent that the major traffic in this zone is because of PWK airport and is quite periodic in nature. The histograms for the X and Z axis shows a lot of empty space, with very few flights.

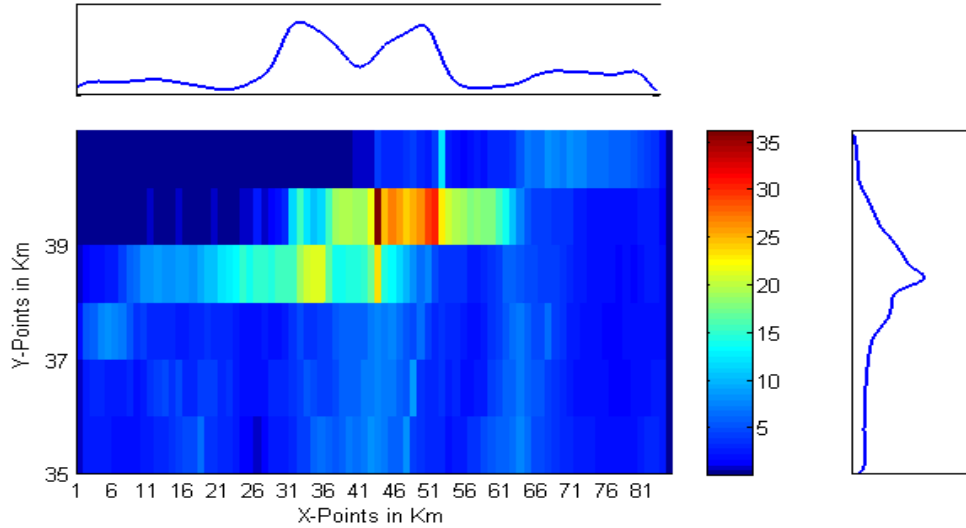


Figure 2.17. Traffic Count for 9 months on the space domain for Zone 4

Figure 2.18 shows that on the time domain it remains quite busy throughout

the day.

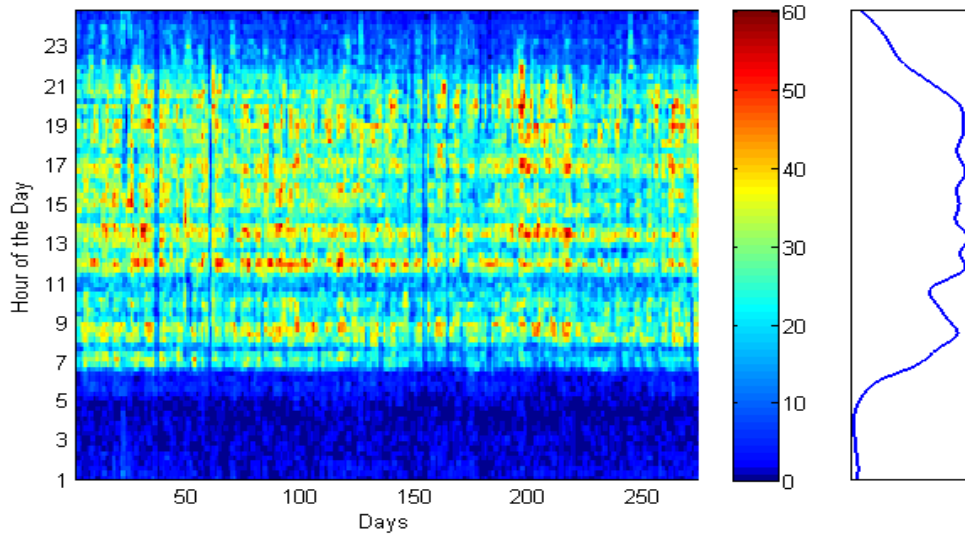


Figure 2.18. Traffic Count for 9 months on the time domain for Zone 4

**2.5.5 Cell Analysis.** As we have seen that each of the 4 zones are unique in its airspace, flight patterns (in space and in time domain) and population density. The space analysis of the zones gives an overall estimates as to which areas are likely to be considered for sharing. The time analysis of the zones gives an overall estimate of the busy time and the periodic nature of the flight times. The time analysis gives the busy hour for the whole zone and not for a specific area. Hence, we need to narrow our analysis down to a space-time analysis of a cell. We have considered 2 cells per zone to show contrasting usage patterns. The two cells per zone approximate location are shown as red circles in Figure 2.10. Figures 2.19 - 2.22 show cell analysis on the time domain for all 4 zones. These waterfall charts are similar to that used analyze the time domain for zones, where the Z axis is the flight count. Please note that the flight count is integer numbers and have the exact color corresponding to the integers in the color bar.

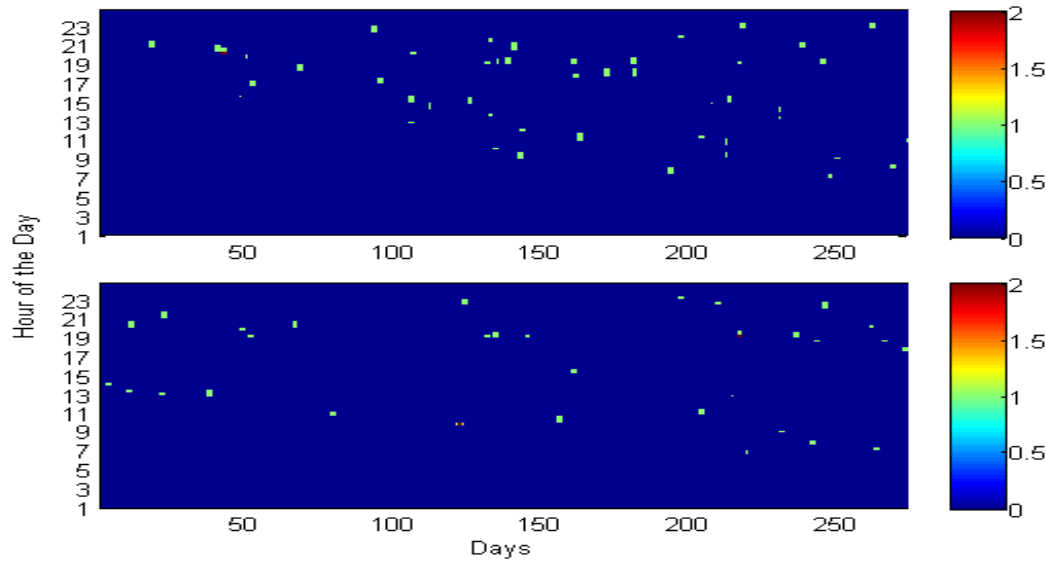


Figure 2.19. Cell analysis on the time domain for Zone 1 (a) (63,23) (b) (65,23)

In Figure 2.19 we have considered two cells which are at downtown Chicago. These cells are present in Zone 1, which seems to be the busiest zone of the four. However, these cells show that with respect to the flight occupancy there is ample amount of white space in the time domain. These cells are quite far from ORD and are located in the city (high demand for LTE), which serves as a good candidate for sharing.

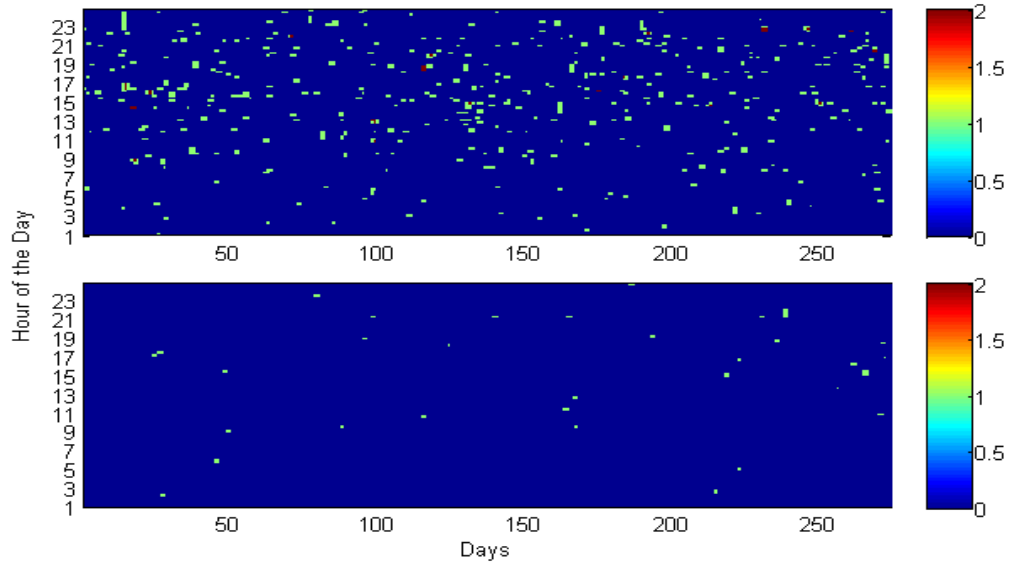


Figure 2.20. Cell analysis on the time domain for Zone 2 (a) (61,4) (b) (61,7)

Figure 2.20 shows two cells with contrasting traffic patterns. The first one is a cell which falls directly under the flight path in Zone 2, while the second figure is away from MDW. Figure 2.21 is comparatively emptier in the time domain, because of the absence of busy airports in that zone.

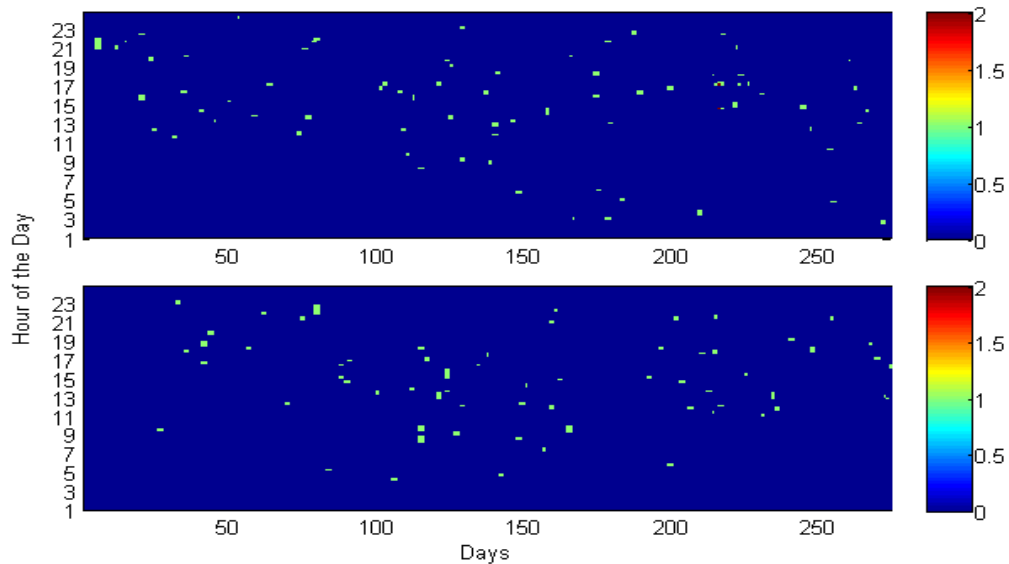


Figure 2.21. Cell analysis on the time domain for Zone 3 (a) (12,16) (b) (14,15)

Again in Figure 2.22 we show two contrasting cells. The first cell seems to have traffic from ORD, PWK and 06C airports. While the second cell is more into the suburbs with very less occupancy of flights.

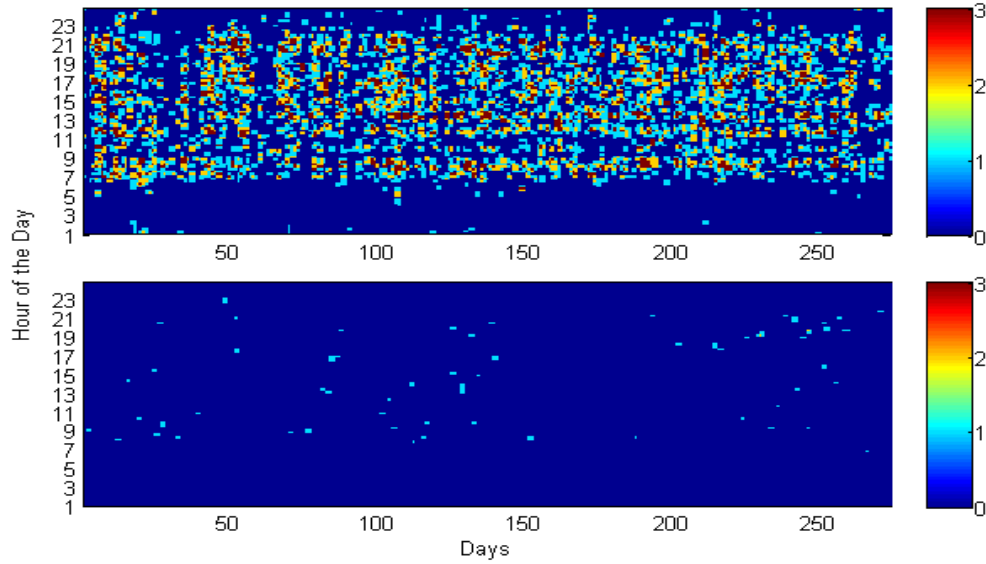


Figure 2.22. Cell analysis on the time domain for Zone 4 (a) (31,38) (b) (59,35)

## 2.6 Likelihood of Occupancy

To quantify this analysis into concrete values that can be used to decide if a cell is a likely candidate for sharing (or not); we take advantage of Empirical Likelihood analysis. For more on Empirical Likelihood refer to Appendix A.

In the time analysis we see that there are busy hour patterns on a daily basis, however we can also analyze the time domain as day of the week. This takes into consideration how the weekend and the weekday flight patterns vary with hour of the day. To analyze the likelihood for a cell we find the Probability Distribution Function (PDF) for a given X and Y coordinate of the cell, for a given day of a week and for a given hour of the day. Figure 2.23 shows the distribution of cell number

$(63,23)^2$ . This cell is in the Chicago downtown area and later in Chapter 4 we will see that it also has the highest demand for LTE. We observe that there is a high probability density at late evening for occupancy of flights in this cell compared to early mornings. Moreover, this cell has a very high density on Saturday and Tuesday. We explained the PDFs for the other cells from each zone in Appendix B

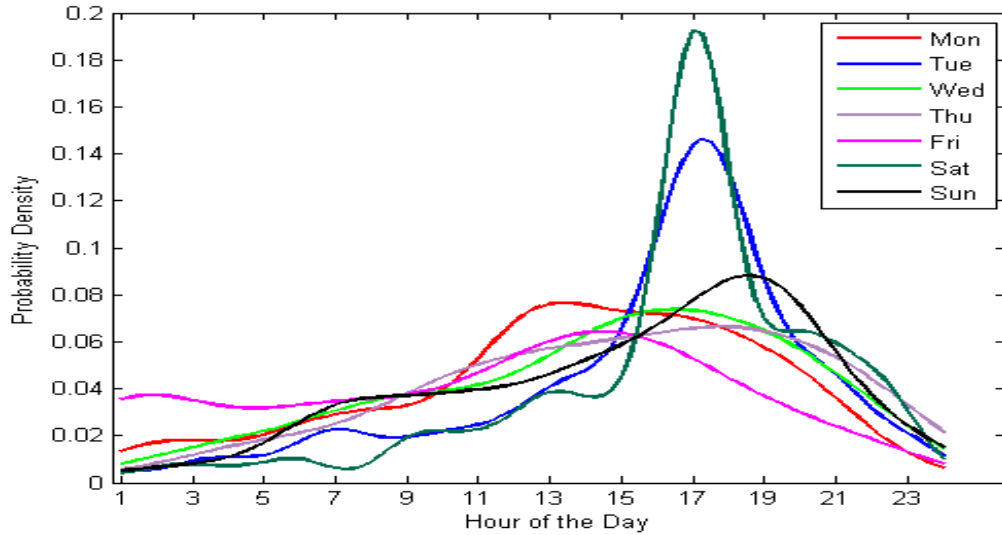


Figure 2.23. Flight occupancy PDF plot for Cell  $(63,23)$  in Zone 1

To find the probability for flight occupancy at a cell for a particular time we need to find the Cumulative Distribution Function (CDF) for the respective PDFs. Figure 2.24 shows the CDF for the cell  $(63,23)$ . The CDFs for all the cells are in Appendix B.

---

<sup>2</sup>The cells are numbered based on the x and y coordinate values as shown in Figure 2.9

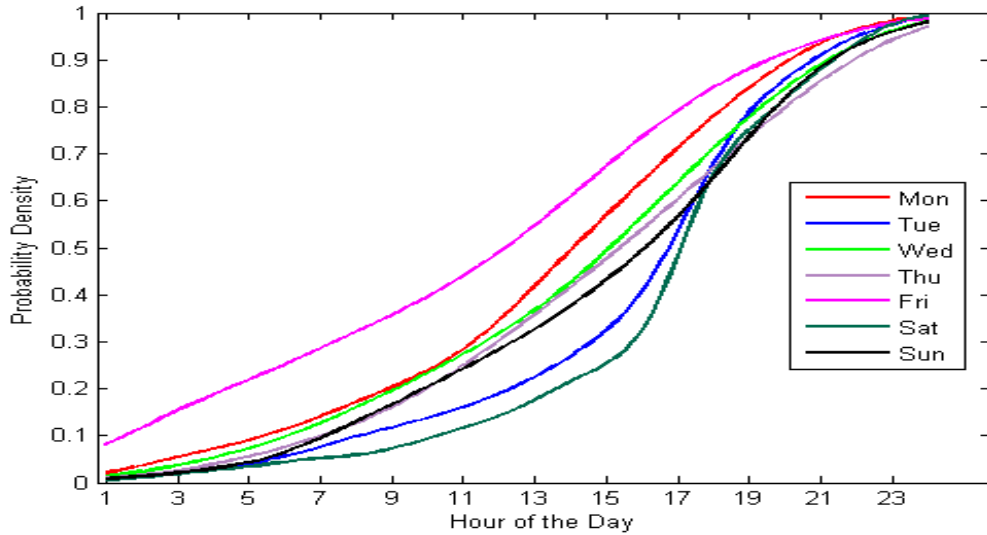


Figure 2.24. Flight occupancy CDF plot for Cell (63,23) in Zone 1

## 2.7 Discussion

Flights do change their paths in case of bad weather (snow, wind, rain) and traffic congestion. We can monitor a particular flight using the ADS-B data and show how often the flight changed its path. Aircraft tilts in various axes when they take turns, so we need to consider the pitch, roll and yaw axis to calculate the effective interference. Moreover, we need to question if the ADS-B data is completely reliable or not, since as explained earlier in US not all commercial aircraft have this system installed. To circumvent this issue MLAT data can be used to detect the aircraft. With NextGen's effort of implementing the ADS-B system will help in easily tracking aircraft.

In this chapter we introduced the area and its airspace we considered in this work. We then divided the area into zones based on the periodic traffic routes and airport classes. We showed how the traffic varied in space and time for these zones. From which some zones emerged out to be easier for sharing in both the domains.

However, when we went one step further and analyzed cells from each zone we saw that even in the busiest zones there are ample opportunities for sharing. The PDF for the cells provide us with a deep insight into the likelihood of occupancy of flights for a given location, day of week and time of day. However, having a high likelihood does not mean that there will always be harmful interference to either the PU or the SU (as it depends on the Euclidean distance and Path Loss). Similarly having less likelihood does not confirm that interference will not be caused to either PU and SU. Hence, we need to find the likelihood of a given cell for a given time interfering with an aircraft and vice versa. This requires a coexistence study between radar and LTE, which is explained in Chapter 3.

## CHAPTER 3

### CO-EXISTENCE STUDY

In this chapter we present a general co-existence analysis to see if there is feasibility for sharing the 200 MHz radio altimeter spectrum with LTE. A preliminary study of coexistence was done in [40]. An altimeter system consists of between 1 and 3 radar altimeters on a single aircraft; and the LTE system includes Base-Stations (BSs) and User Equipment (UEs). This chapter focuses on two cases; (1) the impact of interference from LTE system on radar altimeters, let us name it LTR (LTE to Radar) and (2) the impact of interference from radar altimeters on LTE system, let us name it RTL (Radar to LTE). For all the simulations in this chapter we consider snapshots of the aircraft, BSs and UEs while computing the results. We revisit the RTL and LTR scenarios with the time perspective in the next Chapter.

Before we discuss these two cases, we need to review the Altimeter System and the LTE System in general.

### **3.1 Altimeter System Model**

The sole purpose of the radar is to provide the aircraft with accurate Above the Ground Level (AGL) altitude measurements. The radio altimeters are designed to operate for the entire life of the aircraft which can exceed 30 years. This results in a wide range of equipment age and performance issues.

Typically the radio altimeters have different specifications depending on the manufacturer [33], we have chosen one of the manufacturer whose parameters will bring out the worst case harmful threshold value. Some of the important radio altimeters parameters used in this chapter are listed in Table 3.1.

One of the striking specifications of the radar altimeter is that it can measure from a range of  $6m$  to  $2500m$  (i.e.,  $20ft$  to  $8200ft$ ); this highlights that the radars are

useful and effective only during landing and taking-off at/from the airports. Once it has reached the cruising altitude, which is usually above the 2500m mark the radar is no longer effective, after which the aircraft depends on the Pressure Altimeters and a Global Positioning System (GPS) (or augmented GPS for this purpose) for the altitude measurement. Other than landing and taking off it is also useful for Terrain avoidance and Ground Proximity Warning Systems for instance when flying over tall mountains.

The radar altimeter considered herein employs continuous wave linearly swept frequency modulation [33][35][36][37] and hence is known as a Frequency Modulation Continuous Wave Altimeters (FMCW). Figure 3.1 is a conceptual block diagram of the radar. The transmitted waveform is linearly swept over a frequency range  $\Delta f = 100MHz$ . The instantaneous frequency as a function of time of the swept waveform is illustrated in Figure 3.2. The sweep rate is denoted by  $f_m = 100Hz$ . This waveform is used as interference in the LTE link simulations described later.

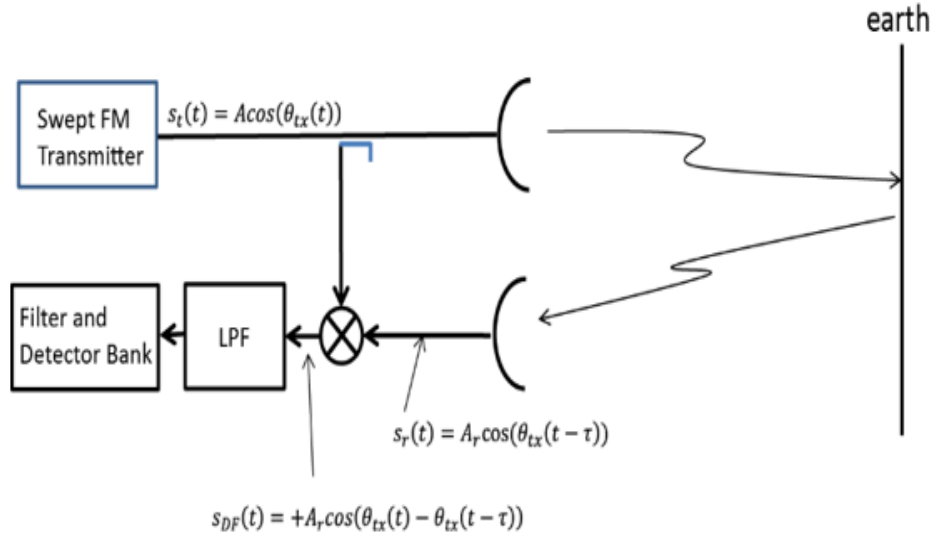


Figure 3.1. Conceptual illustration of FMCW Altimeter

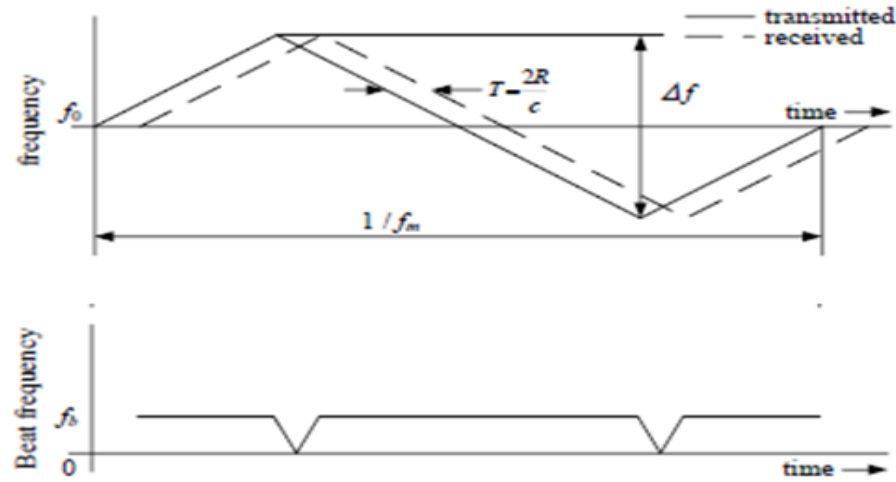


Figure 3.2. Altimeter Transmit and Receive Frequencies as Function of Time

The basic FMCW radio altimeter consists of a homodyne system that samples a fraction of the currently transmitted waveform and supplies it as a reference to the receiver mixer. The FMCW waveform is reflected from the earth and received exactly  $T = \frac{2R}{c}$  seconds after it was transmitted, where  $R$  is the distance from the earth surface and  $c$  is speed of light. Since the frequency of the waveform is continuously changing, the difference frequency between the transmitted and received waveforms is directly proportional to the aircraft altitude. The demodulated difference frequency is illustrated in the lower portion of Figure 3.2. Except for short periods where the sweep is reversing directions, the demodulated difference frequency is constant and may be estimated using, for example, an FFT processor.

The aircraft altitude is a function of the difference between the instantaneous transmitted frequency  $f_2$  and the instantaneous received frequency  $f_1$ . Specifically, the estimated altitude is  $H_o$  calculated from:

$$H_0 = \frac{c * \Delta t}{2} = \frac{c * (f_2 - f_1)}{2 * (\frac{df}{dt})} \quad (3.1)$$

**3.1.1 Altimeter Antenna Pattern.** Radar altimeters use a flat antenna which is fitted on the belly of the aircraft, generally 1 or maximum of 3 radars on large commercial and military aircraft. The antenna is meant to be pointed at the Earth's surface, however due to the possible range of pitch and roll angles performed by the aircraft the radar signals can cover a larger portion of the Earth's surface. Hence, the radar generally has a coverage between 35 and 60 degrees to the 3 dB point (half power) of the antenna pattern. The antenna pattern is essentially cone shaped and is linearly, horizontally polarized.

The altimeter antennas, due to their location on an aircraft, do not have the benefit of being shielded or screened from many of the possible interference sources on the Earth's surface. Instead it can virtually see all possible radiation sources as they escape buildings and via direct transmission from devices operating outside of any structure. The antenna pattern is assumed be conical with the gain of the  $i^{th}$  altimeter toward an LTE antenna  $j$  given by  $G_{ij}^A$  as shown in Equation 3.2 [34].

$$G_{ij}^A = -\frac{12}{\phi_{3dB}^2} \phi_{ij}^2 + G_{(A,0)} \quad (3.2)$$

where  $\phi_{3dB}$  is the 3dB beamwidth of the altimeter antenna,  $\phi_{ij}$  is the direction of the  $j^{th}$  LTE antenna with relative to the  $i^{th}$  altimeter bore site and  $G_{(A,0)}$  is the maximum gain of the altimeter antenna. The interference scenario is illustrated in Figure 3.3

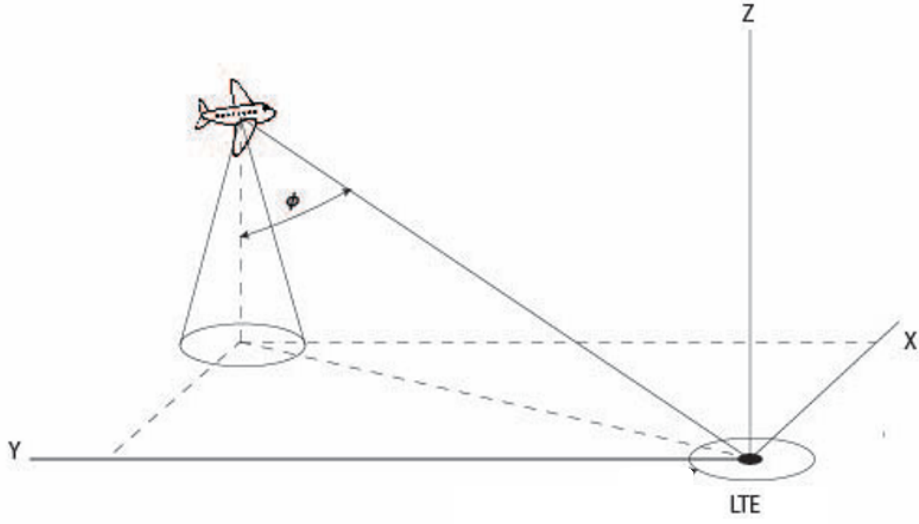


Figure 3.3. Altimeter to LTE Interference Scenario

Table 3.1. Altimeter Model Parameters

Parameter	Setting
$P_A^j$	1W
$G_{(A,0)}$	13dB <sub>i</sub>
Beam-width	60 degrees
Antenna Type	Directional (Conical)
No of Radars per Flight	1 or 3
$S_A$	-120dB <sub>m</sub>
$N_F$	6dB
$I_{T,RF}$	-56dB <sub>m</sub>
$Ht_{MAX}$	2500
$B_{IF}$	0.025MHz
$B_s$	133MHz

### 3.2 LTE System

The LTE system which is the universal standard for 4G is quite complex technology, however in this section we introduce the basics of LTE radio network

planning which are required for understanding the coexistence study.

Major carriers in USA, for example AT&T and Verizon have adopted a version of LTE based on frequency division duplex (FDD), however there are some companies like China Mobile who have LTE based on time division duplex (TDD). Our analysis is based on the FDD variant of LTE. Hence, the 200 MHz spectrum would need to be divided into paired spectrum with sufficient frequency separation to allow simultaneous transmission and reception.

The LTE system uses a range of system bandwidth 1.4,3,5,10,15 and 20 MHz. LTE uses Orthogonal Frequency Division Multiple Access (OFDMA) for the Down-link (DL) and Single-Carrier Orthogonal Frequency Division Multiple Access(SC-OFDMA) for power efficiency for the Up-link (UL). It allows multiple users to schedule transmission on the sub-carriers which are best for them at that time. To overcome the multipath fading problem in UMTS, LTE uses OFDM for downlink thereby transmitting the data over many narrow band carriers instead of spreading the signal over the complete bandwidth. Each sub-carrier is 15 KHz apart.

Resource blocks are defined as the minimum allocation unit in the downlink and uplink shared channels for carrying signaling and traffic. The number of resource blocks at any given time determines the modulation and the bit-rate. On the time-frequency grid a resource block is composed of 12 sub-carriers (i.e., 180KHz) and 7 OFDM symbols (i.e., 0.5ms) [4]. The resource blocks are distributed to the users based on the scheduling mechanisms in the frequency and time dimensions.

The BS is responsible for transmitting and receiving the data to and from the UEs. The geographical area covered by the cellular antenna is called a *cell*. A traditional cell looks like a hexagon, with the omni-directional antenna at the center and the antenna coverage would be the hexagon coverage. However, with

directional antennas the definition of antenna coverage changes. with the cell usually divided into sectors, Tri-Sector (2G-3G) or Six-Sector(4G) [44]. These sectors are made by changing the horizontal beam-width, with the main lobe of the antenna within the beam-width as shown in Figure 3.4 [52]. Moreover, with beamforming, adaptive array and active antenna, the antenna coverage can change shape and fit the capacity and coverage required by the users in that area. The cell coverage is governed by two factors range and interference. The coverage area for a range limited cell is calculated by the path loss and receiver sensitivity, while for an interference limited cell it is calculated by the interference from the adjacent cells operating at the same frequency [42]. To increase the profitability the telecom operators aim at satisfying the maximum number of users with the given resource, which demands a larger coverage. To increase the coverage the large cells are divided into smaller cells. The telecom operators make use of smaller cells to serve more users per square km. Again due to excessive signal attenuation in urban areas a single macro BS is not able to cater to all the users under it, hence pico/femto BS and relay stations are used under the umbrella of the macro cell. This results in a richer user experience and in-building coverage. Moreover, the transmission power, antenna direction and antenna vertical tilts become a key player to maximize the coverage.

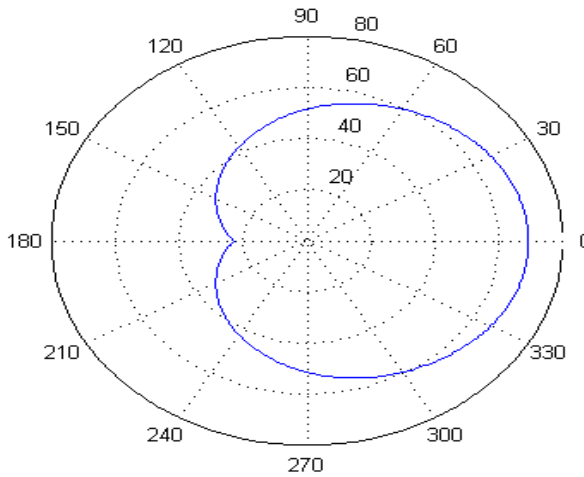


Figure 3.4. LTE BS Azimuth Antenna Pattern

The recent hand held devices (UEs) typically contain planar inverted F antennas (PIFA), which are directional antennas. However, the highly mobile nature of the users using these devices gives an impression that these are omnidirectional antennas.

The maximum transmit power of a BS is represented as  $P_B$ , and it varies by the cell size. In this thesis we mainly consider small cells. The maximum transmit power of a UE is represented as  $P_U^i$ , the maximum transmit power is  $23dBm$  and minimum is  $-40dBm$  [41]. In a real LTE network, an UE transmit power varies from  $P_U^{max}$  and  $P_U^{min}$  depending on its position and data transmission within its serving cell. However, the full power is not utilized and a portion is left for the control channel. Moreover, the BSs and UEs in the present technology tend use power control which involves sensing received power and transmitting a bare minimum power.

**3.2.1 Path Loss Model.** Path loss is an important component in analyzing the link budget for the LTE system. Path loss can occur due to many effects such as

free space loss, reflection, refraction, diffraction, scattering and absorption. Path loss is also frequency dependent and is influenced by the environment (i.e., urban, rural, vegetation) and weather (rain and humidity). For any kind of wireless signal the signal attenuates with distance (i.e. the signal energy disperses). As the distance from the transmitter increases the energy of the signal decreases per each unit of surface area. If we consider an idle case where there is no form of attenuation or impairments; the signal will attenuate over distance since the signal is spread over an ever larger area. This form of attenuation is called free space loss.

Most of the transmitters are located in urban areas where there are many tall buildings which results in no direct line-of-sight (LOS) between the transmitter and receiver. Objects in urban area cause multiple reflections and diffraction, which makes the electromagnetic waves travel along different paths of varying length. This causes multipath fading. Moreover, choice of frequency is also important, as some frequencies are absorbed by environmental elements (e.g. water and oxygen) impacting their ability to travel long distances and some cannot efficiently penetrate through various kinds of obstacles. These different scenarios decreases the signal strength at the receiver and hence effects the data rate. Hence, we need effective path loss models which can predict the mean signal strength for a given TX-RX separation and given environment.

In this thesis we propose to deploy this band for LTE in small cells. The reason being that the central frequency is high which makes it suitable for small coverage areas and the attenuation from the walls and building will likely result in less aggregated power at the altimeter radar. We consider two models the Free-Space Path Loss (FSPL) model and Log-distance Path Loss (LPL) Model. However, more work can be done to build a specific measurement based path loss model for this band, which is beyond the scope of this thesis.

In FSPL the assumption is that there is a clear LOS between the TX-RX. The free space path loss for a TX-RX is given by Equation 3.3.

$$PL(dB)_{FSPL} = \frac{\lambda^2}{4\pi d_{ij}} \quad (3.3)$$

where  $\lambda$  is the wavelength at a selected frequency and  $d_{ij}$  is the Euclidean distance between a TX  $j$  and RX  $i$ .

Many researchers have shown that indoor path loss obeys the log distance path loss model [42] and follows the Equation 3.4. We will be considering LPL model for the small cells distributed inside a building.

$$PL(dB)_{LPL} = PL(d_0) + 10n \log_{10}\left(\frac{d_{ij}}{d_0}\right) + X_\sigma \quad (3.4)$$

where  $n$ <sup>3</sup> is the path loss exponent which indicates the rate at which the path loss increases with distance,  $d_0$  is the close in reference distance<sup>4</sup> and  $X_\sigma$  represents a normal random variable in dB having a standard deviation of  $\sigma dB$  which we have considered 7.0 [42]. While using this model in our simulation we consider that the BSs are inside buildings.

Even number of floors and partitions in the same floor can be considered while modeling for a specific building which is termed as Floor Attenuation Factor (FAF) and Partition Attenuation Factor (PAF) as shown in [42]. However, this is specific for an environment and frequency. Computing the FAF and PAF values in an extended value will help in better estimation of the coverage area of the small cell.

<sup>3</sup>The value depends on the surrounding and building type which we have considered as 2.1

<sup>4</sup>AS the equation does not hold for  $d=0$ , therefore a close in distance is chosen which should lie in the far-field region of the transmitting antenna

Using either of the path loss models in Equation 3.3 or 3.4 will help in computing the received power at a RX  $i$  through Equation 3.5.

$$P_r^{ij} = P_t^j * G_t^j * G_r^i * PL(dB)_{FSPL/LPL} \quad (3.5)$$

where,  $P_t^j$  is the transmit power of a TX  $j$ ,  $G_t^j$  is the gain at the transmitter,  $G_r^i$  is the gain at the receiver.

The altimeter antenna gain is given by Equation 3.2 and the UE antenna gain is considered as  $-3dB_i$  (since it is omni-directional). The BS antenna is directional with gain specified by ITU-R Recommendation F.1336-4 [52] Because of their complexity, detailed formulas are not presented here. The reference is available on the internet. The gain  $G_{BS}^{ij}$  is a function of the azimuth and elevation angles between the LTE base station  $j$  and the aircraft  $i$  and hence Equation 3.6.

$$G_{BS}^{ij} = G_{ITU}(\phi^{ij}, \theta i, j) \quad (3.6)$$

where  $\phi^{ij}$  and  $\theta i, j$  are the azimuth and elevation angle indicate that these angles are functions of the locations of the transmitter and receiver.

Some of the parameters for the BS and the UE are listed in Table 3.2 and 3.3 respectively.

**3.2.2 LTE Activity Profile in Chicagoland.** The measurements were made at the Illinois Institute of Technology (IIT), Chicago, Illinois. The IIT Tower has an unobstructed view in all directions as shown in Figure 3.5. A detailed explanation of the site, measurement setup and data collection is listed in [13]. Several spectrum occupancy measurements were performed in Chicago and proposals for long-term

studies in multiple locations have been made from the spectrum observatory in these papers [14] [15] [45]

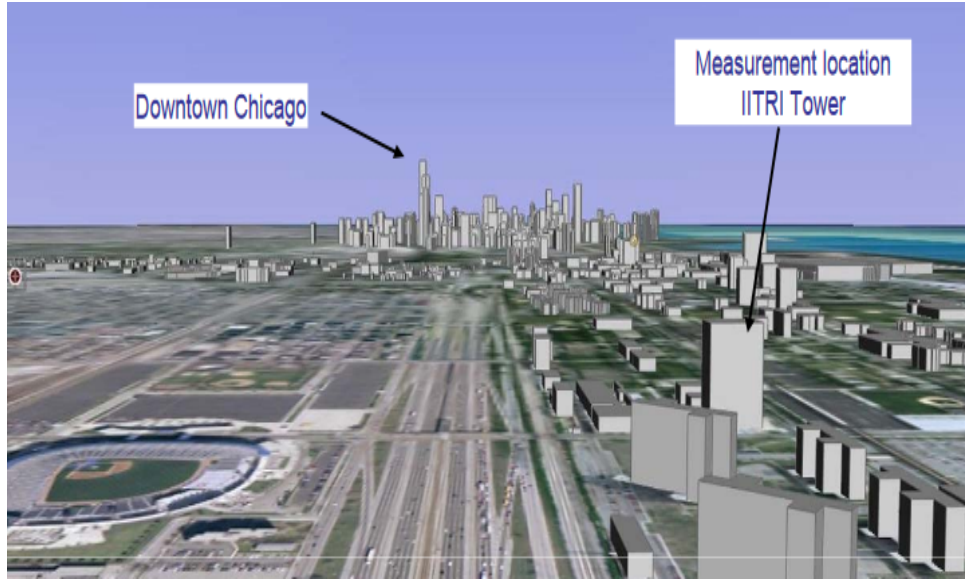


Figure 3.5. The IIT Tower has direct line-of-sight to downtown Chicago and is the tallest building in the vicinity

As explained in the earlier section that the BSs and UEs alter their transmit power based on the environment and the demand. To measure this kind of variation a huge amount of data is required which requires time and infrastructure. Even though if one is able to circumvent these constraints the environment is still very complicated and everything cannot be measured accurately. Hence, we have to make simplified assumptions to estimate the LTE activity. We will analyze the spectrum activity of the existing LTE band which will give us insight to the BS and UE usage pattern. Figure 3.6 represents 2 years of spectrum data for the LTE down-link band  $746 - 756 MHz$ , which is owned by Verizon in Chicagoland. We observe that activity is less in the early morning, and steadily increases throughout the day. From the waterfall chart we see that even at night time the power levels are high and it only goes as low as  $-70 dBm$ . This is because of the BSs' Control Channels, which are active all the time. We do see that there is a significant difference of  $10 dB$  between night and

day time, which can be considered while calculating the likelihood of interference.

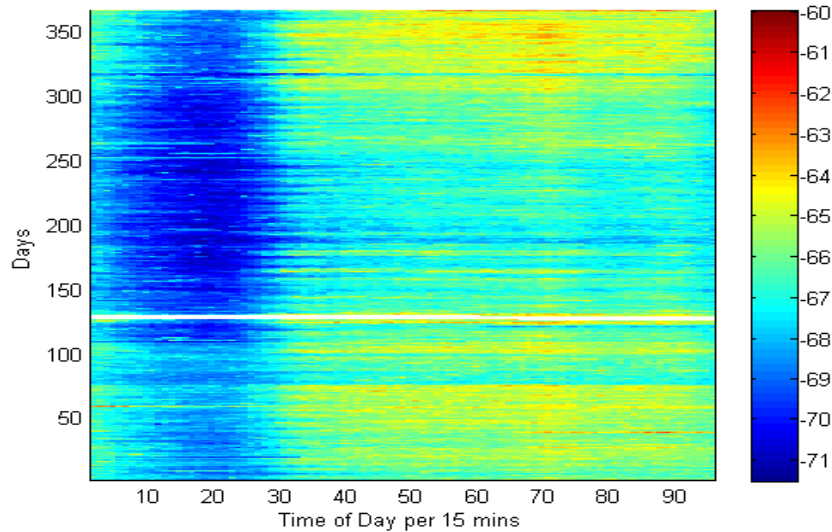


Figure 3.6. Waterfall for 746-756 MHz

To give this a realistic touch we need to generate a LTE Profile for the Chicagoland area which we can use to find the likelihood of interference. We assume a similar LTE Profile for the  $4200 - 4400\text{MHz}$  band as shown in Figure 3.7 in an attempt to predict a realistic the deployment of this band in future. We extract the variation observed in the LTE Profile of  $746 - 756\text{MHz}$  band to help us in Chapter 4 to vary the BS transmit power, the UE transmit power and the number of active users for a given location, a given day of week and a given time of day.

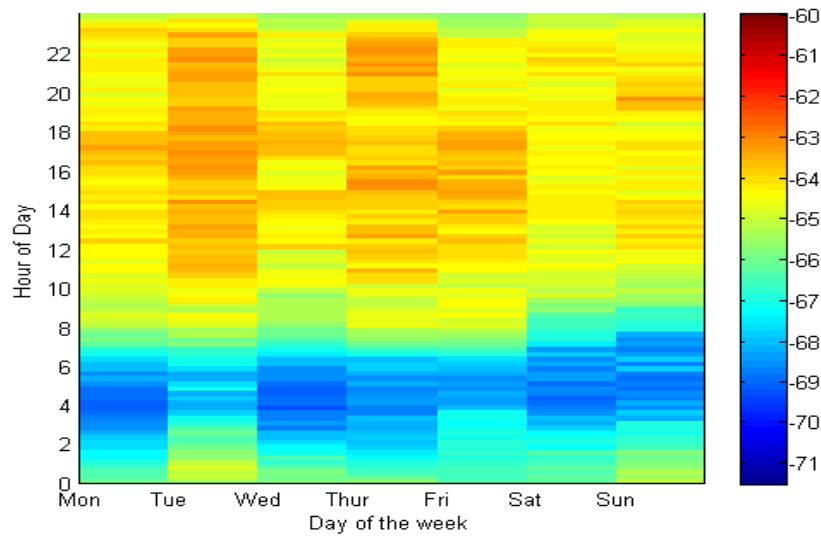


Figure 3.7. LTE Profile for 746-756 MHz

Table 3.2. LTE Model Parameters for BS

Parameter	Setting
$P_B^{max}$	23dBm
$G_{(B,0)}$	13dBi
$S_B$	-105dBm
Bandwidth	10MHz
Antenna Type	Directional (2x2 MIMO)
Azimuthal $-3dB$ Beam-width	60degrees
Vertical $-3dB$ Beam-width	2.7degrees
Height of BS	10m

Table 3.3. LTE Model Parameters for UE

Parameter	Setting
$P_U^{max}$	$23dBm$
$P_U^{min}$	$-40dBm$
$G_{(U,0)}$	$-3dBi$
$S_U$	$-117dBm$
Bandwidth	$10MHz$
Antenna Type	Omnidirectional
Height of UE	$1.5m$

### 3.3 LTE to Radar (LTR) Study

The most critical case of the coexistence study is the interference from the LTE Transmitters (BSs and UEs) to the Radar Altimeters, since this interference could have life threatening consequences. Before we move into simulating these scenarios we need to understand the protection criterion for the altimeter. This protection criterion analysis will provide us with a threshold value which we can use to check for any harmful interference in our simulations.

**3.3.1 Altimeter Protection Criteria.** Harmful interference from LTE can cause loss of altitude accuracy while landing or taking off. Interference can occur from out-of-band and in-band sources. An interfering signal may cause unwanted emission within the IF bandwidth (see description in Section 3.3.1.2 below). Moreover interference can cause an increase in the noise floor, further resulting in a loss of receiver sensitivity. Due to the unique nature of the radar as explained in the previous section, other than interference mitigation through received power from the LTE units, we need to take into consideration some other criteria as well. The three main criterion which we need to consider for a full radar protection are outlined in the subsections below [46]:

**3.3.1.1 Receiver Front-End Overload.** In a radio receiver, the RF front-end is a term used for all the circuitry between the antenna and the first down-conversion. The front-end of the receiver is overloaded when sufficient power from a interfering signal (i.e., LTE in this case) saturates the radio altimeter causing non-linear behavior, like harmonic distortion or inter-modulation.

This potential interference does not exist when Equation 3.7 is satisfied, where  $I_{RF}$  is the total signal power at the receiver input from the LTE BSs and UEs,  $I_{T,RF}$  is the input threshold at which the receiver front-end overload occurs, the value is listed in Table 3.1.

$$I_{RF} < I_{T,RF} \quad (3.7)$$

**3.3.1.2 Receiver Desensitization.** The receiver desensitization occurs when a sufficient portion of the interfering signal falls into the Intermediate Frequency (IF) bandwidth of the radio altimeter. An IF is a frequency at which a carrier wave is shifted as an intermediate step during transmission or reception. The altimeter operates in a homodyne configuration using a linear frequency modulated signal, therefore interference in the IF filter bandwidth is time dependent.

The threshold for harmful interference is an average power level at the output of the receiver IF bandpass filter. The IF filter bandwidth is denoted by  $B_{IF}$  and the value is listed in Table 3.1. The threshold is also dependent on the total noise power at the output of the IF bandpass filter. Equation 3.8 [46] gives the total noise in dBm which is dependent on the power spectral density, IF bandwidth and the receiver noise figure denoted by  $N_F$ .

$$N = -114dBm/MHz + 10 \log_{10} B_{IF} + N_F \quad (3.8)$$

The interference power in the IF filter output is not simply the interference power at the receiver input translated to the IF, because the receiver local oscillator sweeps in frequency, the interference (assumed to have a constant frequency) sweeps through the IF bandpass filter. For each altimeter frequency sweep (assumed triangular), the signal appears in the IF filter twice, once on the positive sweep and once on the negative sweep. The resulting interference signal at the IF filter output is a pulsed signal. The interference duty cycle  $R_s$  of this pulse is given by Equation 3.9 [46]

$$R_s = \frac{2B_{IF}}{B_s} \quad (3.9)$$

The amount of interference signal power at the IF filter output is proportional to the interference duty cycle and hence is given by Equation 3.10 [46].

$$I_{IF} = I_{RF} + 10 \log_{10} R_s \quad (3.10)$$

The maximum acceptable interference at the IF filter output can be considered to be 6dB less than the Noise  $N$  as shown in Equation 3.11 [47].

$$I_{IF} < N - 6 \quad (3.11)$$

Using Equations 3.8 through 3.11 we get the threshold for the interfering signal  $I_{RF}$ .

$$I_{RF} < -114dBm/MHz + N_F + 10 \log_{10} \frac{B_{IF}}{R_s} - 6 \quad (3.12)$$

**3.3.1.3 False Altitude Report.** A FMCW based radio altimeter works by mixing the received waveform with the local transmit oscillator. The difference frequency is proportional to the altitude. The performance of the spectrum analysis (and thus the estimate of the difference frequency and subsequently the altitude) is a function of signal-to-interference ratio at the input to the detector. The interference will be quantified using its power spectral density per 100 Hz at the input to the detector.

It appears that the requirement for accurate frequency analysis is that the interference power spectral density  $PSD_I$  using a 100 Hz bandwidth at the input to the detector be less than -143 dBm/100 Hz [46]. The Equation for calculating this power spectral density is

$$PSD_I = I_{IF} + 10 \log_{10} \frac{100}{B_{IF}} \quad (3.13)$$

The value  $I_{IF}$  is the total interference power at the IF filter output accounting for the local oscillator sweeping as described for the desensitization analysis in Equation 3.10. This calculation presumes that the interference power is uniformly spread in frequency across the IF bandwidth. The factor of 100 is due to wanting the PSD units to be dBm/100Hz.

Harmful interference is experienced whenever Equation 3.14 is satisfied.

$$PSD_I > -143dBm/100Hz \quad (3.14)$$

Combining Equation 3.10, 3.13 and 3.14 we get the threshold for the interfering signal  $I_{RF}$ .

$$I_{RF} < -143dBm/100Hz - 10\log(200/B_s) \quad (3.15)$$

**3.3.1.4 Final Threshold Value.** Radio altimeters are operational at all phases of the flight, hence for complete protection all possible interference scenarios should be considered. Hence, Equations 3.7, 3.12 and 3.15 should be satisfied to prevent any harmful interference. By putting in the values from the Table 3.1 we can find an overall threshold value for the interfering signal  $I_{RF}$ .

$$I_{RF} < \min(-56dBm, -95.77, -72.73) = -95.77dBm \quad (3.16)$$

This value is specific for an altimeter specification, however we found this altimeter type to be the worst case. Hence, to avoid any harmful interference the total aggregated interference from the LTE access points should be less than  $-95.77dBm$ . From this point we state this value as  $R_{TH}$ .

**3.3.2 BS Effect on Radar.** Let us consider a BS setup which transmits at a maximum transmit power along with the other BS parameters mentioned in Table 3.2. The simulation is snapshot based so we make the aircraft static at different locations to see the variation in received power as a function of X,Y,Z coordinates. We consider the aircraft to be static at (X,Y) coordinates of (100,100),(750,750),(1400,1400) and name them Case A,B and C respectively. Let us assume an aircraft for each coordinate pair varies its altitude between 50ft till 60,000ft (15.24m till 18288m) as shown in the Figure 3.8. Let the antenna azimuth pattern for the BS [43] be as shown in Figure 3.4, and all BSs are pointed toward the right hand side of the figure (in the direction of the aircraft). In Figure 3.8 the gray shade shows the BS at coordinate (750,750) footprint using the main lobe of the antenna considering the link budget

discussed in Section 3.2.1. This is a general scenario which we will be using throughout the chapter unless mentioned otherwise.

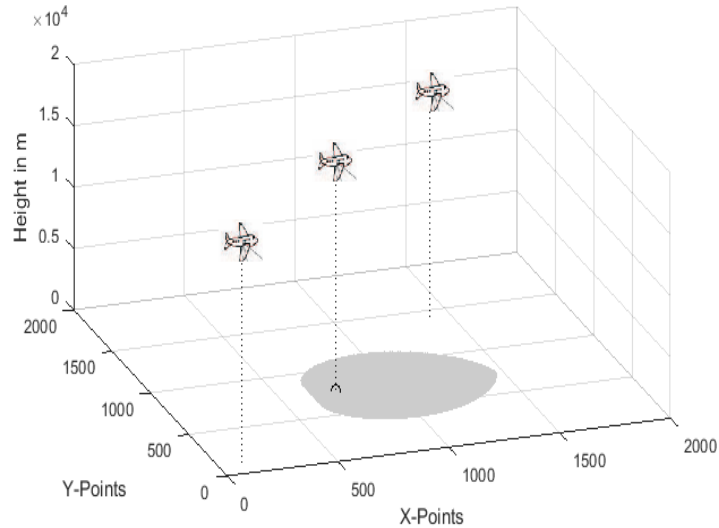


Figure 3.8. Scenario with Aircraft positions and BS antenna direction

In Figure 3.9 we considered the same scenario but now with 5 BSs and with the same antenna direction as the one shown in Figure 3.8. Hence, making Case A to be always behind and Case C to be always in front of the main lobe of the BS antenna. While Case B is just over the antenna.

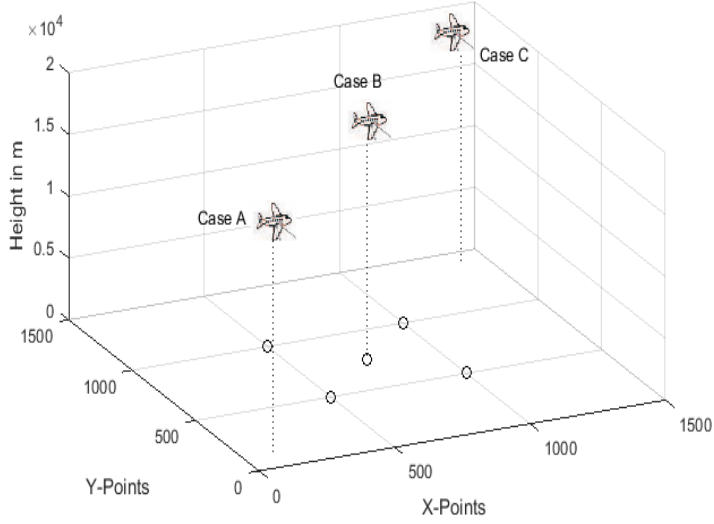


Figure 3.9. Same scenario as Figure 3.8 with 5 BSs

We consider both FSPL and LPL models and calculate the received power at the different aircraft snapshots; the results are shown in Figure 3.10. We compare the results for the 3 cases with the altimeter threshold  $R_{TH}$ . The plots from both the models have a similar curve, however there is a significant drop off nearly  $20dB$  when the BS were used inside a building (i.e. in LPL). Moreover, in all the three cases in FSPL it takes a larger altitude for the aircraft to go below the  $R_{TH}$  as compared to LPL. In both the models, Case A has a steeper slope compared to Case B and C, due to its positional advantage of sitting behind the directional view of the antenna. Case B and C curves are very close to each other, however the received power at Case C is larger than Case B. In Case B the aircraft is just over the antenna, however the antenna has a vertical tilt which faces downwards and provides a vertical loss. In Case C the aircraft is more exposed to the main lobe compared to Case B, which results in a higher received power compared to Case C. It almost takes an aircraft altitude of  $5000m$  for the curve to converge to the  $R_{TH}$  when the aircraft is in the direction on the main lobe of the BSs. This specific scenario is not such an issue but

that taking into account the details of relative locations of the aircraft with the main lobe of the BSs is an issue.

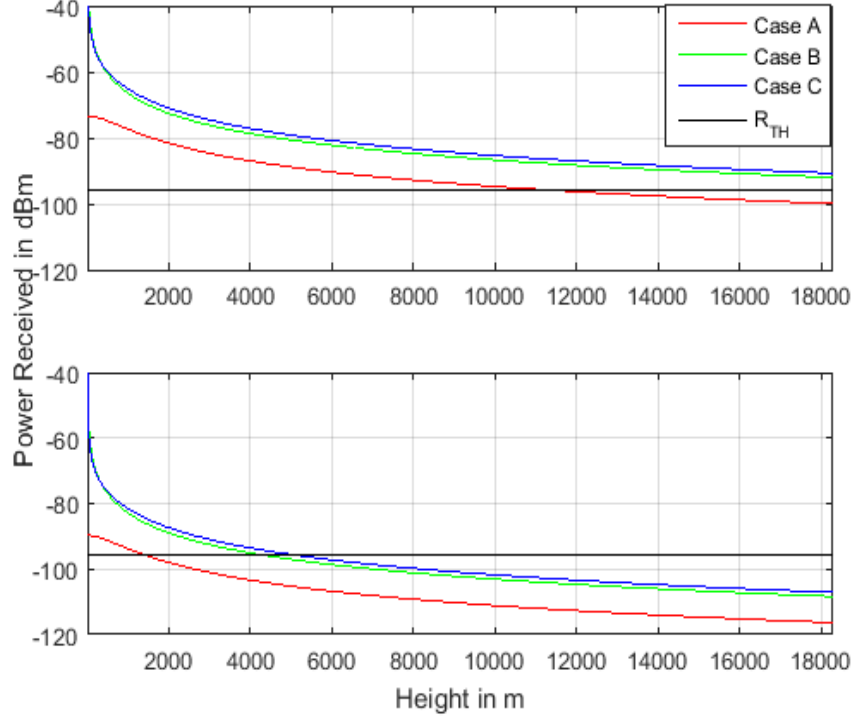


Figure 3.10. Received Power at the radio altimeter from the BSs through (a) FSPL and (b) LPL

**3.3.3 UE Effect on Radar.** Let us consider the same scenario of the flights as shown in Figure 3.8. Let us consider a public gathering, e.g. a sports Game Night, with 10,000 people at the point (75,750). Since, the UEs are omni-directional in nature the gain would be the same for both Case A and C. So, we modify the location of Case C to (1000,1000) to get a better understanding.

Figure 3.11 shows that after the 2000m altitude mark all three cases converge to the same received power. This shows that for the UE's omnidirectionality is not so sensitive to the position of the aircraft on the X-Y plane.

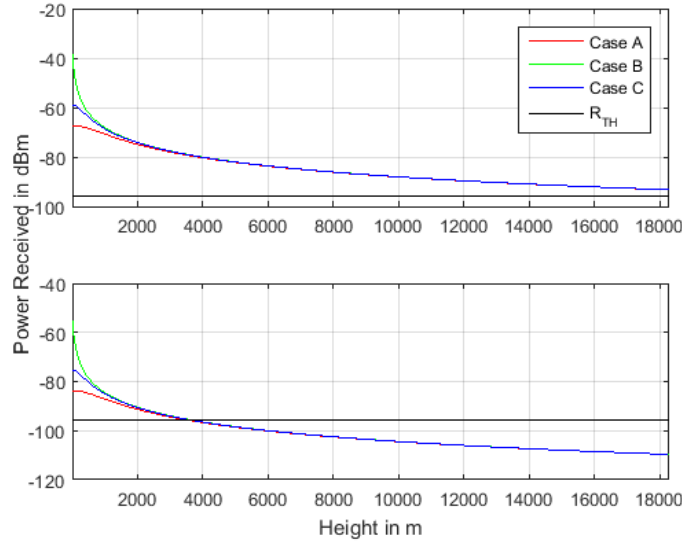


Figure 3.11. Received Power at the radio altimeter from 10,000 UEs through (a) FSPL and (b) LPL

In Figure 3.12 we see a magnified version. By using the result from Equation 3.16 it is clear that with FSPL (outdoor scenario) the aircraft will need to be at nearly 20,000m before harmless sharing is possible. However, with the users deployed indoors it will take an aircraft elevation of a little more than 2000m to enable sharing.

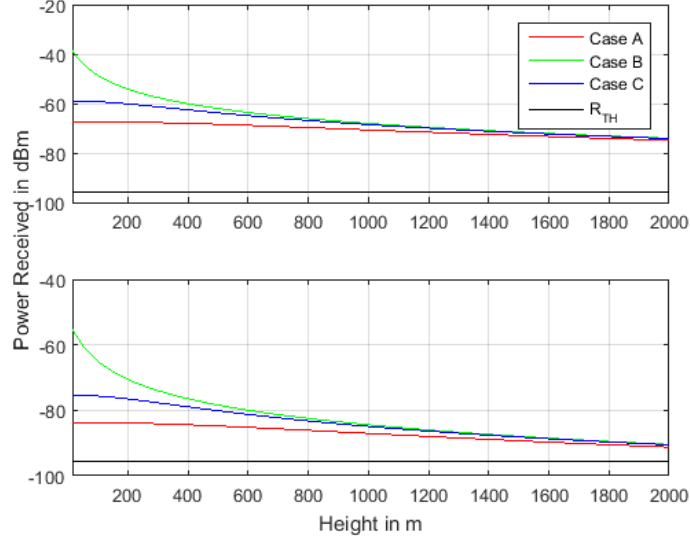


Figure 3.12. Magnified version of Figure 3.11

In Figure 3.13 we consider a UE density of 100. In this case the received power is significantly decreased for both FSPL and LPL cases. Now, with the user count decreased 10 times a aircraft need be at less than 2000 m for harmless sharing in an outdoor scenario.

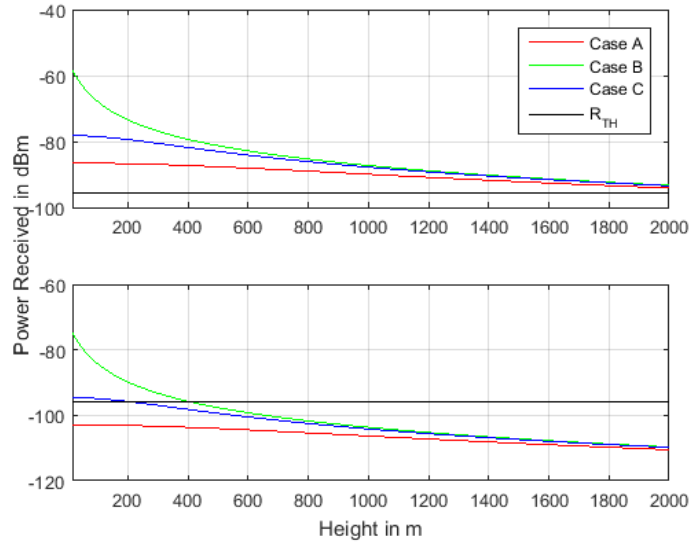


Figure 3.13. Received Power at the radio altimeter from 100 UEs through (a) FSPL and (b) LPL

**3.3.4 Combined Effect of BS and UE on Radar.** In a real life scenario both the BS and UE will be present, moreover the down-link and up-link would be allocated in the same  $4.2 - 4.4\text{GHz}$  band with a guard band between them. Hence, there could be an aggregated interference from the BSs and UEs in the band. Figure 3.14 shows an aggregated received power at the aircraft for the scenario as earlier (i.e., 5 BS and 100 UEs).

In this scenario the BS Effect dominates the UE Effect

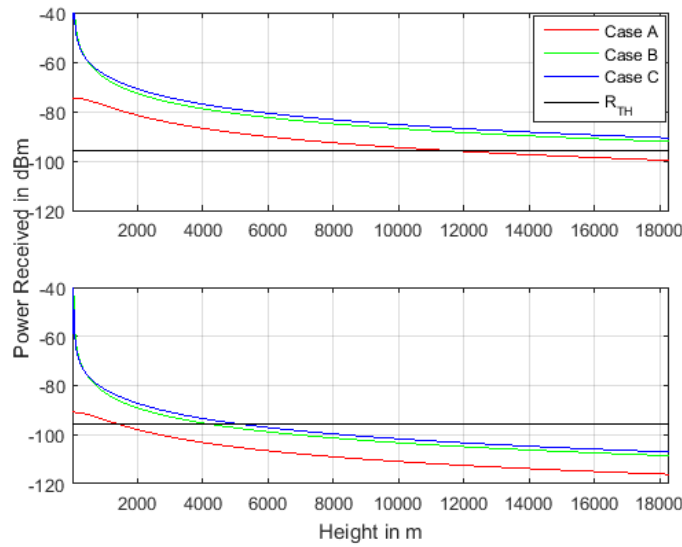


Figure 3.14. Received Power at the radio altimeter from 5 BSs and 100 UEs through (a) FSPL and (b) LPL

### 3.4 Radar to LTE (RTL) Study

This scenario is important for the Users to meet their high data demand. LTE has a lot of methods through which packet losses can be dealt with. However, the Interference from the Radar should not be so strong that the throughput drops below a threshold. In this section, we will show the received power from the aircraft to the BS and UE as a function of the Altitude and the Speed of the aircraft.

**3.4.1 LTE Downlink Analysis.** Consider altimeter interference to the down-

link (i.e. the link from the LTE access point to the user handset) in a small-cell LTE deployment. The Mathworks LTE Toolbox [48] has been used to estimate LTE performance. The LTE Toolbox enables rapid and accurate standards-compliant modeling of LTE systems in a *MATLAB<sup>TM</sup>* environment. Among other capabilities, the Toolbox facilitates end-to-end performance simulations for the LTE test configurations defined in the 3GPP standard TS 36.101 [49]. Further, the LTE Toolbox facilitates modeling of the standards-defined multipath channel environments [50] as well as LTE MIMO transmit and receive technology. It is noted that the LTE Toolbox is highly complex and allows the setting of a vast array of LTE parameters and configurations. Definitions and details for these parameters are given in the documentation for the Toolbox.

LTE downlink bit error rate and throughput were estimated in an environment that included interference from the radar altimeter. Specifically, the LTE Physical Downlink Shared Channel (PDSCH) [51] and associated control, synchronization, and channel estimation sub-channels were modeled. The altimeter interference was modeled using the built-in MATLAB swept frequency generator. Several LTE MIMO configurations were modeled; the results for a single transmit antenna/dual receive antenna systems are considered herein. The LTE Toolbox includes all of the multipath channels defined in 3GPP TS 36.104 Annex B [50]. Simulation runs were made for many parameter combinations. The simulation parameters for the results presented in this paper are given in Table 3.4 .

Table 3.4. LTE Toolbox Parameters

Parameter	Setting
SNR	40dB
Number of transmit antennas	1
Number of receive antennas	2
Information Modulation	QPSK or 16QAM
PMI Delay	8ms
Maximum Doppler Frequency	70Hz
MIMO Correlation	Low
Measurement Channels <sup>5</sup>	R.2 and R.3(TM1), R.11 (TM4)
Model Type	GMEDS <sup>6</sup> (Rayleigh Fading)
Delay Profile	Extended Typical Urban Model (ETU)

Simulated throughput results for QPSK and 16QAM are presented in Figure 3.15 for interference from either 1 Radar or 3 Radars. As expected, higher modulation order (i.e.16QAM) results in higher throughput at high SINR. QPSK achieves higher throughput at low SINR. At any particular SINR the LTE adaptive modulation and coding algorithm selects the modulation scheme having the highest throughput. If we compare the 1 Radar and 3 Radar curves we see that the 3 radars contribute very significantly to the decrease in throughput for a given SIR. However, LTE has many interference mitigation mechanisms which can be used in case of 3 radars. For the mitigation scheme assumed for this analysis, the system changes the modulation scheme from 16QAM to QPSK when there is high interference. This adaptive modulation and coding scheme is modeled by the hull of the two results of Figure 3.15.

---

<sup>5</sup>Measurement channels R.2 and R.3 were used for single antenna transmission whereas R.11 was used for closed loop spatial multiplex transmission.

<sup>6</sup>Rayleigh fading modeled using the Generalized Method of Exact Doppler Spread (GMEDS)

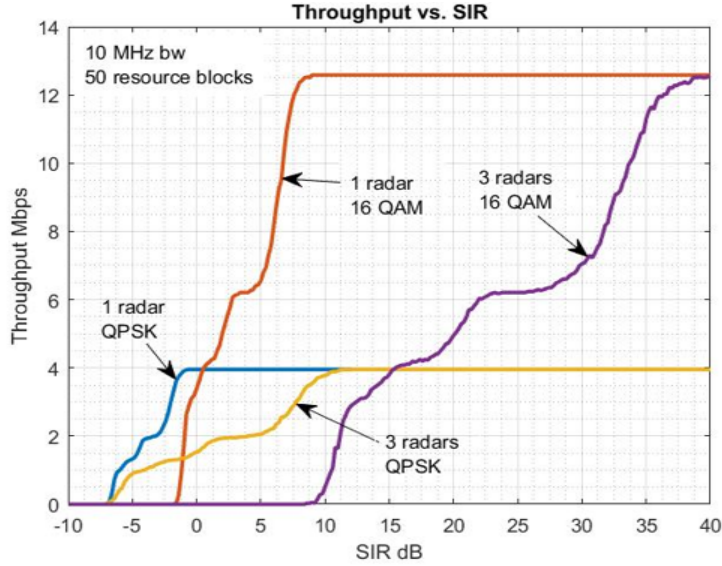


Figure 3.15. Throughput Measurement at the UE for different SINR with 1 and 3 Radars Altimeters

Let us assume a scenario as shown in Figure 3.16 with a flight path shown in blue. For an initial simple scenario, it is assumed that a single UE (marked in red) is located at four different locations along the course of the flight.

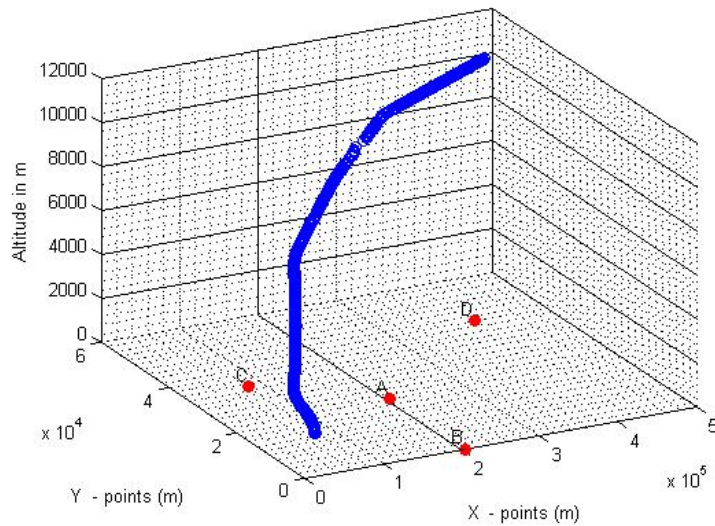


Figure 3.16. Aircraft Flight Path and LTE User Equipment Locations Scenario

Figure 3.17 illustrates the output of the system analysis showing throughput as a function of time, for 3 radar altimeters on a single flight. Observe that the throughput is at its maximum until the aircraft is approximately over the UE. The UE throughput dips significantly as the aircraft passes directly overhead and then gradually increases as the aircraft passes the UE. As shown in Figure 3.17, the throughput of Users A, B and C is highly impacted by the flight path. Although, User D is located directly below the flight path, the throughput for User D remains almost unaltered with time since the flight has gained enough altitude to avoid any significant interference from the radar altimeter to User D. Therefore, it is important to consider the latitude, longitude and altitude when evaluating the sharing potential. Preliminary analysis shows that interference is reduced significantly as an aircraft approaches the range of typical cruising altitudes indicating that the potential for sharing increases with the distance from a major airport.

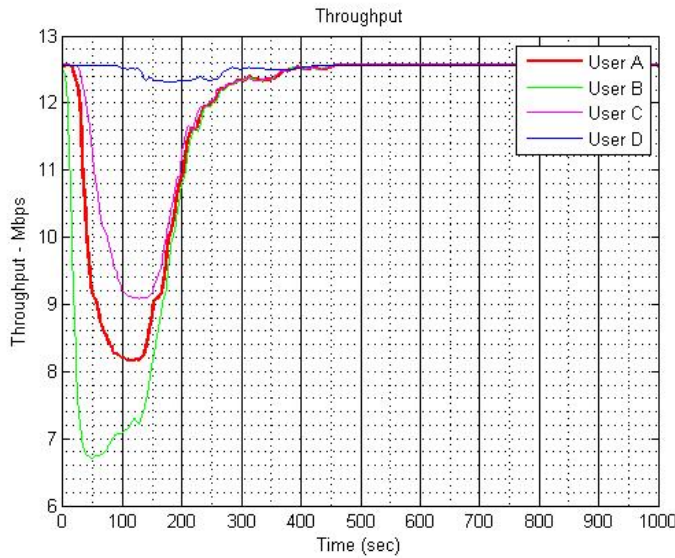


Figure 3.17. UE Throughput vs Time for 3 Radar

### 3.4.2 LTE Uplink Analysis.

A similar analysis is required at the BS receiver, however LTE has different technologies to mitigate interference and this is dependent on the telecom operator to determine what technique(s) it wants to implement. The transient nature of the aircraft causes interference at the BS for a lesser duration. Average speed of an aircraft is about 878-926 km/h, this makes the footprint of an aircraft to interfere with the LTE system only momentarily. For simplicity we consider the BS sensitivity  $S_B$  as a measure for the LTE up-link.

Let us consider a scenario with 5 BSs and the aircraft static over BS2 as shown in Figure 3.18. We vary the height of the aircraft from 50ft to 60,000ft.

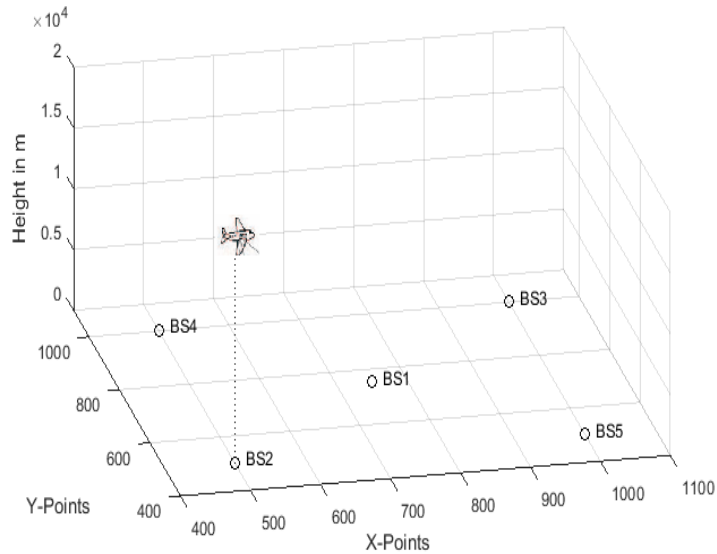


Figure 3.18. Scenario for Uplink Analysis

Figure 3.19 shows the received powers at 5 BS from an aircraft altimeter. Observe that the curves for BS1 and BS3 converge to the same point after 1000m. This is because the aircraft is slightly away from the main lobes of BS1 and BS3.

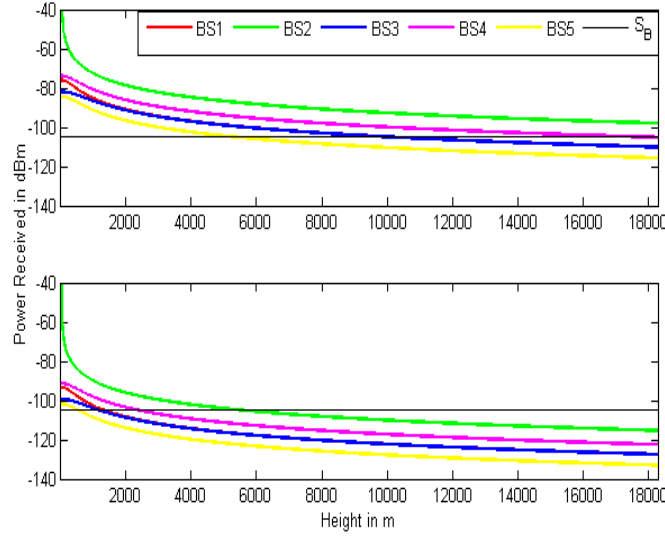


Figure 3.19. Power Received at the BS from the Radar Altimeter through (a) FSPL  
(b) LPL

### 3.5 Discussion

In this chapter we provide a deep study on the Radar and LTE systems. We talk about the protection criterion for the altimeter radar and simulate scenarios to see the effect of distance on received power at the aircraft. We introduce the LTE technology in brief, path loss models being used and other parameters we used for our scenarios. Using the LTE Toolbox we found the relationship between throughput and SIR at the down-link. We showed simulations to see the effect of radars on down-link and up-link. LTE Profile which captured the LTE activity in Chicagoland area was introduced which will be used in the next chapter.

This chapter tried to lay the technical ground for the sharing approach we will be proposing in Chapter 4. However, there are some challenges in the coexistence study which needs to be dealt with before deployment can be made. A proper propagation model (outdoor and indoor) for this band needs to be developed. In the propagation model different scenarios needs to be considered i.e. take-off vs.

landing, unique characteristics of different airports (e.g. obstacles that create unique flight patterns), terrain characteristics around the airport (e.g. over water vs. over mountains vs. over cities, etc. In this work, we discuss about small cells, however it needs to be studied if the band is also available for macro cells, for which outdoor propagation models need to be developed. Factors like housing patterns, demographic changes and urban sprawls effect the demand for LTE. Identifying this change in LTE pattern based on geographic location and time is necessary for making deployment strategies.

## CHAPTER 4

### SHARING APPROACH

As introduced earlier there are generally at least two types of stakeholder when it comes to spectrum sharing, incumbent users (or Primary Users (PUs)) and Secondary Users (SUs). There are various ways that the spectrum can be shared usually segmented into a category of zone geographically surrounding the PU (or PUs). This Chapter will discuss the various sharing approaches.

Before we can form any zones around an area Likelihood analysis for Interference for LTR and RTL is required.

#### **4.1 Interference Likelihood**

To compute the likelihood of interference for LTR and RTL interference scenarios we need to predict the characteristics of the activity of the PU and SU. The PU can be predicted using the ADS-B data discussed in Chapter 2, while the LTE Profile introduced in Section 3.7, can predict the alteration in BS power and UE activity with time. However, we need to have the demand of LTE in order to get the full picture, for example, there would clearly be more LTE demand and therefore more BSs in an urban area compared to rural area. The area we have considered is a blend of urban, sub-urban and rural area, and hence a LTE demand per cell is required.

Data was extracted from Antennasearch.com which provides the coordinates of registered antennas and towers at a given location. We can generally assume the demand for LTE as a function of the BS deployment in this area. Figure 4.1 shows a heat map for the BS distribution in the area around the City of Chicago generally known as Chicagoland.

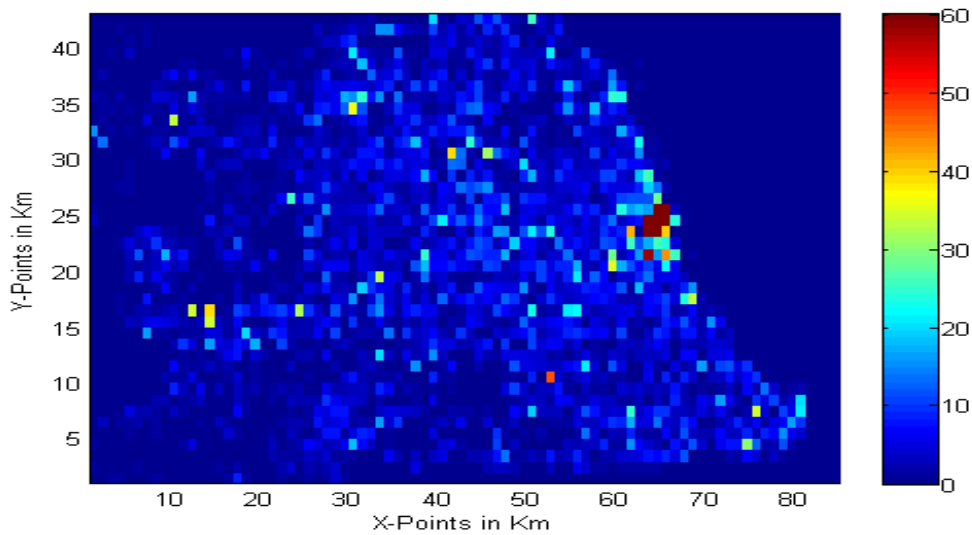


Figure 4.1. Existing Base Station Antenna Heat Map for Chicagoland

For the UE concentration it is assumed that a single antenna can cater to a maximum of 10 UEs, since we have assumed small cells in this thesis. This is a simplifying assumption which will be accurate only in the central city and not in the rural area where macrocell BSs still dominate, but for our purposes this is an acceptable simplification. We continue explaining the interference likelihood with cell (63,23) which we took as an example for occupancy likelihood in Chapter 2. This cell has roughly 136 BSs which is justifiable as it is in Downtown Chicago. The maximum users in the cell were considered 1360, and the number of active users varies with time of the day and day of the week as stated in LTE Profile.

Though not the current reality, for simplifying purposes we considered the current locations of the antennas to deploy the small cells. We considered these cells are indoor and hence considered Log-distance Path Loss Model for the simulations in this chapter.

**4.1.1 Likelihood of LTR Interference.** To find the likelihood of aggregate

interference at the radar altimeter from a cell, we need to consider the Flight Path and therefore the radar altimeter occupancy in and around the cell, LTE Activity (to calculate the BS transmit power, and UE count and transmit power, as a function of time) and the physical constraint of the radar altimeter of  $2500\text{ft}$ . The radar is mainly used for take-off and landing, and can only accurately measure the height upto  $2500\text{ft}$  above the ground. Therefor sharing can be done without harming the operation of the airplane in scenarios when an aircraft is at a height more than  $2500\text{ft}$  even if the radar altimeter is receiving interference from the LTE that is greater than the threshold value of  $-95.7\text{dBm}$ <sup>7</sup>. A buffer of  $2500\text{ft}$  is added for safety and consider the aircraft height threshold at  $5000\text{ft}$ . However, this buffer margin can be lowered after negotiations between the FAA and the Telcos when it is in the deployment stage.

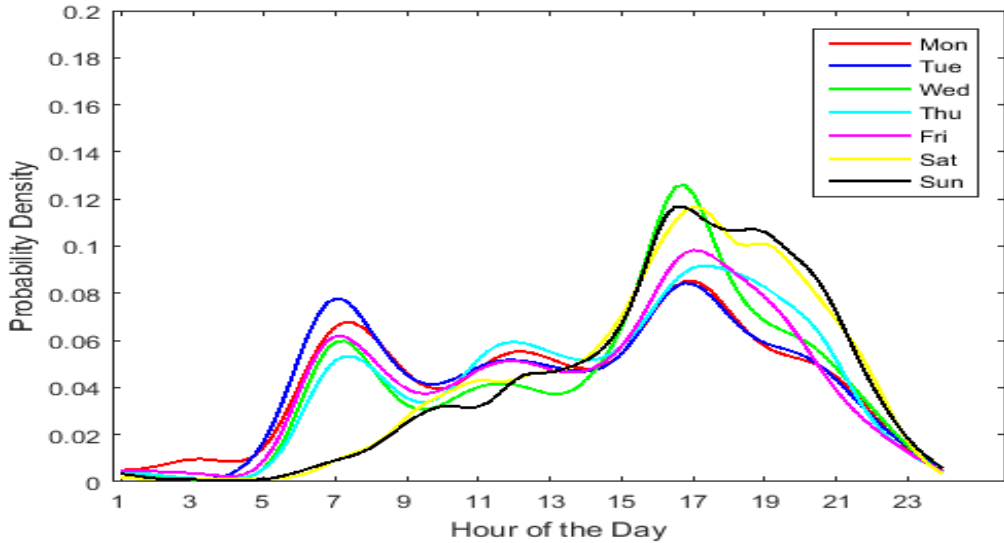


Figure 4.2. LTR Interference PDF plot for Cell (63,23) in Zone 1

Figure 4.2 shows the PDF plot for the LTR interference for a given day of the week and give time of the day. We can observe that there are two prominent spikes at *7am* and *5pm* during weekdays. While in weekends the spike is mainly from *5 – 7pm*.

---

<sup>7</sup>Refer Equation 3.16

This plot helps us to estimate time boundaries during which the likelihood of LTR interference will be less. Figure 4.3 is a CDF plot for Figure 4.2 which we will use later in this Chapter to find the exact probability of interference for a given time.

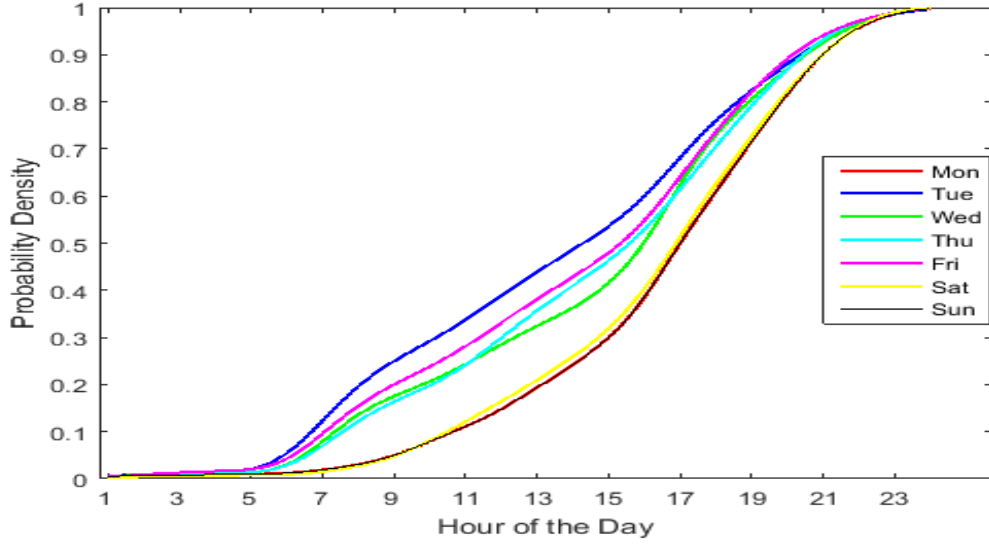


Figure 4.3. LTR Interference CDF plot for Cell (63,23) in Zone 1

For analysis on other cells as introduced in Section 2.5.5 refer to Appendix C.

**4.1.2 Likelihood of RTL UE Interference.** To assess how the UEs are affected by interference from the radar altimeters, we need to compare the fall in throughput (as shown in Section 3.4.1) when an aircraft is close enough to interfere with the UEs. The activity of UEs are varied based on the LTE Profile. We assume that the UEs have 100% throughput in the absence of the aircraft (which is not the case, since there will be path loss between the UE and the BS, and co-channel interference which is out of scope). So, the PDF in Figure 4.4 shows the likelihood of a throughput value when interference is observed at a given day of week for a particular time. In this plot we considered 5 – 6pm, because we saw in the previous section there are high chances of LTR interference at this time, and we would like to observe the worst case.

The PDF plot for 5 – 6pm tends to accumulate at particular throughput values of 2.5, 3.8, 4.0Mbps and few ranges of peaks from 5.0 to 6.0Mbps.

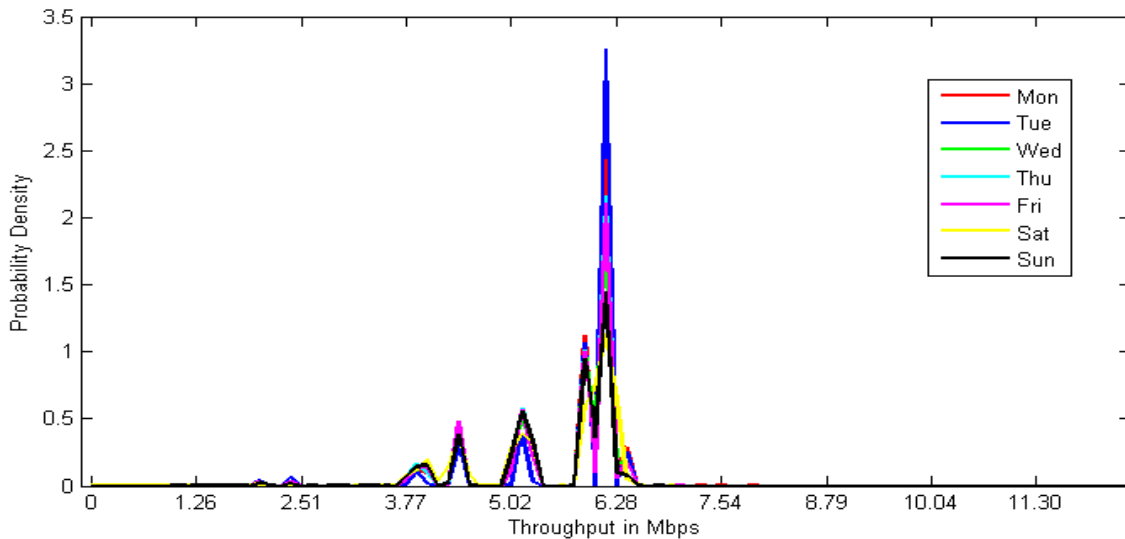


Figure 4.4. RTL UE Throughput PDF plot for Cell (63,23) in Zone 1 at 5 pm-6 pm

Figure 4.5 shows the CDF plot for Figure 4.4, which would give the probability of throughput value at 5 – 6pm for a given day of the week.

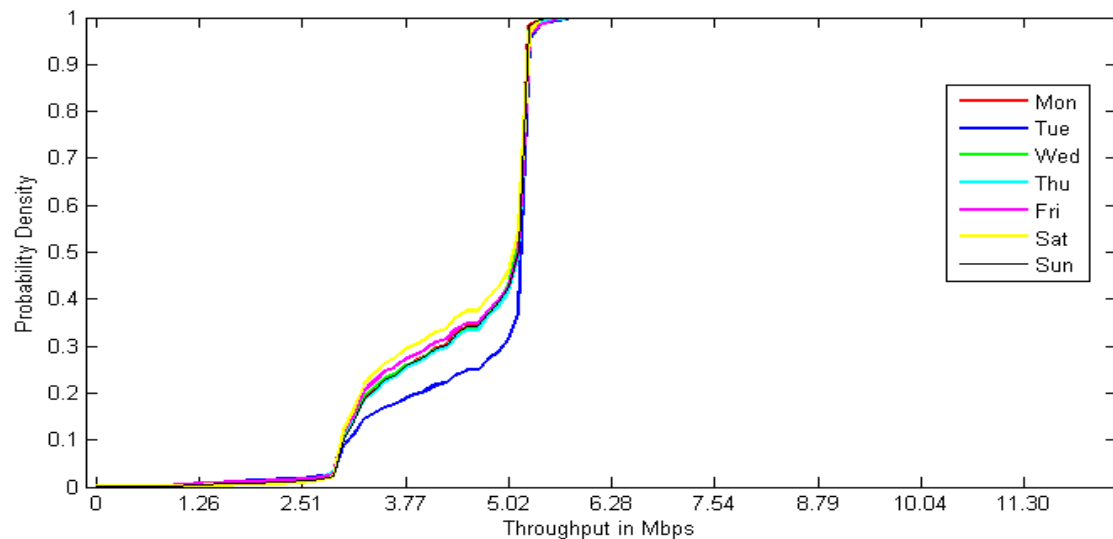


Figure 4.5. RTL UE Throughput CDF plot for Cell (63,23) in Zone 1 at 5 pm-6 pm

For analysis on other cells as introduced in Section 2.5.5 refer to Appendix D

**4.1.3 Likelihood of RTL BS Interference.** To assess how the BSs are affected when an aircraft is close to a cell we compare the sensitivity of the LTE BS (as shown in Section 3.4.2) with the received power from the radar altimeters. The PDF plot in Figure 4.6 shows similar peaks as that in Figure 4.2. There is a lot of aberration in the probability densities which might be due to the BS location, elevation and antenna direction. We considered the BS location and elevation information from the data we extracted from Antennasearch.com. The likelihood of RTL BS interference increases after 5am and descends after 9pm for every day of the week.

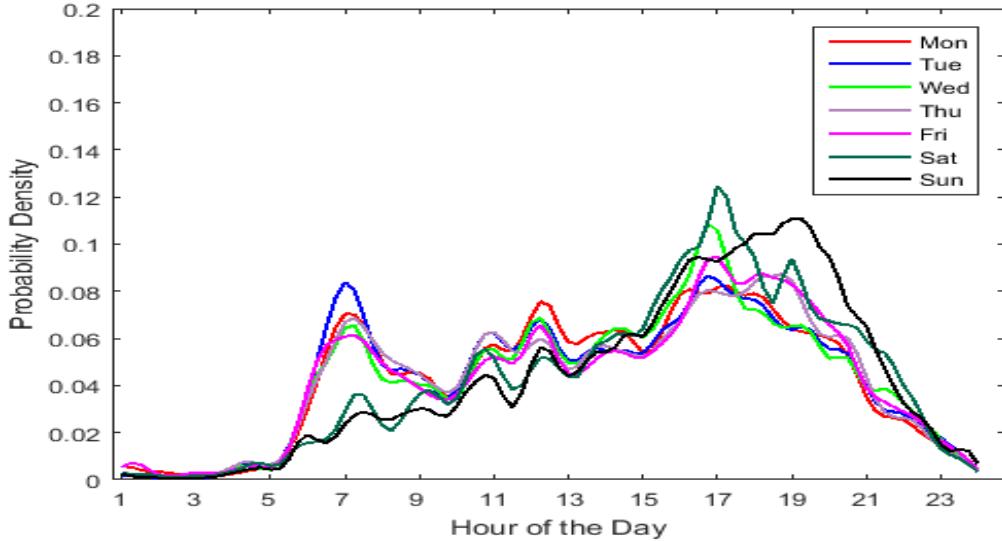


Figure 4.6. RTL BS Interference PDF plot for Cell (63,23) in Zone 1

Figure 4.7 shows the CDF plot for Figure 4.6, which would give the probability of interference at the BSs for a given time of the day and given day of the week.

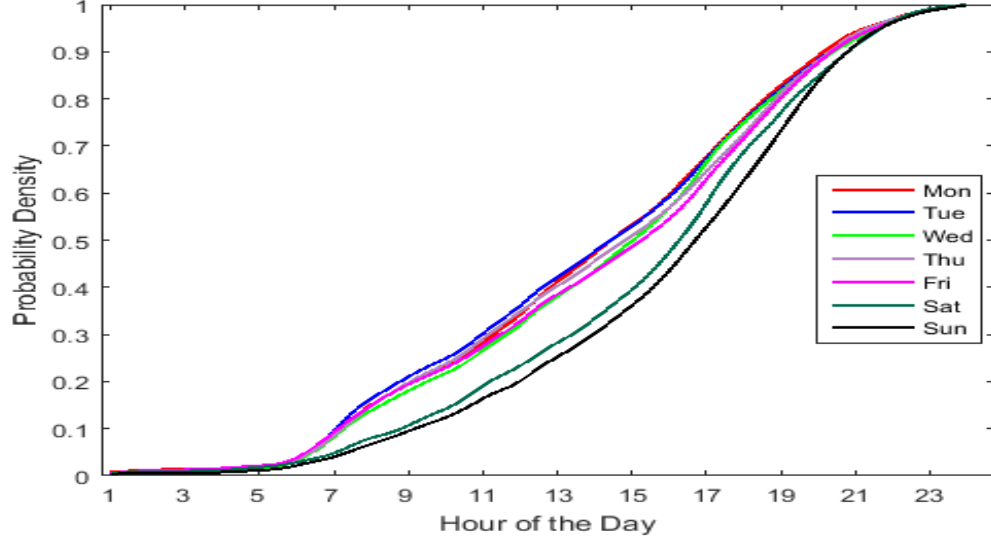


Figure 4.7. RTL BS Interference CDF plot for Cell (63,23) in Zone 1

For analysis on other cells as introduced in Section 2.5.5 refer to Appendix E

## 4.2 Exclusion and Coordination Zone Formation

To ensure interference protection a static spatial boundary is defined around each PU, the simplest approach is to require SUs to operate only outside of that boundary. SU operation within this boundary is presumed to cause harmful interference to the PU. This kind of static boundary is called an Exclusion Zone. There has been much work on defining Exclusion Zones which consists of methods such as F-curves [53] which is heavily used in TV bands.

Figure 2.4 shows an overlay of flights in a time frame of 90 days, around the Chicagoland . As we can see, the flights do have well defined paths, which they tend to repeat, i.e. highways in the air. Still from this kind of an overlay analysis we can easily strike out those places which fall under these defined paths, and form an Exclusion Zone around it.

However, every other cell in the given grid seems to have been visited by an aircraft at some time or another. Given this scenario it is difficult to form permanent static boundaries or exclusion zones in any given grid that also enable spectrum sharing. Even if we come up with some static zones which are never visited by flights or not interfered by surround cells, the spectrum demand in that area may not be sufficiently high to encourage the telecom operators to try to deploy their systems and utilize the spectrum. Moreover, the fact that a cell has been visited by an aircraft does not, in itself, cause that cell to be in an exclusion zone. Only when altimeter received interference level is above the harmful interference threshold should the cell be in an exclusion zone.

To mitigate this we propose to make these zones dynamic or form Co-ordination Zones. The coordination area is that area, so defined that any interference between the earth based station in question in the zone and terrestrial stations outside this area may be considered as negligible. The coordination contour would dynamically shrink and grow based on the aircraft position and the BS variables/parameters. In case of the aircraft the variable may be the altitude of the aircraft, where as for the BS the variables would be the transmit power, height of the antenna, vertical and horizontal angles and the environment in which it is deployed. The NTIA recently defined Coordination zones in AWS-3 bands (specifically 16751710 MHz and 17551780 MHz) for sharing it with Wireless Broadband Systems (WBSs) [54] [55]

### **4.3 Approach**

The Likelihood of Interference in Section 4.1 helps us make proper decisions on which cells are appropriate for sharing or at what times selective cells can be used. We suggest four approaches for sharing this band based on the ADS-B results and co-existence study in Chapters 2 & 3. We propose that there can be levels of restrictions on space-time for the PU and SU. We therefore propose four restriction

levels such that when deployment for this band starts. The regulatory authorities (FCC in the U.S.) might want to start with a proposal for an Exclusion Zone around the airports, then migrating to a dynamic spectrum sharing model that is able to seamlessly handoff the BS from the Radar band to the Normal LTE band when there are no airplane in the vicinity. These four proposed classes of zones are as follows:

- Level 0 (L0) - In this approach there will be a strict implementation of an Exclusion Zone. Under this Level, only cells with a interference likelihood of 0 will only be allowed to share this band. This approach is quite popular with TV and Weather Radars, since they are static. For this we would require years of data to validate that a flight has never visited a cell at an altitude where interference is possible or has not been near enough to that cell to cause interference. Moreover, we cannot predict human activity or chance, which might lead to an emergency landing or unexpected reroutes. With this transient nature of the airplane based radars and the FAA's restricted control on the Class G airspace, it is uncertain to say that there will be a cell with interference likelihood count of 0.
- Level 1 (L1) - In this level we consider an only slightly less conservative approach and try to find the cells which are unlikely or less likely to be visited by flights. We use cells which on average are visited by 10 flights per day or less as shown in Figure 2.9. We choose the value 10 for Chicagoland, as it brings out the popular flight paths and leaves lots of space on the grid for sharing. This value will need to be specific for an area, hence similar analysis as shown in Chapter 2 is required for a new area. The red cells in Figure 2.9 would be exclusion zones where the SU will not be allowed to use this band. In this level there would be a need for constant measuring of ADS-B data, since the cells which have an average of less than 10 need to have coordination between the SUs and

the PU. The flight occupancy likelihood should be used while drawing exclusion zones and providing limited access to the cells surrounding it. Even the blue cells at the boundary of the red cells need to be highly coordinated to prevent interference to the red cells, hence buffer cells needs to be maintained in case of change in flight pattern, emergency, weather conditions or other airplane impacts.

- Level 2 (L2) - In this level we consider a *Hybrid-Exclusion Zone* where the cells in the excluded zones will have an opportunity to share the band in the time domain. White spaces in the time domain should be used in this level, hence making this band available in otherwise excluded cells at certain times when it is very unlikely to cause or receive harmful interference. On the space level it will follow the exclusion zone principles and all the BS will be handed off in case of interference.
- Level 3 (L3) - This is a pure Coordination Zone implementation with complete dependence on sensing of flights with no exclusion zone. In L3 all the cells are included and coordination is done in the space-time domain. However, if selective coordination zones are to be implemented (for particular cells only) the PDFs shown earlier in this chapter can help in intelligently choosing the cells as good candidates for L3. The difference with L2 is that each BS will be dealt separately.

Table 4.1 summarizes the important aspects of the four levels of deployment strategies.

Table 4.1. Zone deployment levels

Level	Domain of Operation	Zone formation Criteria	BS handoff
L0	Space	Interference	-
L1	Space	Occupancy & Interference	All
L2	Space & Time	Interference	All
L3	Time	Interference	Subset

#### 4.4 L2 Analysis

In this level when a flight is detected that is anticipated to receive an interference greater than the threshold value, all the base stations are handed off to non-interfering frequencies for a certain time, generally known as the Backoff Time. The BSs in the cell will be provided with a Sanction Table which provides information if the BSs sanctioned to use the band for a given day of week and hour of the day. Cells in the exclusion zones check the Sanction Table and will use the band accordingly.

**4.4.1 Sanction Table.** The sanction table will help to implement the Hybrid Exclusion zones as it will take care of the timely allocation of the band to the BSs in a cell. The sanction table will be time slots which are good for sharing, and have likelihood of interference less than a threshold value; it will be calculated based on the PDF and CDF plots of a cell. The CDF in Section 4.1.1 will provide the exact probability of aircraft close enough to get interference from the BS in the cell for a given time slot. We ignore the RTL scenario as it is a business decision and is dependent on how much interference the telecom operators are willing to accept and how the link budget is calculated. In case both LTR and RTL is considered then the sanction table will be based on the conditional probability of the both the scenarios for a given time.

The sanction table will have Boolean values with a size of  $7 \times 24$  (days of week  $\times$  hours of the day) and needs to be determined before hand. Rather than sanctioning BSs on an hourly basis, they can be sanctioned every  $n$  hours, based on the busy times. As stated in the time analysis of Zone 1 in Figure 2.12, the busy times are cyclical (the red and yellow lines). We found that for Zone 1 these busy hours would last for on average  $30.6\text{min}$  and at max  $2.75\text{Hrs}$  over  $10\text{months}$  of data. Therefore, we take a conservative approach and consider sanctioning the BSs every  $3\text{hrs}$ ; this might decrease the usability but will keep the handoffs under control. Now the sanction table size becomes  $7 \times 8$  and we need to populate it using the probability of interference to an aircraft  $Pr_{LTR}^{w,t}$  for every  $3\text{hrs}$  using Equation 4.1. The  $Pr_{LTR}^{w,t}$  calculates the probability for a given day of week  $w$  and time of day  $t$  through the CDF values.

$$Pr_{LTR}^{w,t} = CDF(w, 3t) - CDF(w, 3(t-1)) \quad (4.1)$$

To convert these probability values to Boolean values we need a threshold probability to compare with. One can handcraft the sanction table, however it would require the government and the telco companies to make that decision. The least conservative way to populate the sanction table is to make all the values in the table *True*, which means the BSs are allowed to access the spectrum all the time. This case is more like an L3 level deployment with the exception in how the BSs will be handed off, collectively or separately. Hence, we check if  $Pr_{LTR}^{w,t} < 1$  and the threshold value here is 1.

To find a threshold value we compare it with the mean probability of every  $3\text{hrs}$  from the CDF plot in Figure 4.3. Let us consider the distribution of probability for  $3pm$  to  $6pm$  for all seven days of week, as shown in Figure 4.8. The mean for the

distribution  $\mu = 0.2603$  with a standard deviation of  $\sigma = 0.0389$ .

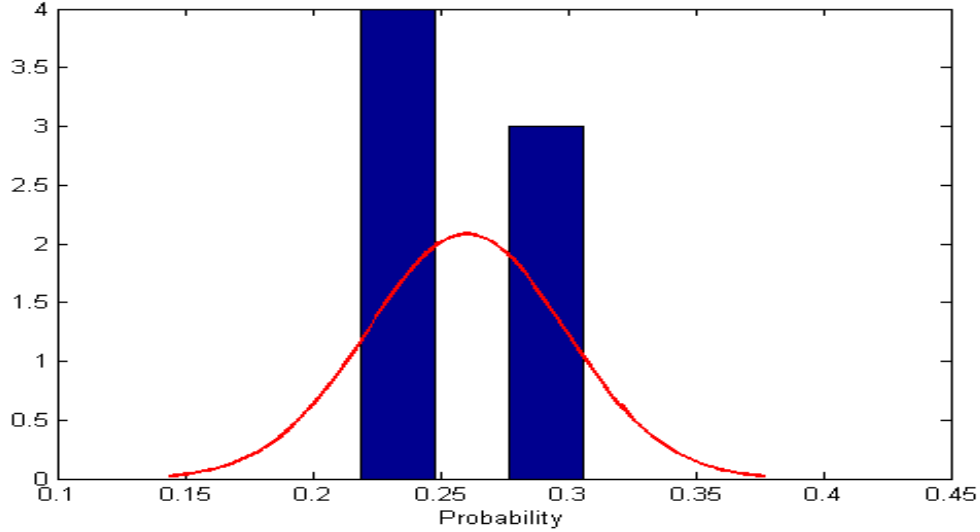


Figure 4.8. Probability distribution for 3pm to 6pm for all days of week

Similarly, distributions can be drawn for all 8 time slots of the day to find the threshold value, hence populating the sanction table with the respective truth values. We consider four sub cases in L2 to populate the Sanction table in the order of least to most conservative approach. We name this sub cases at L2.1,L2.2,L2.3 and L2.4, which are as follows:

- $Pr_{LTR}^{w,t} < \mu - \sigma$
- $Pr_{LTR}^{w,t} < \mu$
- $Pr_{LTR}^{w,t} < \mu + \sigma$
- $Pr_{LTR}^{w,t} < 1$

**4.4.2 L2 Algorithm.** A pseudo code for Level L2 for a particular cell is shown in Algorithm 1. The algorithm takes the sanction table as an input *Sanction*, which

will return a Boolean value for a given day of week  $w$  and time of day  $t$ . It also takes a back-off time  $T_{BackOff}$  in sec, which is the time for which the BSs will not use this band. The back-off time needs to be selected very efficiently and should be a function of occupancy of flights in and around the cell. We assumed the back-off time to be  $5min$ , which we calculated based on the mean time of interference to a flight in Zone 1.  $S_B$  is the set of BS in the cell and  $LTEProfile$  is the LTE activity as introduced in Section 3.2.2. According to the LTE Profile it is clear that the major traffic is in the day time, which is when this band should be used to increase the overall capacity.

Let  $T$  be a timer which checks if the back-off time has crossed; we initialize it as 0. The variables  $t$  and  $w$  has the current time and day of the week. In line 6 it is checked if for a given  $(w, t)$  the cell is allowed to share the band or not and that the backoff time has passed; then we activate all the BSs in the cell by populating the set  $ActiveBS$  with  $S_B$ . The set  $S_A$  is populated from the ADS-B sensors, which will have the co-ordinates of the aircraft for time  $t$ . Then the transmit power of BS  $P_B$ , transmit power of UE  $P_U$  and the active number of users  $N_U$  is calculated based on the  $LTEProfile_{w,t}$  for a  $(w, t)$  pair. Line 13 checks if the aggregated interference is less than  $-95.7dBm$  and the aircraft height  $S_A(z)$  is greater than  $3000ft$ <sup>8</sup>. If both conditions are met then  $ActiveBS$  set is emptied and the back-off timer  $T$  is started.

---

<sup>8</sup>Refer Section 4.1.1

---

**Algorithm 1:** Algorithm for L2

---

**Input:** *Sanction*,  $T_{BackOff}$ ,  $S_B$ , *LTEProfile***Output:** *ActiveBS*

```

1 begin
2   Set  $T = 0$ 
3   while True do
4     Set  $t = CurrentTime()$ 
5     Set  $w = DayOfWeek()$ 
6     if  $Sanction_{w,t} == True$  and  $t > T$  then
7       Set  $ActiveBS = S_B$  ; // Allow BSs to use the spectrum
8       Set  $S_A = ReadADSBDData()$ 
9       Set  $P_B = P_B^{max} * LTEProfile_{w,t}$ 
10      Set  $P_U = P_U^{max} * LTEProfile_{w,t}$ 
11      Set  $N_U = 10 * |S_B| * LTEProfile_{w,t}$ 
12       $I = ComputeInterference(S_A, ActiveBS, P_B, N_U, P_U)$ 
13      if  $I_j > -95.7$  and  $S_A(j, z) >= 5000ft \forall j \in S_A$  then
14         $ActiveBS = \phi$  ; // Handoff all BSs from this spectrum
15         $T = T + T_{BackOff}$ 

```

---

Algorithm 2 is for the function *ComputeInterference()* which calculates the aggregated interference at the aircraft from the BSs and UEs, as introduced in Chapter 3.

---

**Algorithm 2:** Algorithm for ComputeInterference

---

```

1 ComputeInterference( $S_A, ActiveBS, P_B, N_U, P_U$ )
2 begin
3   for  $i \in ActiveBS$  do
4      $I = \sum_{n=1}^{|ActiveBS|} P_B * G_B^n * G_A^j * PL(dB)_{LPL} \forall j \in S_A$ 
      ;
      // For  $G_A$  &  $G_B$  refer Equation 3.2 & 3.6
5   Set  $S_U = Random(N_U)$ 
6   for  $i \in S_U$  do
7      $I = I + \sum_{n=1}^{N_U} P_U * G_U^n * G_A^j * PL(dB)_{LPL} \forall j \in S_A$ 
      ;
      // For  $G_U$  refer Table 3.3
8   return I;

```

---

**4.4.3 L2 Simulation Results.** We show the spectrum usage for each of the cases discussed in Section 4.4.1. As we move from the most to least conservative approach we see that the spectrum usage increase and at the same time the handoffs also increases, shown in Figures 4.9 - 4.12. The blue lines in the waterfall graphs signify that either the sanction table had a *False* value for a given  $(w, t)$  pair or the BSs had to handoff since it did not obey the interference threshold values. The red lines signify that all the BSs are using the spectrum in that cell for that time.

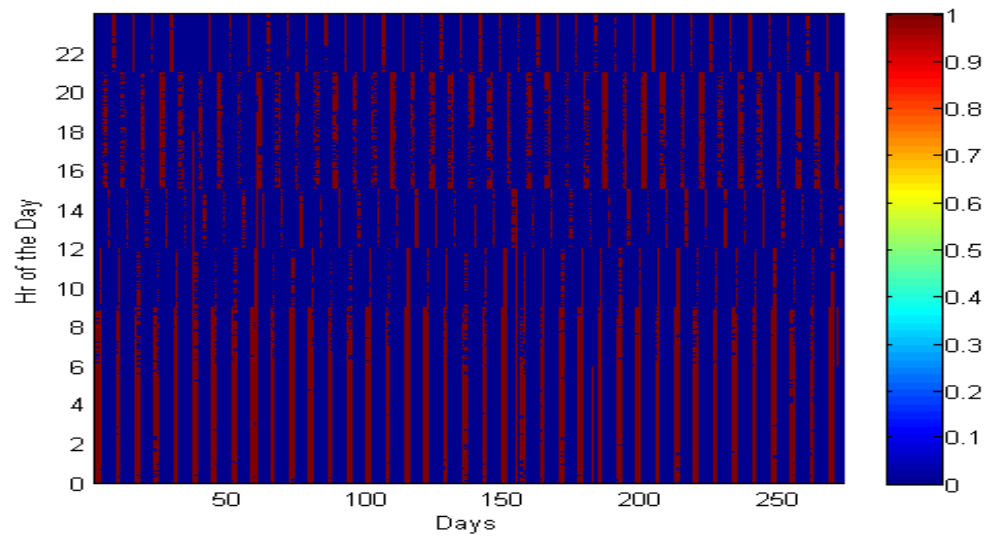


Figure 4.9. L2 implementation for Cell (63,23) in Zone 1 with  $Pr_{LTR}^{w,t} < \mu - \sigma$

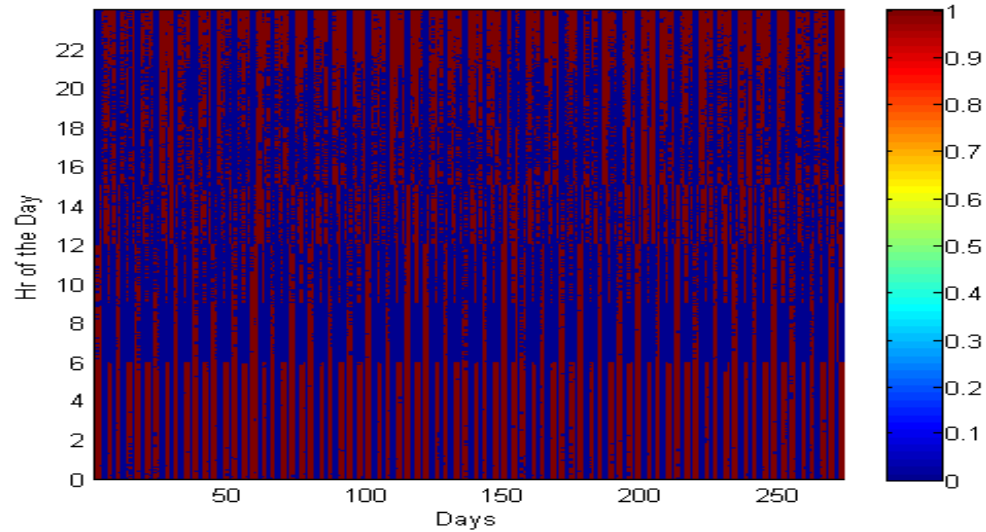


Figure 4.10. L2 implementation for Cell (63,23) in Zone 1 with  $Pr_{LTR}^{w,t} < \mu$

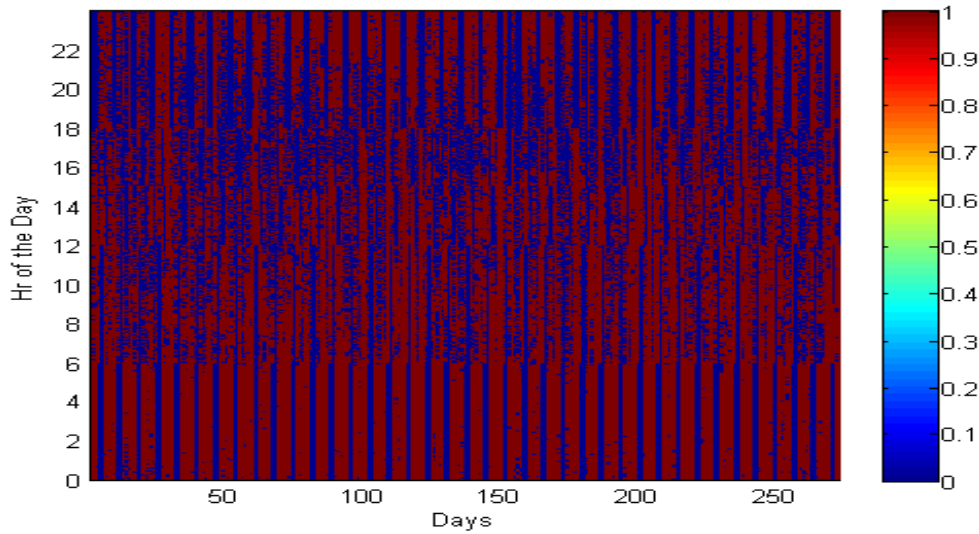


Figure 4.11. L2 implementation for Cell (63,23) in Zone 1 with  $Pr_{LTR}^{w,t} < \mu + \sigma$

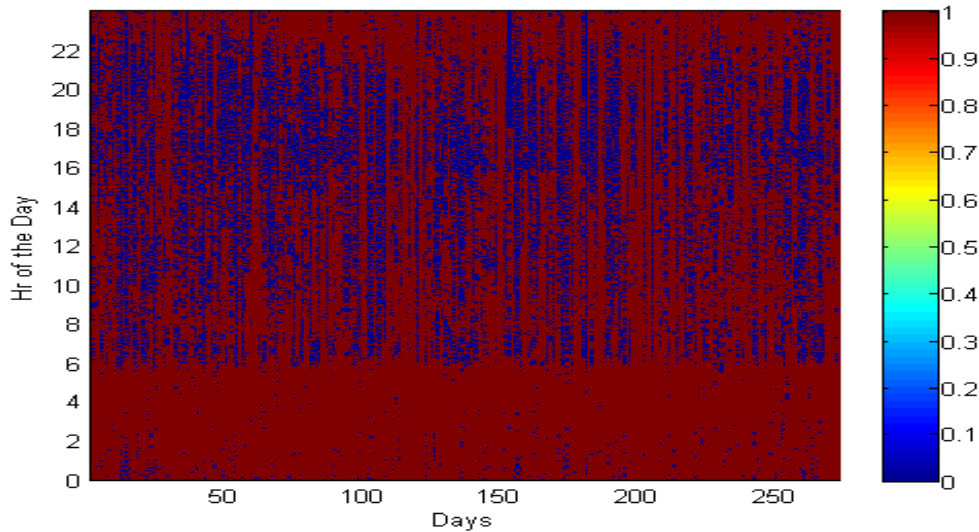


Figure 4.12. L2 implementation for Cell (63,23) in Zone 1 with  $Pr_{LTR}^{w,t} < 1$

## 4.5 L3 Analysis

In level L3, when a flight is detected a selected number of BSs are handed off based on some criteria, so that the threshold for avoiding harmful interference is

met. The algorithm 3 is similar to that of Algorithm 1 in many aspects, however the subtle difference is that each BS is dealt with individually. In L2 there was only one back-off timer for the cell, in L3 there will be back-off timers for each BS in the cell. L3 does not have any sanction table and hence the preliminary checking in line 7 is to check if at least one BS has passed its back-off time; after which only those BSs will be populated into the *ActiveBS* set. The secondary check in line 15 loops until the  $|ActiveBS| = \phi$  or a set of *ActiveBS* has been obtained which obeys the threshold. Every time the condition fails a BS  $j$  is removed from the *ActiveBS* set and the back-off timer for the BS  $k$  is started. One can improve the algorithm by improving the choice of  $k$  in line 16 of Algorithm 3 so that a *ActiveBS* set can be reached quickly.

---

**Algorithm 3:** Algorithm for L3

---

**Input:**  $T_{BackOff}$ ,  $S_B$ ,  $LTEProfile_{w,t}, S_A$

```

1 begin
2   Set  $T_i = 0 \forall i \in ActiveBS$ 
3   Set  $ActiveBS = S_B$ 
4   while True do
5     Set  $t = CurrentTime()$ 
6     Set  $w = DayOfWeek()$ 
7     if  $t > T_i \exists i \in ActiveBS$  then
8       Add BS  $i$  to set  $ActiveBS \forall i \in t > T_i$ 
9       Set  $S_A = ReadADSBData$ 
10      Set  $P_B = P_B^{max} * LTEProfile_{w,t}$ 
11      Set  $P_U = P_U^{max} * LTEProfile_{w,t}$ 
12      Set  $N_U = 10 * |S_B| * LTEProfile_{w,t}$ 
13      while  $|ActiveBS| \neq \phi$  do
14         $I = ComputeInterference(S_A, ActiveBS, P_B, N_U, P_U)$ 
15        if  $I_j > -95.7$  and  $S_A(j, z) \geq 5000ft \forall j \in S_A$  then
16          Find BS  $k$  with least Euclidean distance  $\forall j \in S_A$ 
17          Remove  $k$  from  $ActiveBS$ 
18           $T_k = T_k + T_{BackOff}$ 
19        else
20          break

```

---

Figure 4.13 shows the average usage time in hours of the 136 BSs in the cell when L3 deployment was considered. The BSs usage of the spectrum varies from maximum 88% to minimum 9%. This shows that all the BSs do not require to handoff in every case there is an aircraft which is close enough to receive interference from the BSs. There can be a subset of BSs which can still operate and not provide

harmful interference to the aircraft.

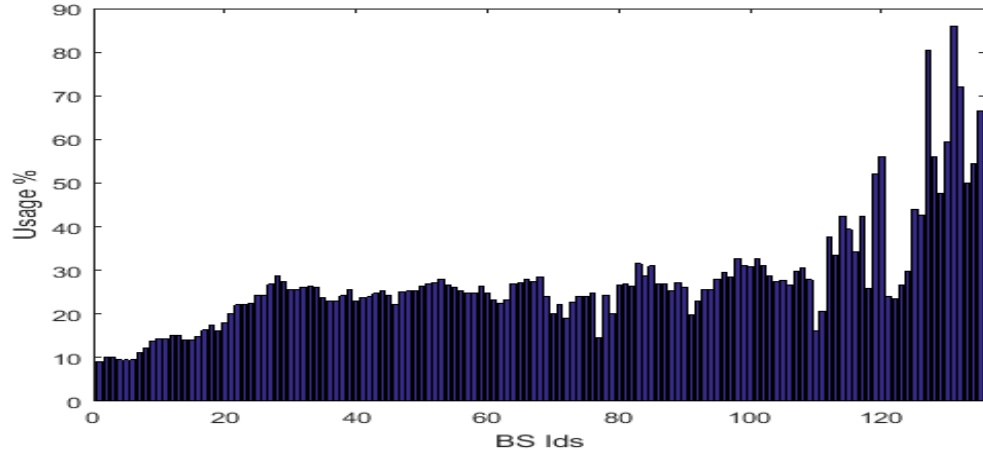


Figure 4.13. L3 average BS usage for Cell (63,23) in Zone 1

#### 4.6 L2 and L3 Comparison

In this Section we compare the average handoffs and spectrum usage for the BSs for L2 (all 4 cases) and L3 deployments. Figure 4.14 shows the daily average usage by the 136 BSs in the Cell (63,23) for different deployment scenarios. The deviation for L3 greater than the L2 sub classes, since the BSs in L3 class goes through irregular handoffs. This is quite evident from the Figure 4.13 where the daily usage varies a lot for the BSs. With each sub class of L2 there is an improvement in the usage.

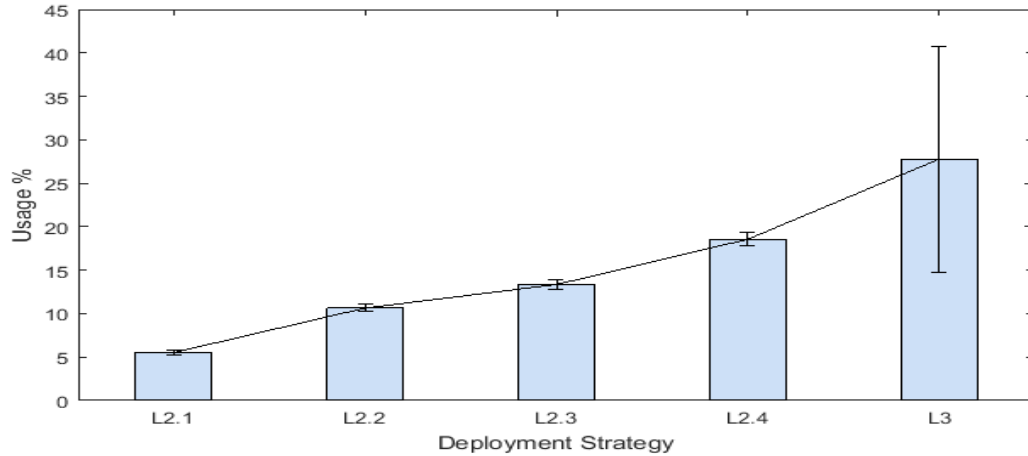


Figure 4.14. Average spectrum usage for Cell (63,23) in Zone 1

Figure 4.15 shows a similar trend as that of the spectrum usage. If we compare the usage and the handoff graphs we see that with each class both the usage and number of handoffs increases. To select a perfect class for an area there needs to be a tradeoff between the usage time and number of handoffs. L2.1 and L2.2 are the least conservative approaches and can be used in cells with moderate likelihood of interference. L2.3 and L2.4 are quite comparable for this cell, but it might change for a different area. Due to the huge deviation in L3 it might not be always a good option for deployment compared to L2.4. However, if a fairness is implemented within the BSs for handoffs, then this variation can be minimized.

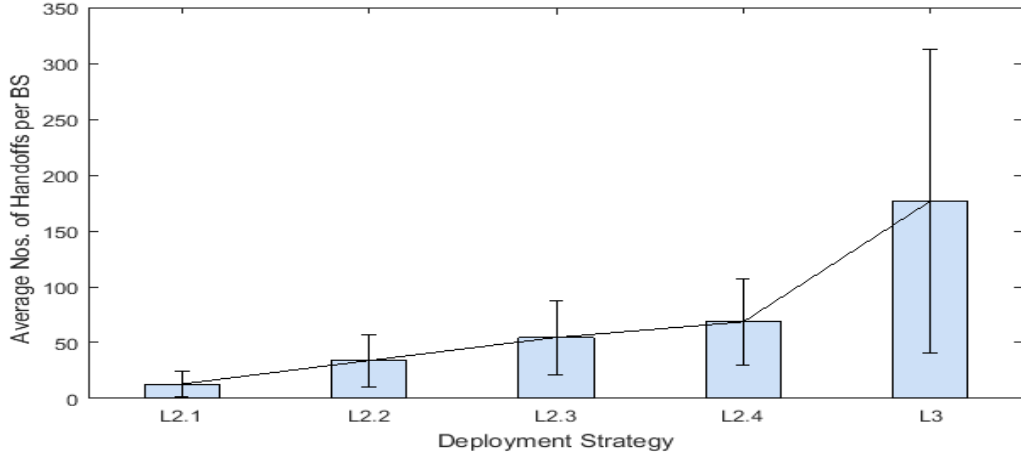


Figure 4.15. Average Number of BS Handoff for Cell (63,23) in Zone 1

## 4.7 Discussion

In this chapter we combined the altimeter radar tracking data, the interference threshold values, LTE Profile and BS deployment in Chicagoland to get LTR and RTL likelihood values. With the help of these likelihood values we proposed to form Exclusion and Coordination Zones. We did find the likelihood for LTR and RTL scenarios, however for the simulation we used the LTR results as we cannot decide on a threshold for the RTL scenario; which is a business decision. We suggest that there can be four levels of restriction in the space-time domain, namely L0,L1,L2 and L3. L0 and L1 are conservative approaches which take only the space domain, and can work as a starting point for regulating agencies to start deployment of this band. However, to have a better usage of this spectrum L2 or L3 deployment is required which takes in the time domain. It was observed that there was improvement in spectrum usage as we went from the L2 sub classes to L3. The number of handoffs also increased in the same pattern, hence a trade-off needs to be established between the usage and number of handoffs. This is again a business decision where the Telcos have to consider the return on investment, since handoffs are costly.

## CHAPTER 5

### CONCLUSION AND FUTURE WORK

#### **5.1 Summary**

Spectrum sharing has gained a serious focus from academia, industry and policy makers. It is one of the most prominent proposed solutions to meet the demand for spectrum and for ending the current spectrum crunch. Even with the new and effective technologies, spectrum sharing poses challenges for its stakeholders (PUs and SUs). The technical, administrative and psychological challenges can be dealt with through the collaboration of the various spectrum stakeholders. Proper and clear policy needs to be implemented so that the challenges faced by the stakeholders can be minimized.

This thesis has focused on sensing the whereabouts of the PU (aircraft) so that their trajectory can be predicted and an intelligent sharing method between the PU and SU can be implemented. In Chapter 2 we introduced a mechanism for tracking the aircraft using the ADS-B data, which is right now open sourced. We analyzed the historical data to emphasize the potential white spaces present in the  $4.2 - 4.4\text{GHz}$  band in the space-time domain. The commercial aircraft tend to follow a particular path which is repeated periodically. Even the busy time of the aircraft in a given area were cyclical. The PDF and CDF charts for the occupancy of flights in a particular cell at a given time brought out the point that there are specific time periods during which the likelihood of flight presence is less and others when it is decidedly greater. However, observing the direct presence or absence of an aircraft in the cell does not ensure that the stakeholders will not interfere with each other.

In Chapter 3 we introduced the Altimeter Radar and LTE working principles which we needed to consider while making decisions on coexistence. Different inter-

ference scenarios like LTR and RTL were implemented to see how interference varies with cell placements, BS antenna direction and radar height. We assume a small cell (with directional antenna) deployment with a conservative path loss model, in a way to predict the deployment when this band will be available in the future. We studied the LTE Profile of Chicago using the spectrum data, so that a realistic touch can be given to the simulations.

In Chapter 4 we combined the location data of the aircraft, LTE usage profile and the interference study to get the likelihood of LTR and RTL interference for a given time. On the basis of these results we proposed sharing strategies namely L0, L1, L2 and L3. In L0 and L1 we propose to form strict exclusion zones based on the interference tolerance count; L0 tolerates no interference while L1 tolerates some interference. While forming exclusion zones in L1 we check cells with the least likelihood of interference, so that in case flights or LTE users receive interference they take steps to mitigate it. In L2 and L3 we also consider the time domain for sharing. In L2 a hybrid exclusion zone in the time domain is proposed, where time periods for sharing are predefined using Sanction tables. The SUs use the band in accordance with the Sanction table, with and back-off in time techniques deployed in case of interference. The sanction table is built based on the Likelihood of LTR interference, since deciding a threshold for the RTL interference is a business decision. We see that as we move from building a more to less conservative Sanction table, the band usage increases. However that will come with a cost i.e. handoffs, when the PU wants to use the band the BSs need to handoff. Hence, a trade-off needs to be set between usability and the number of handoffs while building the sanction table. Moreover, in L3, which is a pure coordination zone implementation, not all BSs need to handoff in the case of the presence of an aircraft. Switching off a subset of BSs will result in a decrease in aggregated interference, so that the altimeter protection threshold is met.

The ITU has already recommended the use of this band inside the aircraft as explained in Section 1.3. Throughout the thesis we did take some assumptions, since the environment is too complicated to take a full set of accurate measurements and to consider all small parameters. Through our findings, we propose that using the “ADS-B” aircraft sensing mechanism, LTE interference mitigation techniques, and forming coordination zones in space-time domain; the  $4.2 - 4.4\text{GHz}$  band can be made available for sharing outside the aircraft.

## 5.2 Future Work

The method suggested herein may be extended to enable evaluation of intelligent sharing methods in other bands. It is suggested that this type of analysis including the use of ADS-B data might ultimately be integrated with an intelligent sharing system.

More work needs to be done to deal with the technical, administrative and psychological challenges. Proper measurement based propagation models need to be made specifically for this band. In case of small cell and indoor deployments the FAF and the PAF values need to be calculated for different scenarios. Moreover, outdoor propagation models can also be developed so that even the macro cells can use this band for short range.

While calculating the LTR threshold we considered the parameters for a particular manufacturer which resulted in the worst case threshold of  $-95.7\text{dBm}$ . However, there were other manufacturers whose parameters would result in much lower threshold (like,  $-111.87\text{dBm}$ ). If along with the radar location information, the radar manufacturer’s information was also known then the sharing opportunities could have been increased.

In Chapter 4 we introduced the L3 sharing strategy, where we computed the

subset of active BSs which would obey the threshold values based on the Euclidean distance. However, improvements can be made on selecting the subset of active BS. Rather than always trying to compute the BS subset; the system can learn the BSs which are most likely to get switched off at a given time. This would reduce the complexity of the L3 algorithm. Again, from the L3 results it is certain that there would be some set of BSs which would go through handoffs and some which will not. The algorithm can be improved to implement fairness by finding the subset of BSs which obey the thresholds and have also collectively gone through less handoffs.

There needs to be a collaboration between the Telcos and the FAA so that a smooth transition of band usage can happen when interference is detected. The Telcos need to build a trust factor so the psychological barrier in the common public can be dissolved. The policy makers will work as a key catalyst for rolling out this band to LTE. By following these techniques it is believed that this valuable spectrum can be shared with commercial LTE systems enhancing these systems for their numerous users nationwide!

APPENDIX A  
EMPIRICAL LIKELIHOOD

Empirical likelihood (EL) is a non-parametric method likelihood ratio function which is data-driven. In EL we do not need to specify a family of distribution for the data, like bootstrap and jackknife. It was first introduced by Owen in [56].

Similar to parametric likelihood methods, EL makes an automatic determination of the shape of confidence regions. It has very favorable asymptotic power and can be thought as a bootstrap without resample. This method is used when the parametric distribution cannot properly describe the data. This is perfect for our work as the flight pattern and LTE usage is highly time dependent; varies with time of day and day of week.

## A.1 Kernel Distribution

We used Kernel Distribution which is a non-parametric representation of the probability distribution function (PDF). In some fields such as signal processing and econometrics it is also termed the ParzenRosenblatt window method. The function is defined by a smoothing function and a bandwidth value that controls the smoothness of the resulting density curve [57]. Let  $(x_1, x_2, \dots, x_n)$  be an Independent and Identically Distributed (IID)<sup>9</sup> sample drawn from some distribution with an unknown density  $f$ . We are trying to find the shape of the function  $f$  for a bandwidth  $h$ . The kernel density estimator is the estimated PDF over a sample set is given by the Equation A.1

$$f_h(x) = \frac{1}{nh} \sum_{i=1}^n K\left(\frac{x - x_i}{h}\right) \quad (\text{A.1})$$

where n is the sample size,  $K(\cdot)$  is the kernel smoothing function, h is the band-

---

<sup>9</sup>In probability theory, a collection of random variables is said to be IID if each random variable has the same probability distribution and all variables are mutually independent.

width. One wants to choose  $h$  as small as the data allows, however there is trade-off between the bias of the estimator and its variance. We considered the recommended Silverman's bandwidth for our simulations.

The kernel smoothing function defines the shape of the curve  $f_h$  for a bandwidth  $h$  which is used to generate the PDF. It is similar to a histogram and builds a function to represent the probability distribution using the sample data. Histograms due to the bin count approach produces a discrete PDF; which is not suitable for our data. Hence, we used the kernel distribution which builds the PDF by creating an individual probability density curve for each data value, then summing the smooth curves. This approach creates one smooth, continuous probability density function for the data set.

APPENDIX B  
PDF AND CDF OF FIGHT OCCUPANCY FOR CELLS

This Appendix is a continuation of Section 2.6. We have the PDF and CDF plots of Flight Occupancy for all the cells we have considered in Section 2.5.5.

### B.1 Zone 1

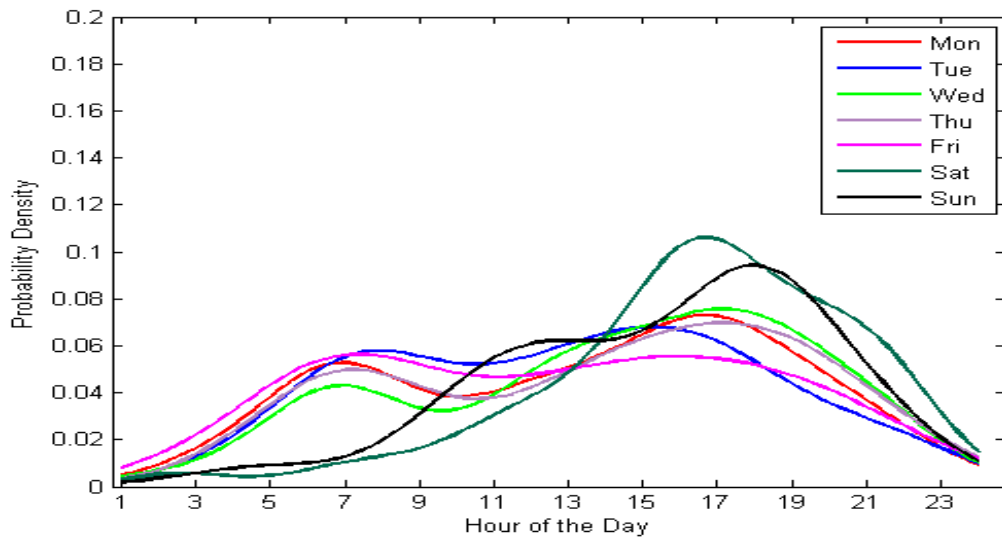


Figure B.1. Flight Occupancy PDF plot for Cell (65,23) in Zone 1

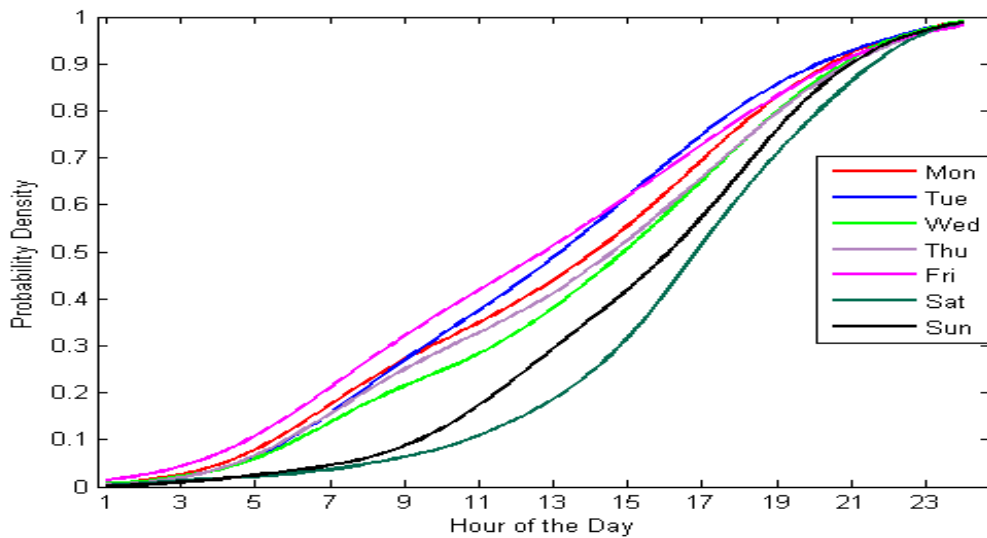


Figure B.2. Flight Occupancy CDF plot for Cell (65,23) in Zone 1

## B.2 Zone 2

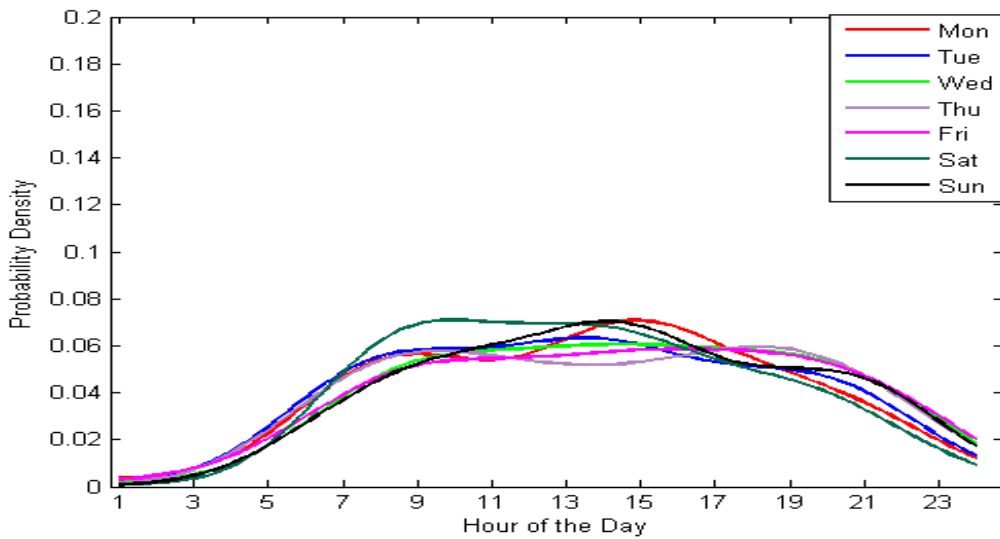


Figure B.3. Fight Occupancy PDF plot for Cell (61,4) in Zone 2

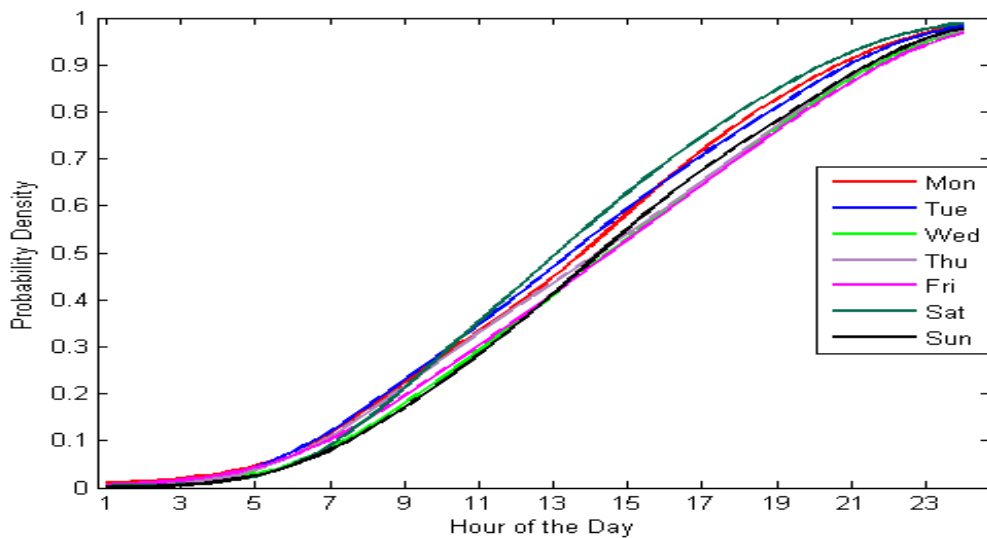


Figure B.4. Fight Occupancy CDF plot for Cell (61,4) in Zone 2

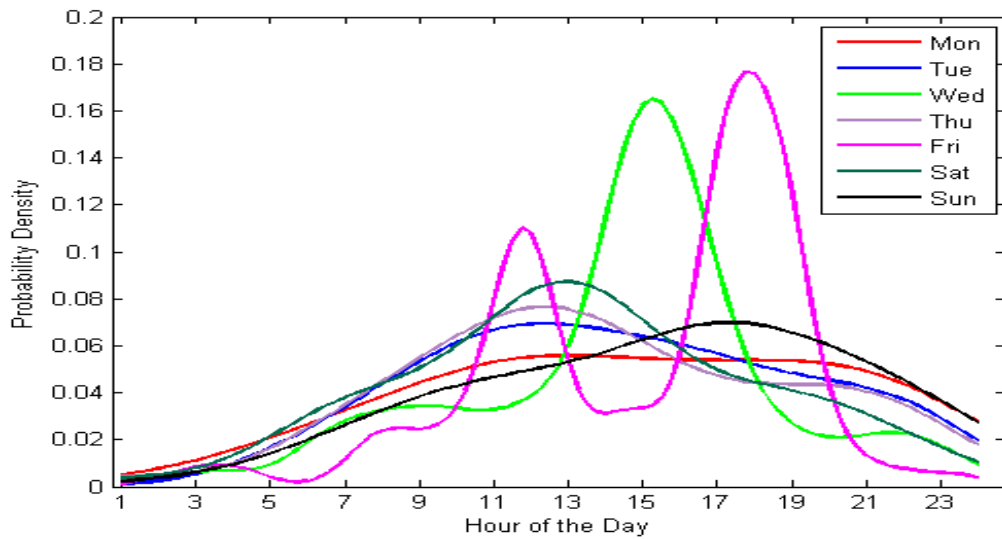


Figure B.5. Fight Occupancy PDF plot for Cell (61,7) in Zone 2

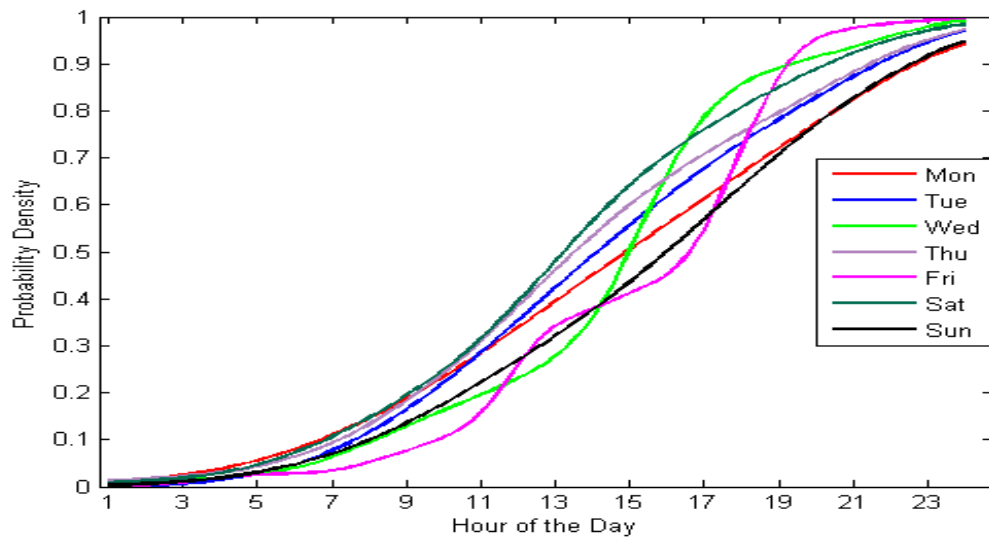


Figure B.6. Fight Occupancy CDF plot for Cell (61,7) in Zone 2

### B.3 Zone 3

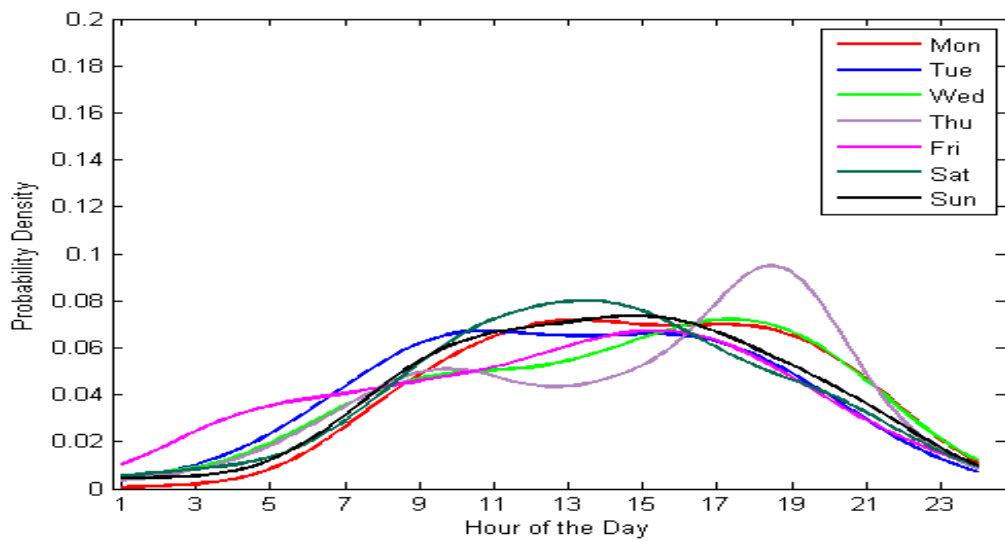


Figure B.7. Fight Occupancy PDF plot for Cell (12,16) in Zone 3

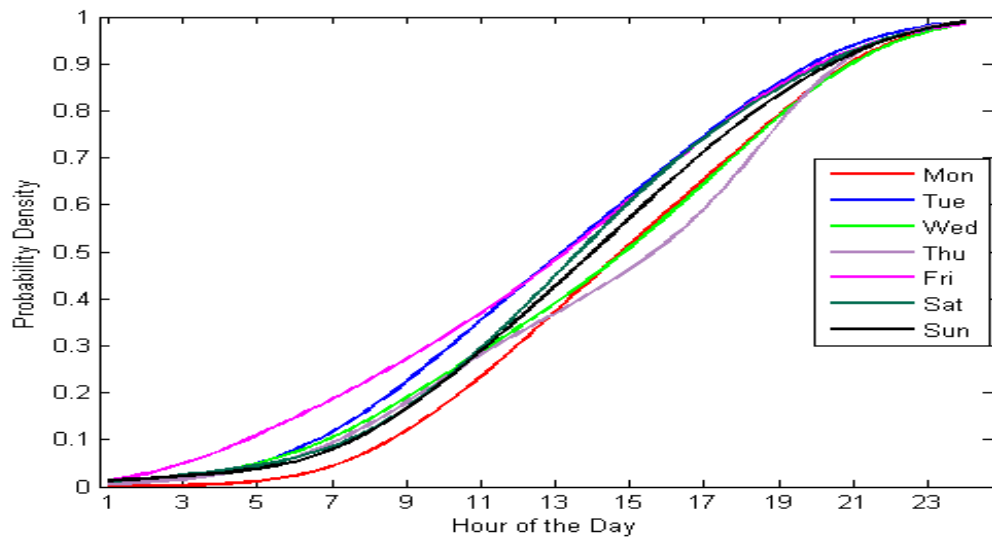


Figure B.8. Fight Occupancy CDF plot for Cell (12,16) in Zone 3

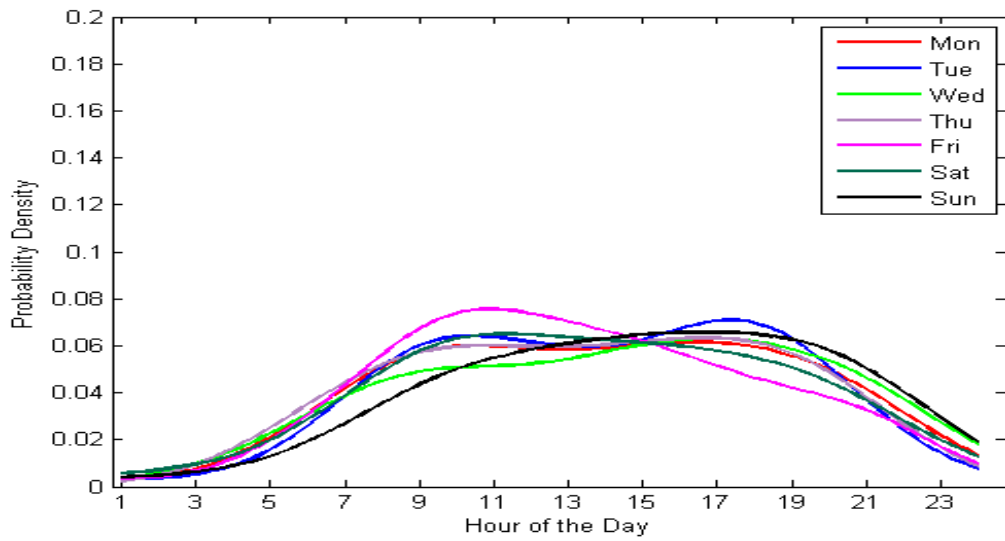


Figure B.9. Fight Occupancy PDF plot for Cell (14,15) in Zone 3

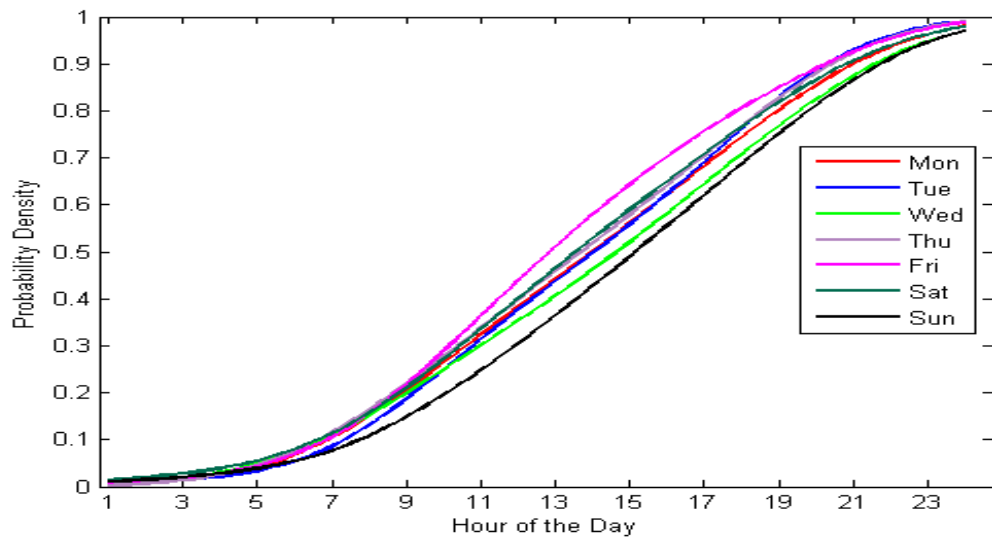


Figure B.10. Fight Occupancy CDF plot for Cell (14,15) in Zone 3

#### B.4 Zone 4

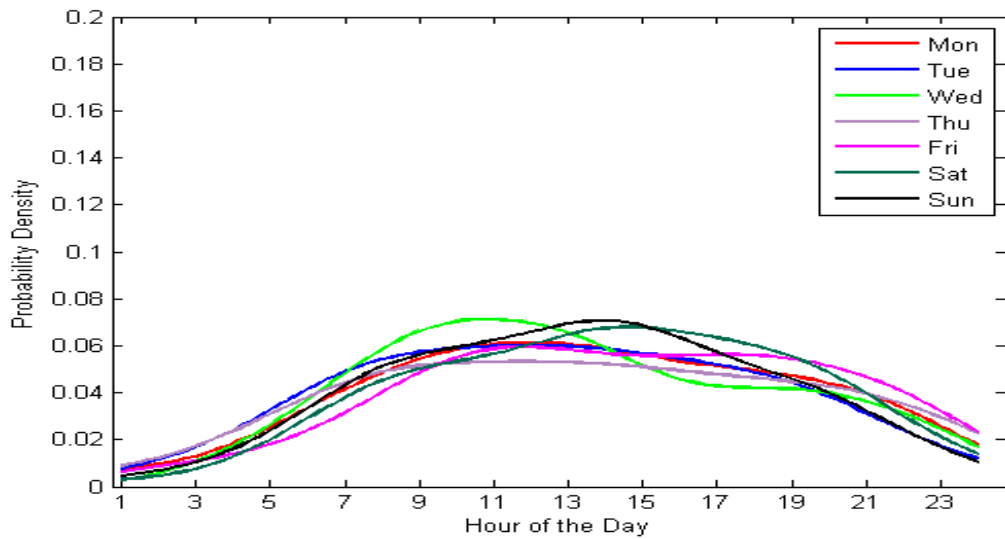


Figure B.11. Fight Occupancy PDF plot for Cell (31,38) in Zone 4

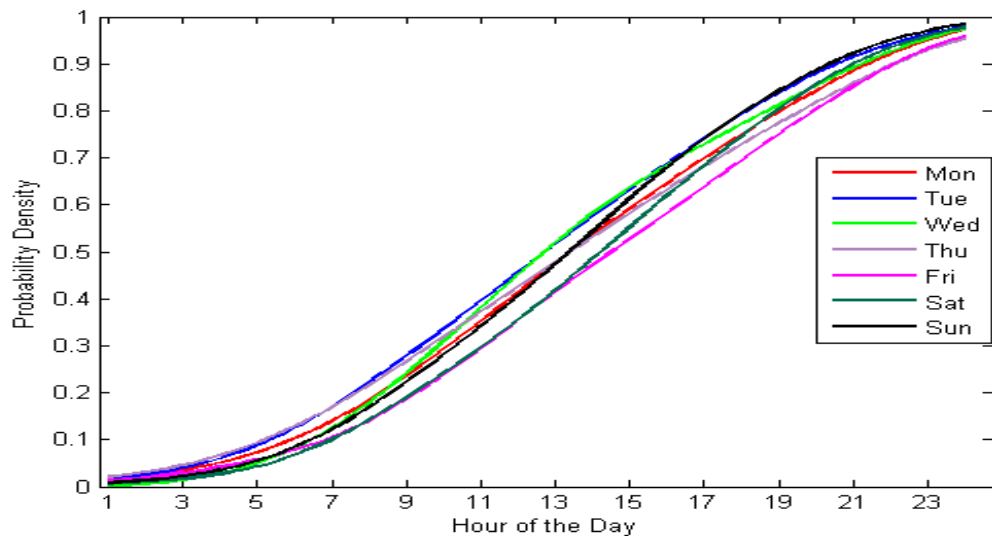


Figure B.12. Fight Occupancy CDF plot for Cell (31,38) in Zone 4

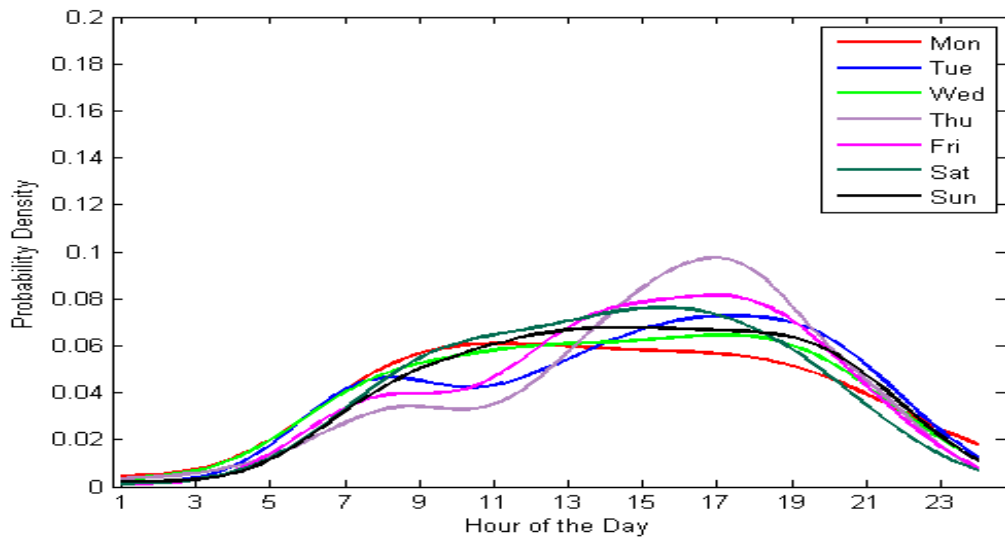


Figure B.13. Fight Occupancy PDF plot for Cell (59,35) in Zone 4

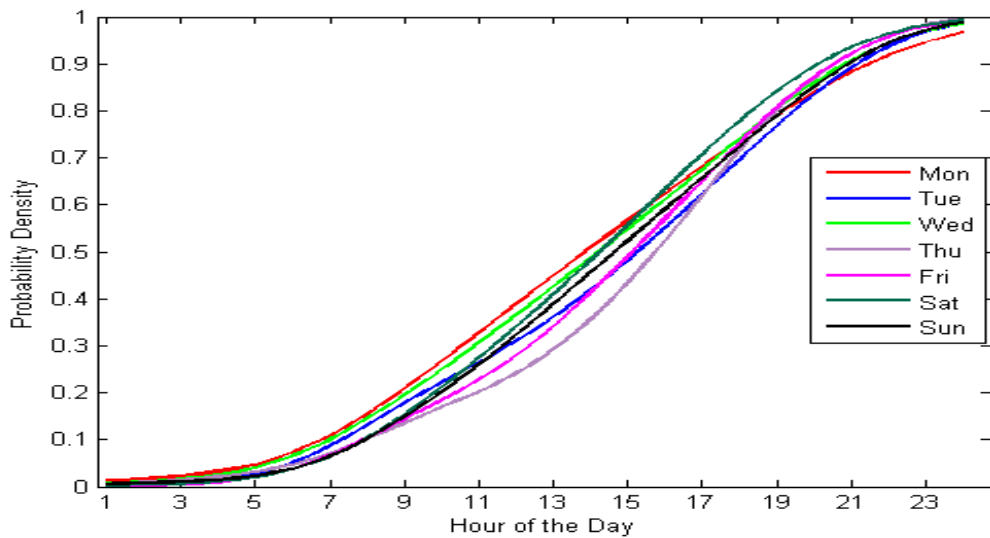


Figure B.14. Fight Occupancy CDF plot for Cell (59,35) in Zone 4

APPENDIX C  
PDF AND CDF OF LTR INTERFERENCE FROM CELLS

This Appendix is a continuation of Section 4.1.1. We have the PDF and CDF plots of LTR interference for all the cells we have considered in Section 2.5.5.

### C.1 Zone 1

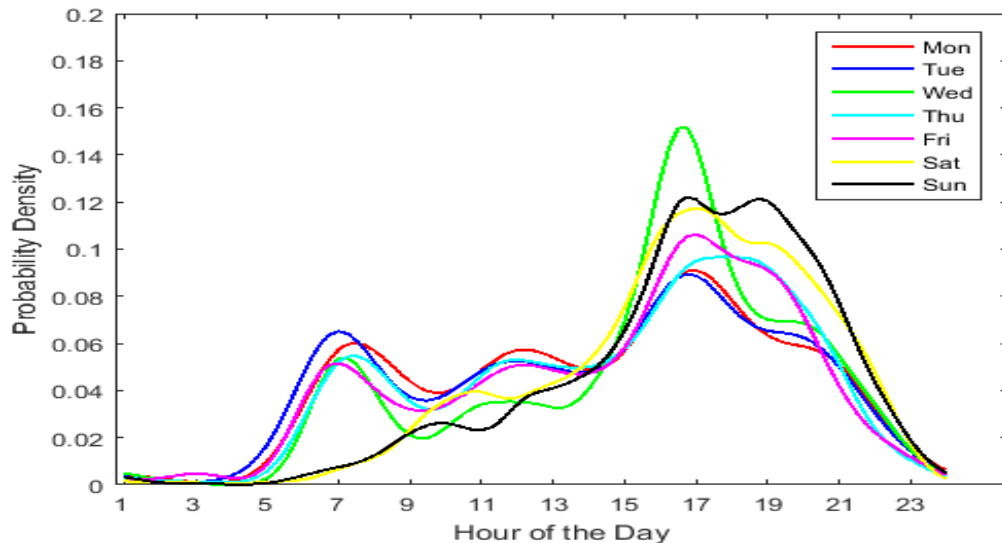


Figure C.1. LTR Interference PDF plot for Cell (65,23) in Zone 1

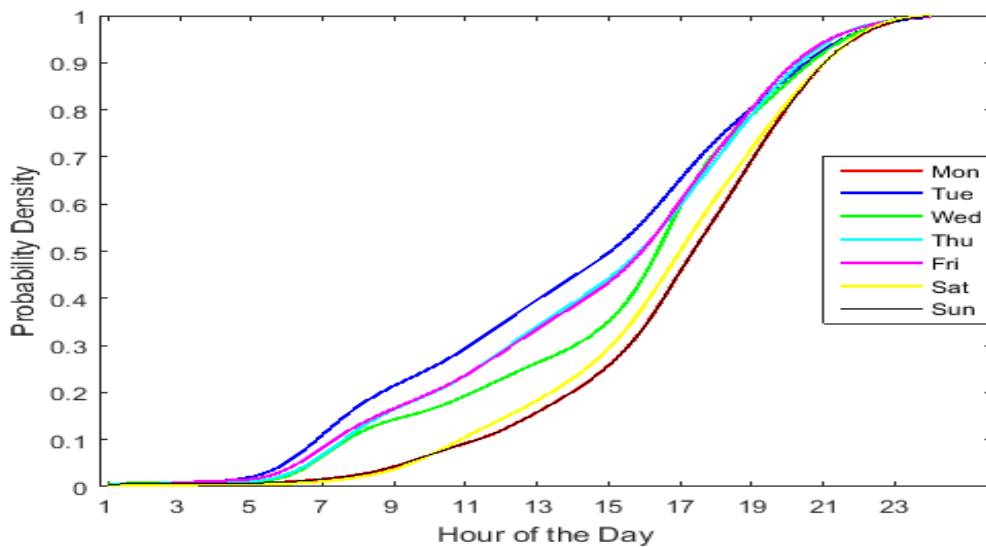


Figure C.2. LTR Interference CDF plot for Cell (65,23) in Zone 1

## C.2 Zone 2

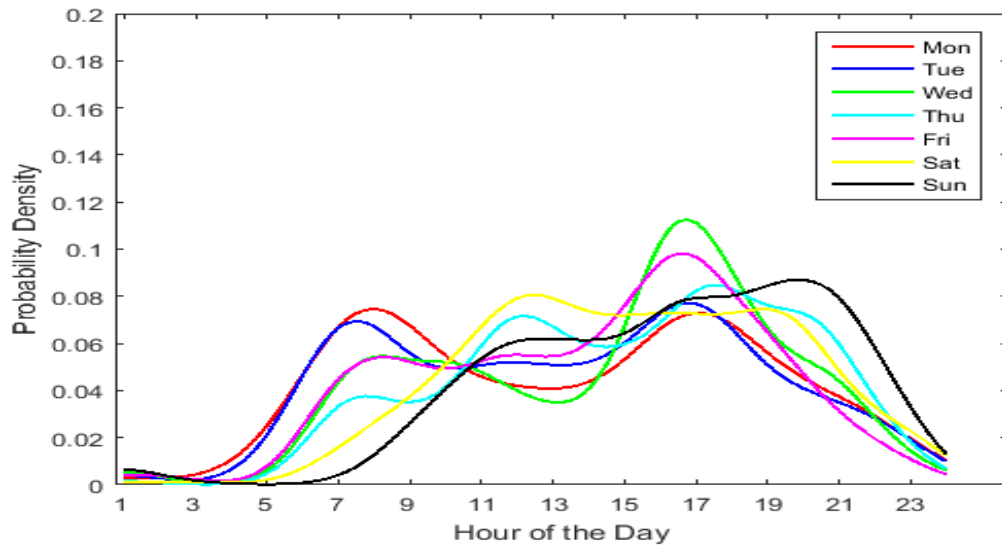


Figure C.3. LTR Interference PDF plot for Cell (61,4) in Zone 2

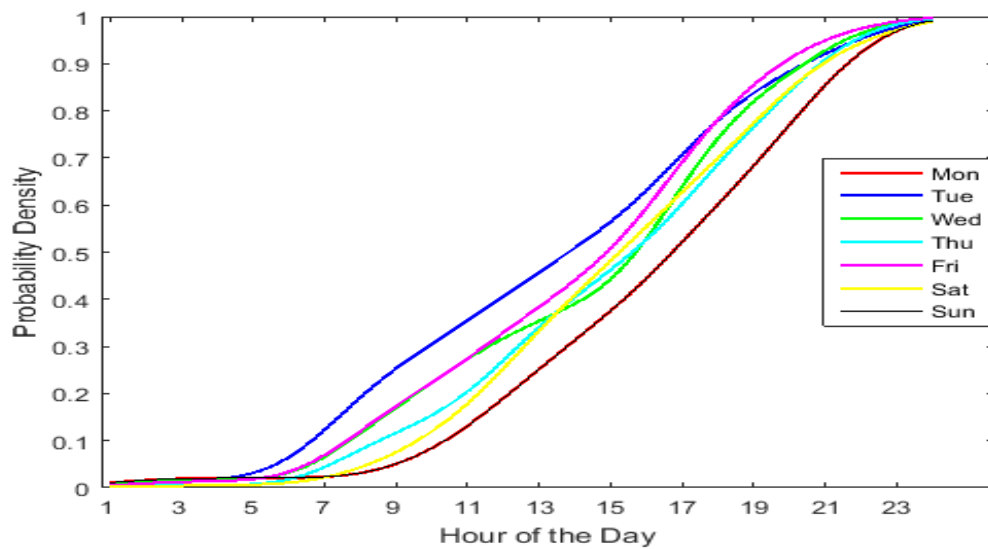


Figure C.4. LTR Interference CDF plot for Cell (61,4) in Zone 2

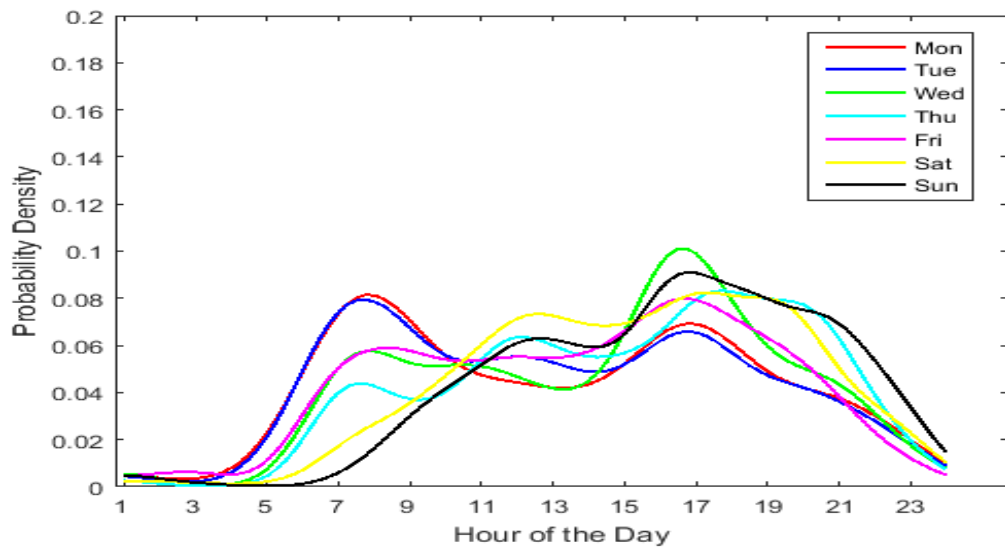


Figure C.5. LTR Interference PDF plot for Cell (61,7) in Zone 2

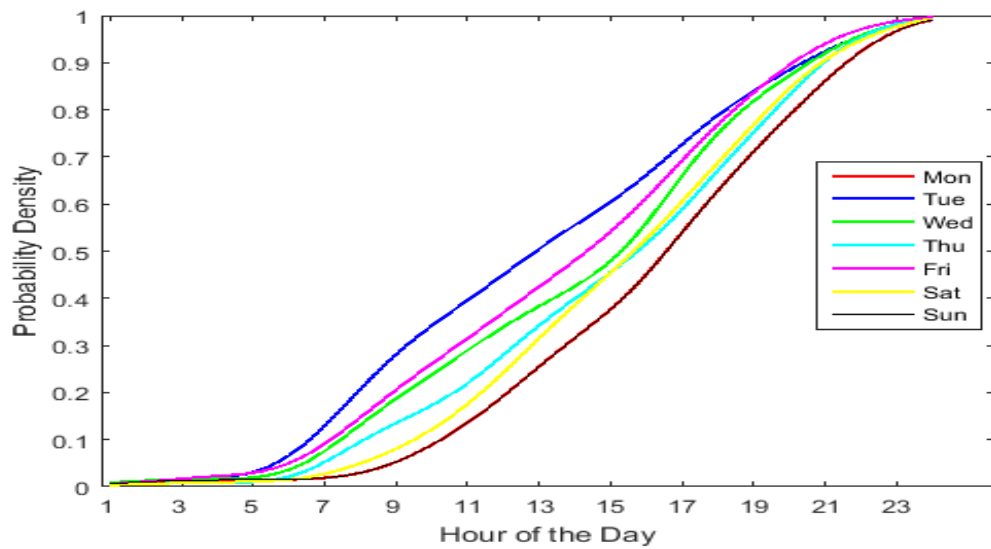


Figure C.6. LTR Interference CDF plot for Cell (61,7) in Zone 2

### C.3 Zone 3

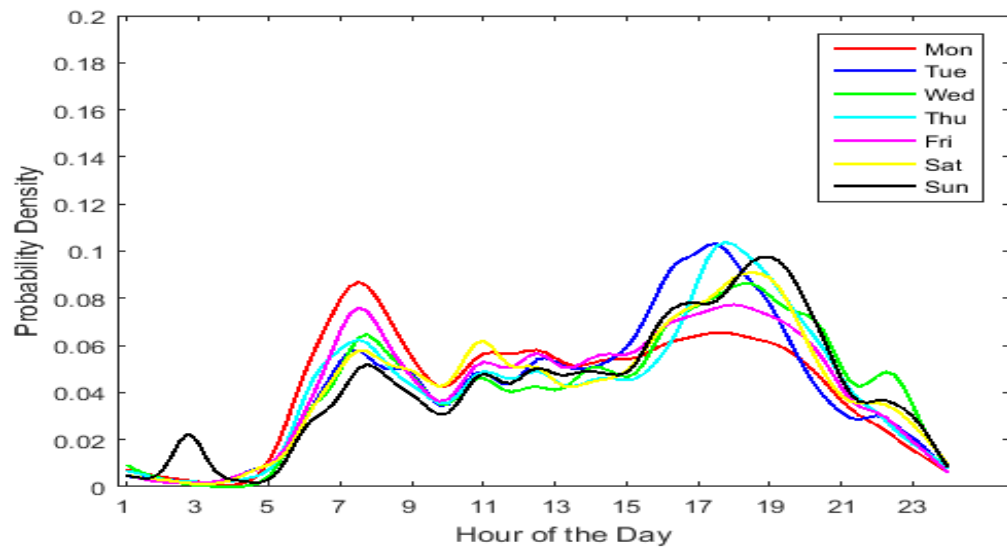


Figure C.7. LTR Interference PDF plot for Cell (12,16) in Zone 3

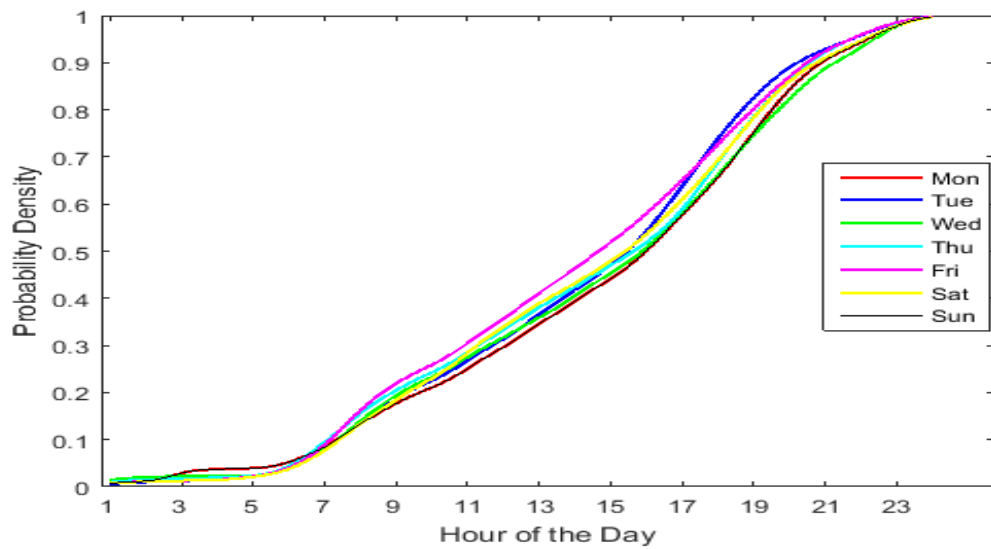


Figure C.8. LTR Interference CDF plot for Cell (12,16) in Zone 3

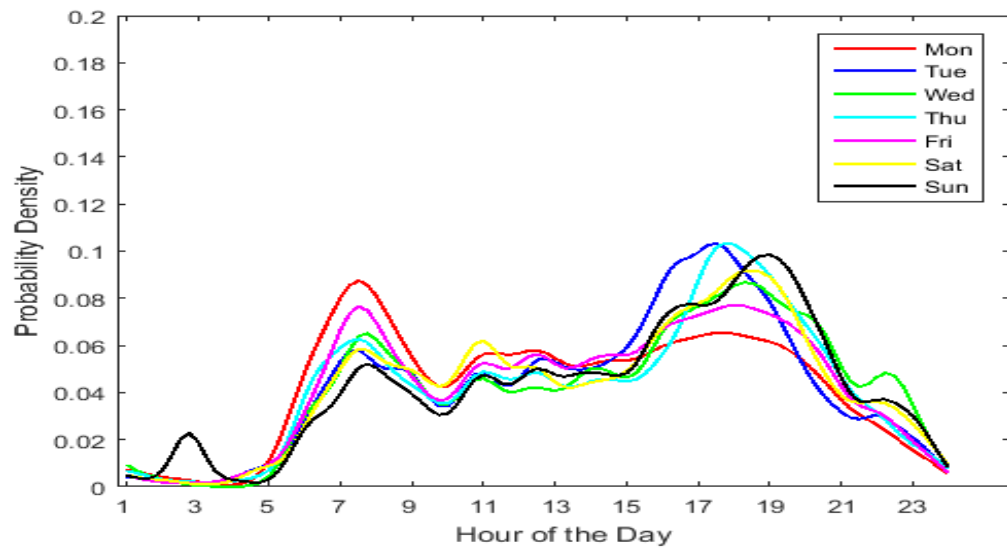


Figure C.9. LTR Interference PDF plot for Cell (14,15) in Zone 3

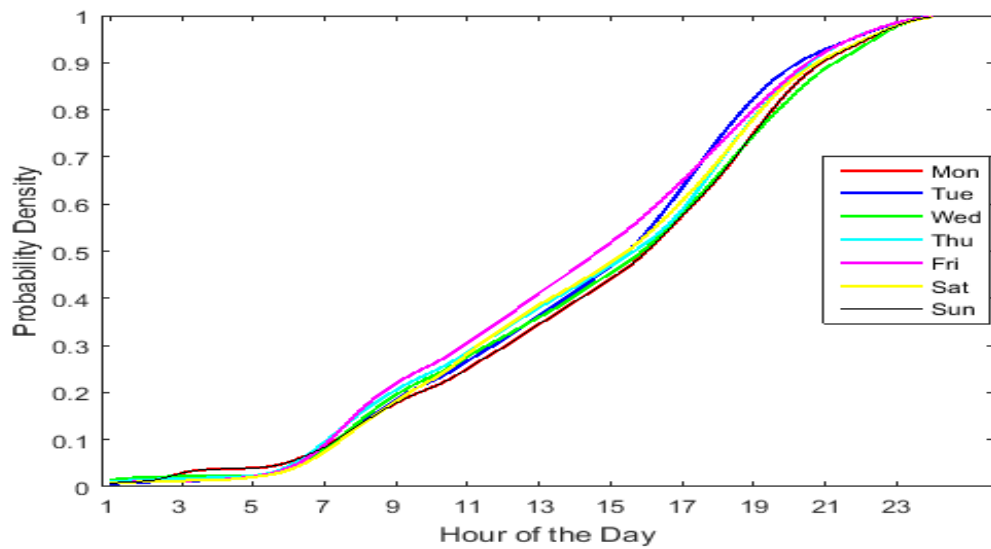


Figure C.10. LTR Interference CDF plot for Cell (14,15) in Zone 3

#### C.4 Zone 4

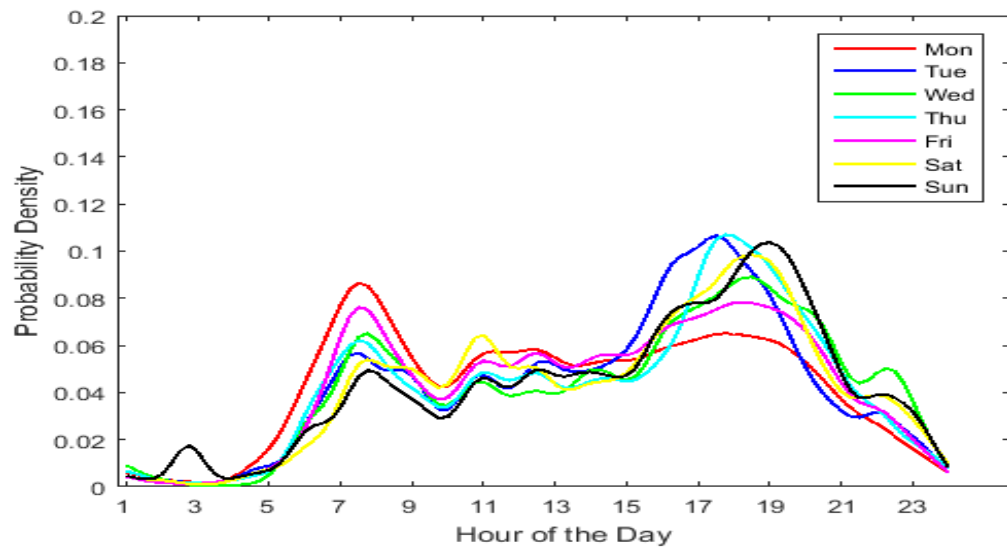


Figure C.11. LTR Interference PDF plot for Cell (31,38) in Zone 4

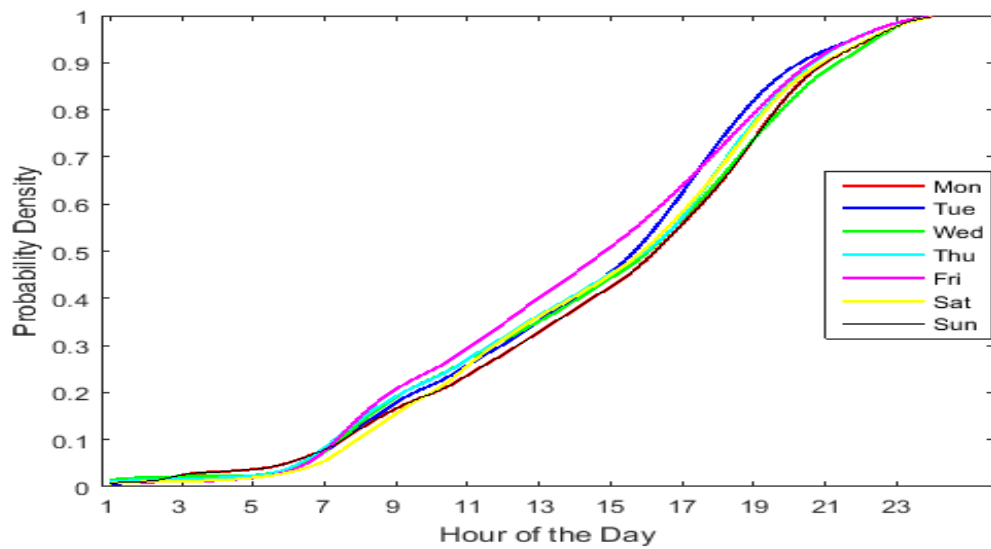


Figure C.12. LTR Interference CDF plot for Cell (31,38) in Zone 4

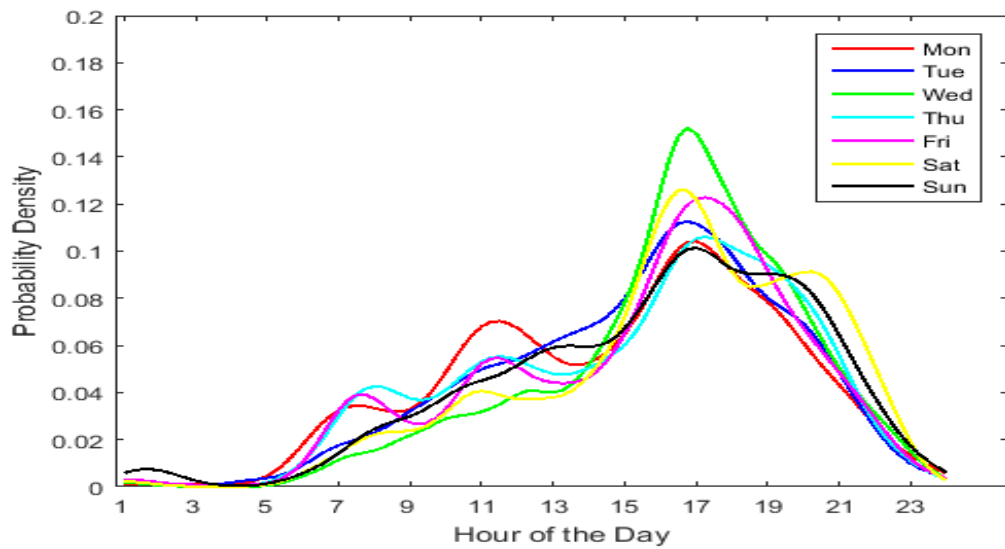


Figure C.13. LTR Interference PDF plot for Cell (59,35) in Zone 4

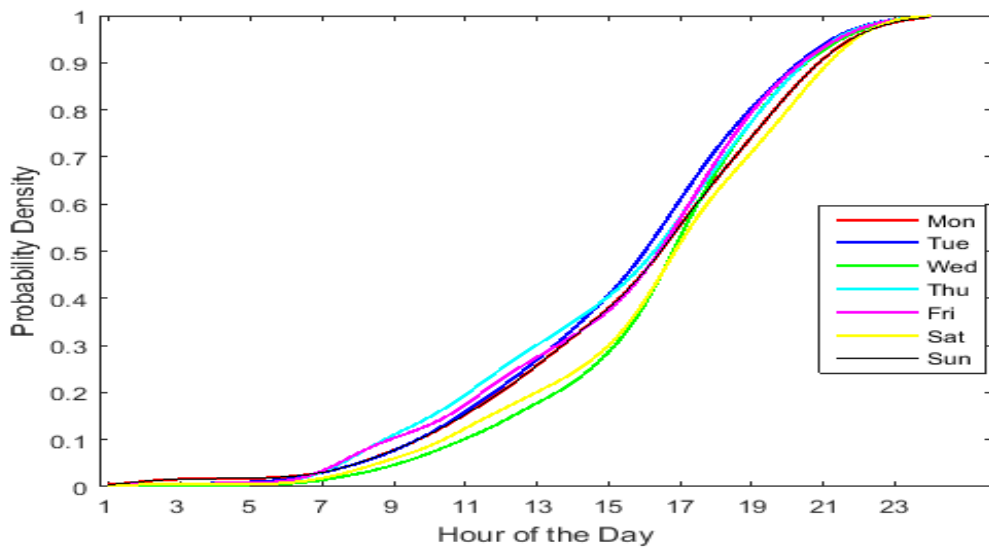


Figure C.14. LTR Interference CDF plot for Cell (59,35) in Zone 4

APPENDIX D  
PDF AND CDF OF RTL UE INTERFERENCE

This Appendix is a continuation of Section 4.1.2. We have the PDF and CDF plots of LTR interference for all the cells we have considered in Section 2.5.5.

### D.1 Zone 1

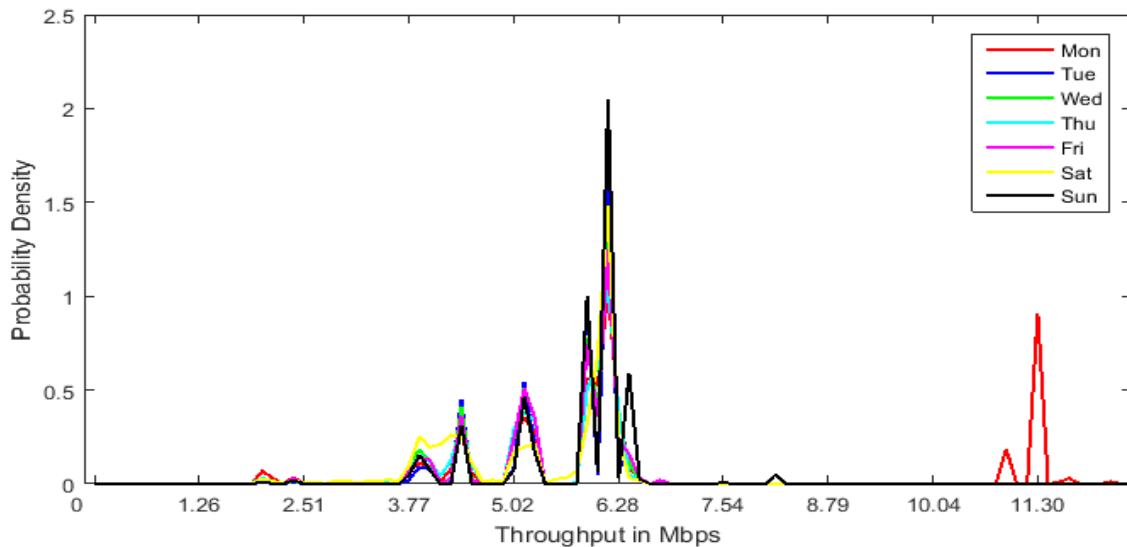


Figure D.1. RTL UE Interference PDF plot for Cell (65,23) in Zone 1

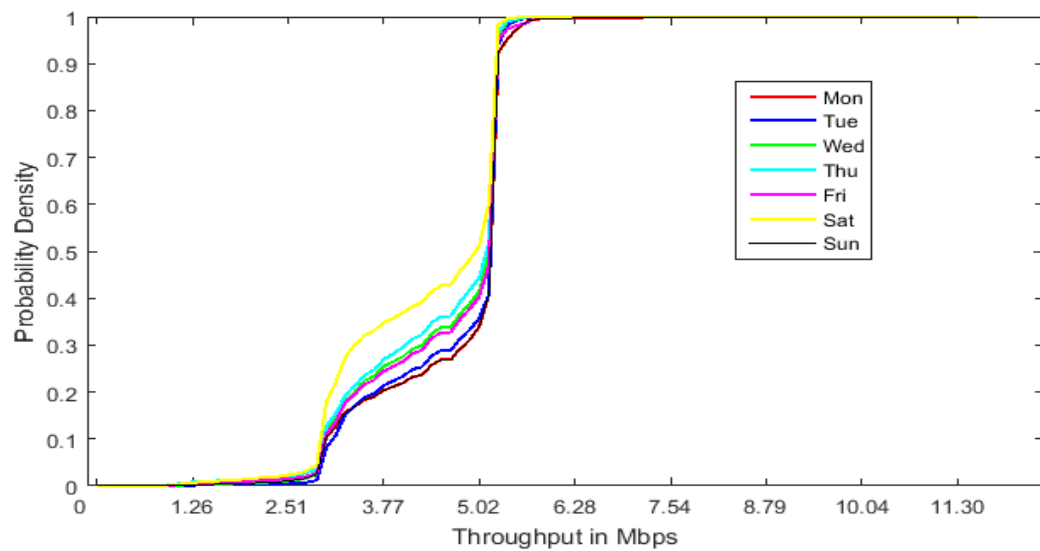


Figure D.2. RTL UE Interference CDF plot for Cell (65,23) in Zone 1

## D.2 Zone 2

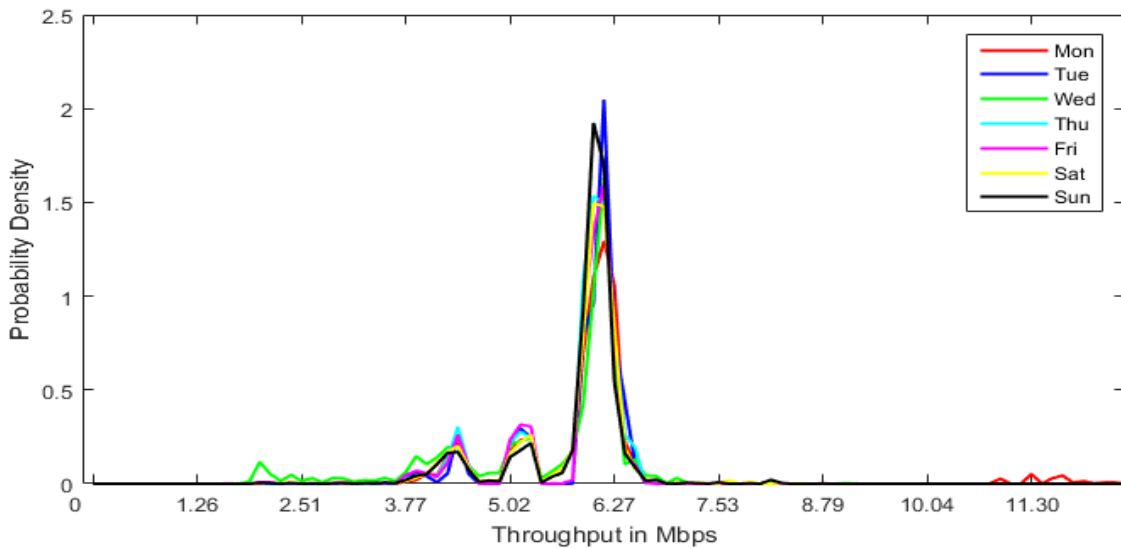


Figure D.3. RTL UE Interference PDF plot for Cell (61,4) in Zone 2

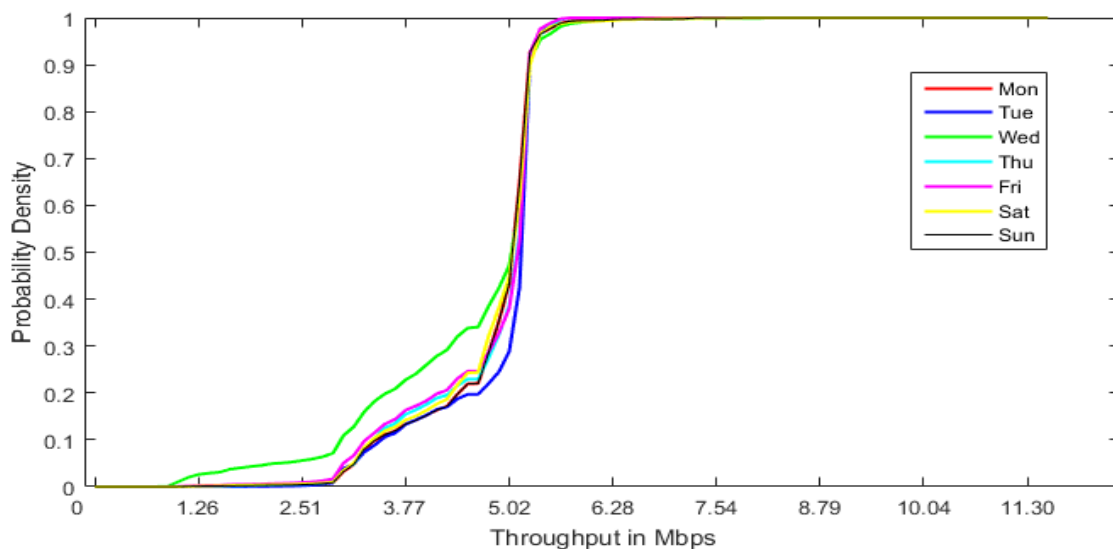


Figure D.4. RTL UE Interference CDF plot for Cell (61,4) in Zone 2

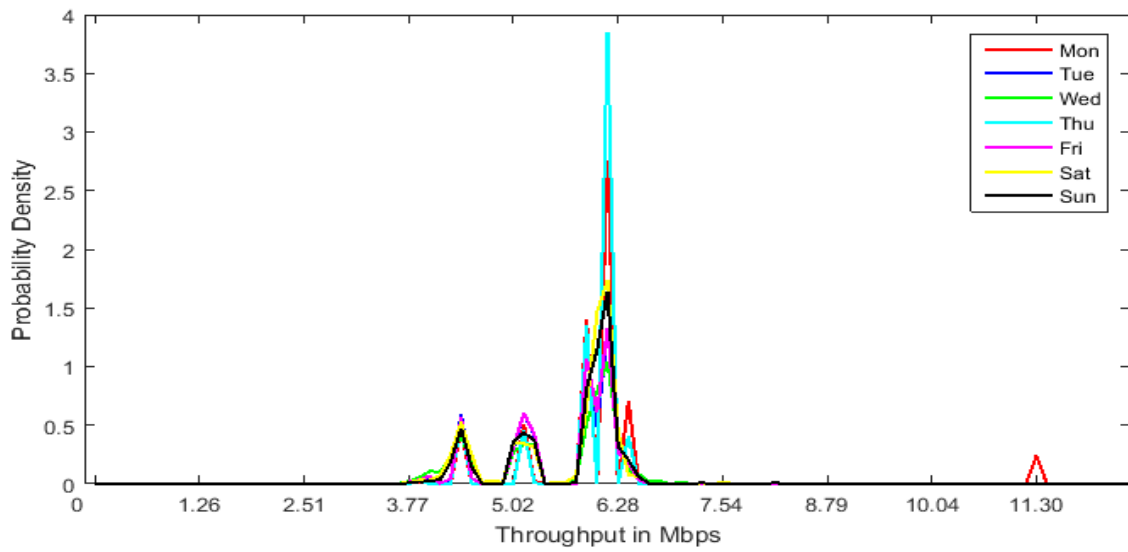


Figure D.5. RTL UE Interference PDF plot for Cell (61,7) in Zone 2

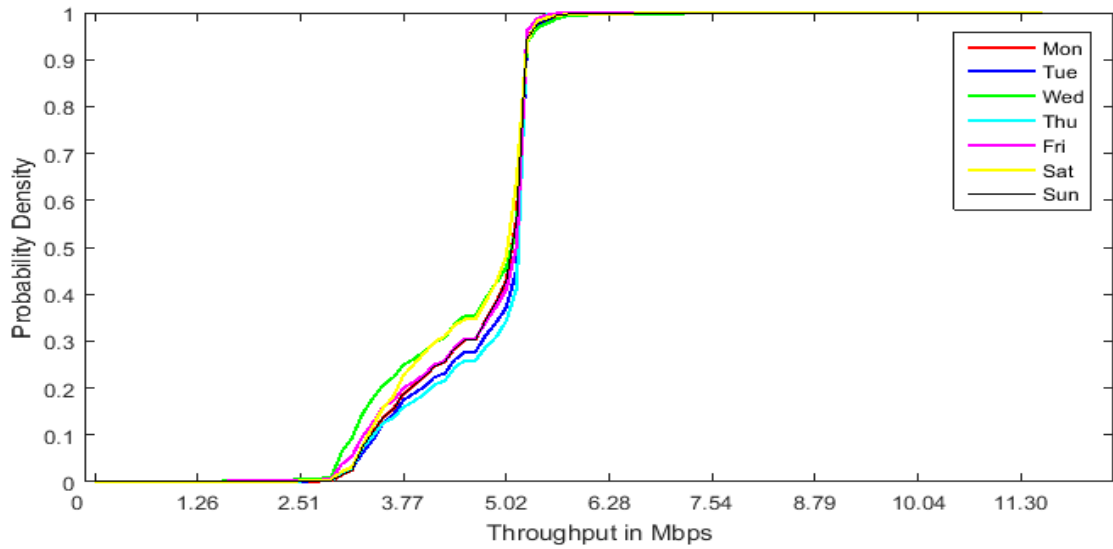


Figure D.6. RTL UE Interference CDF plot for Cell (61,7) in Zone 2

### D.3 Zone 3

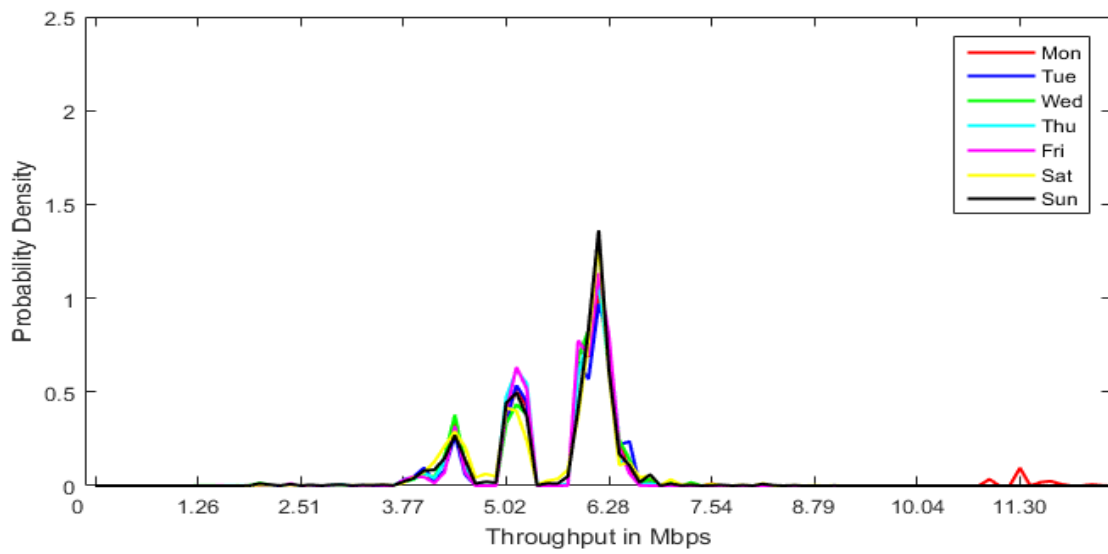


Figure D.7. RTL UE Interference PDF plot for Cell (12,16) in Zone 3

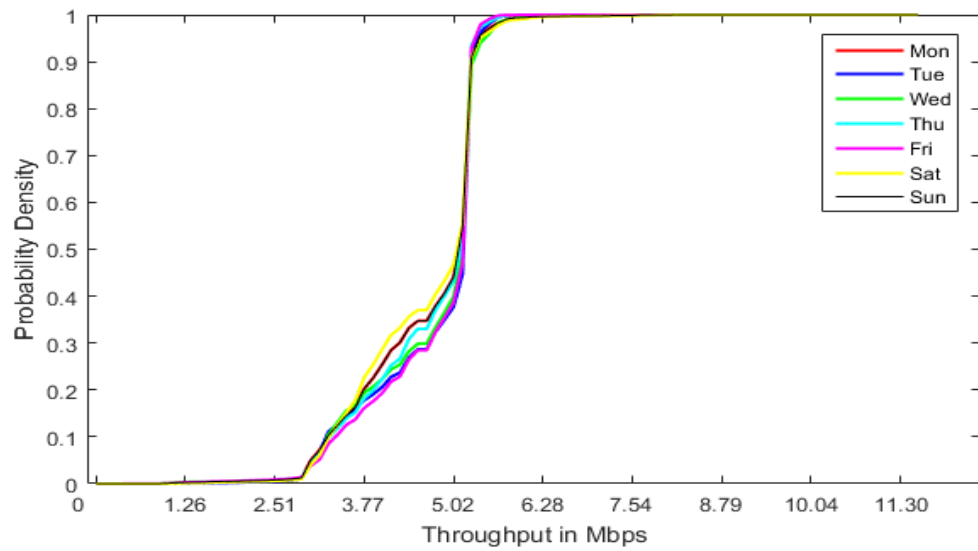


Figure D.8. RTL UE Interference CDF plot for Cell (12,16) in Zone 3

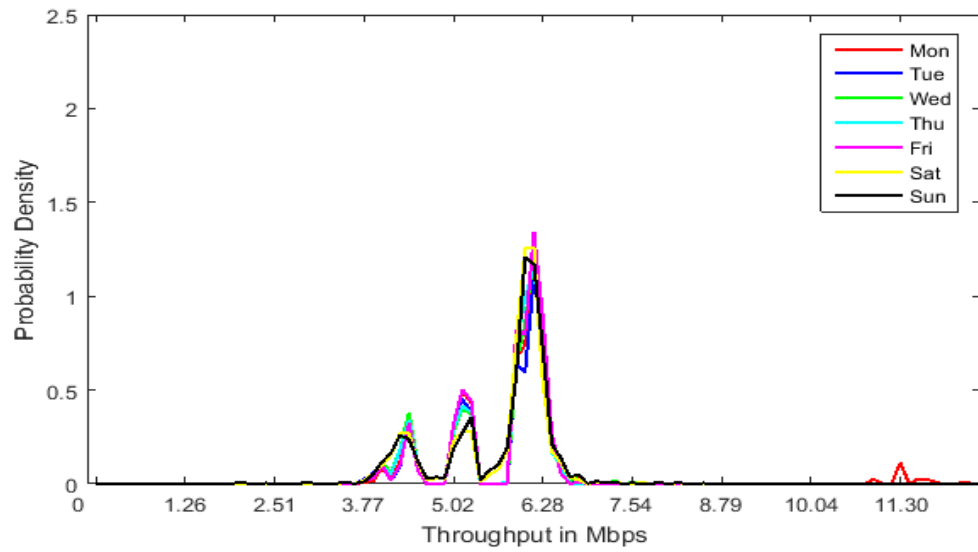


Figure D.9. RTL UE Interference PDF plot for Cell (14,15) in Zone 3

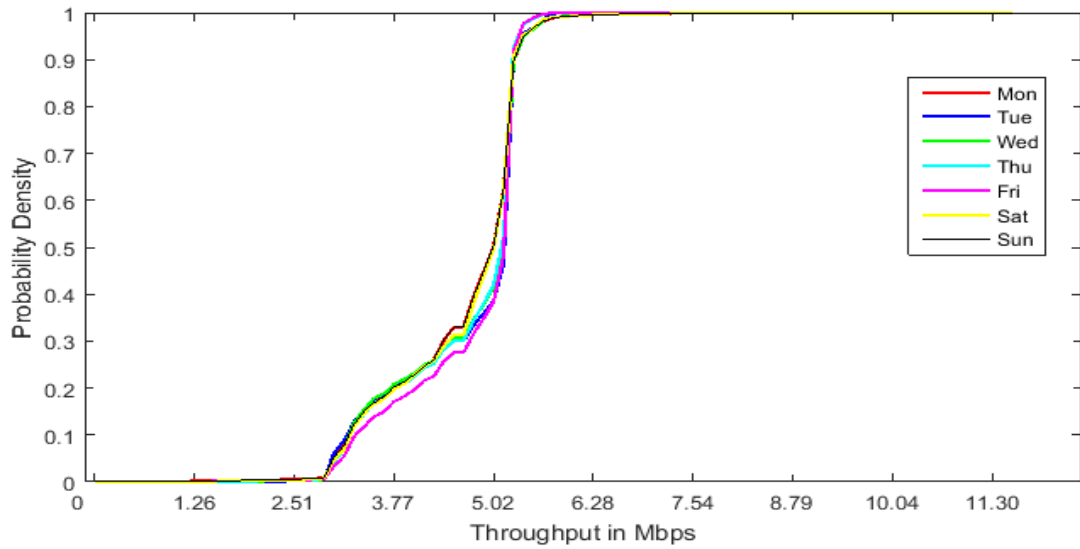


Figure D.10. RTL UE Interference CDF plot for Cell (14,15) in Zone 3

#### D.4 Zone 4

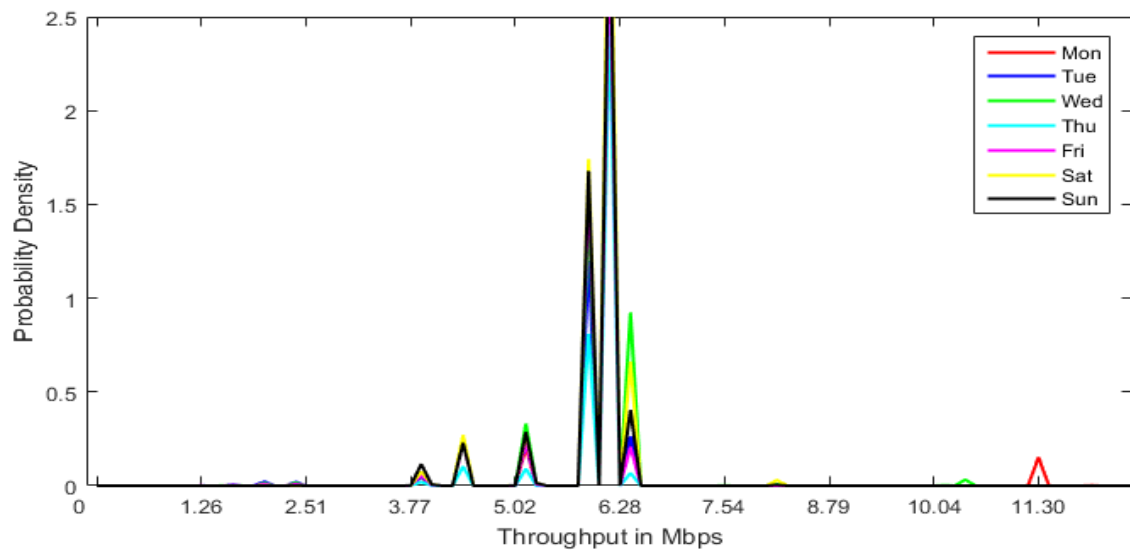


Figure D.11. RTL UE Interference PDF plot for Cell (31,38) in Zone 4

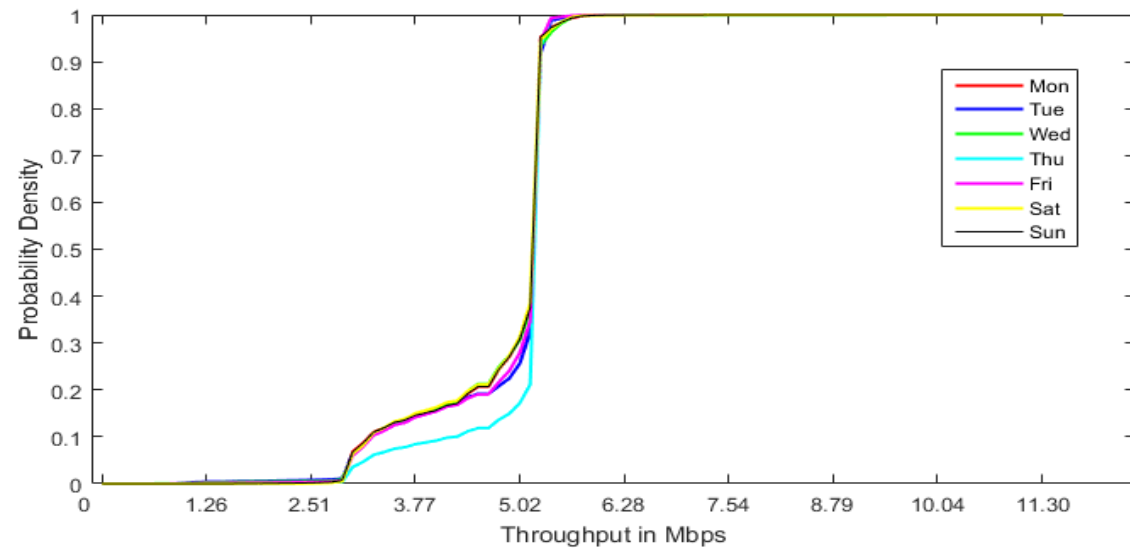


Figure D.12. RTL UE Interference CDF plot for Cell (31,38) in Zone 4

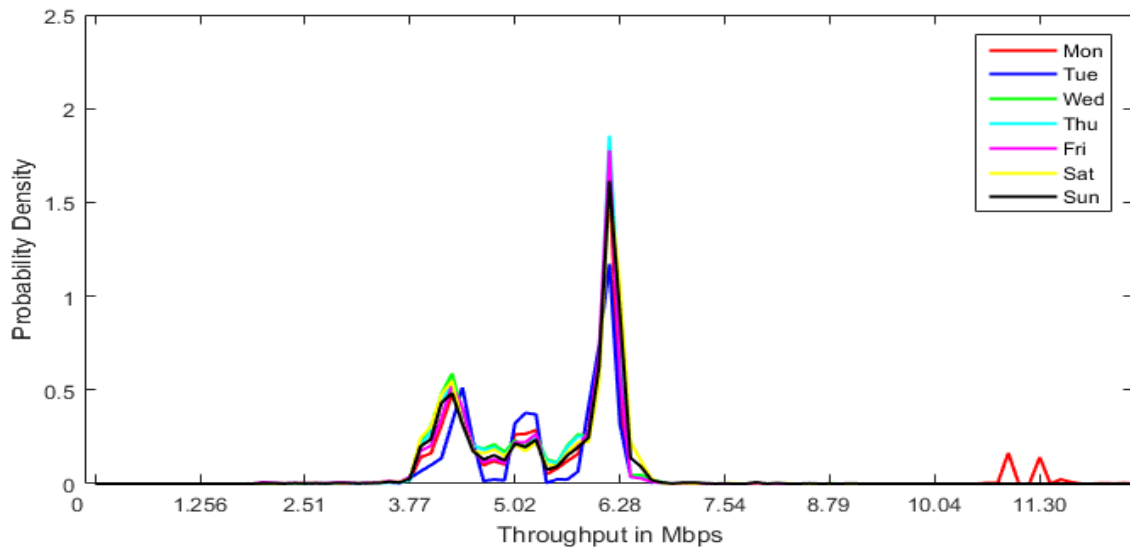


Figure D.13. RTL UE Interference PDF plot for Cell (59,35) in Zone 4

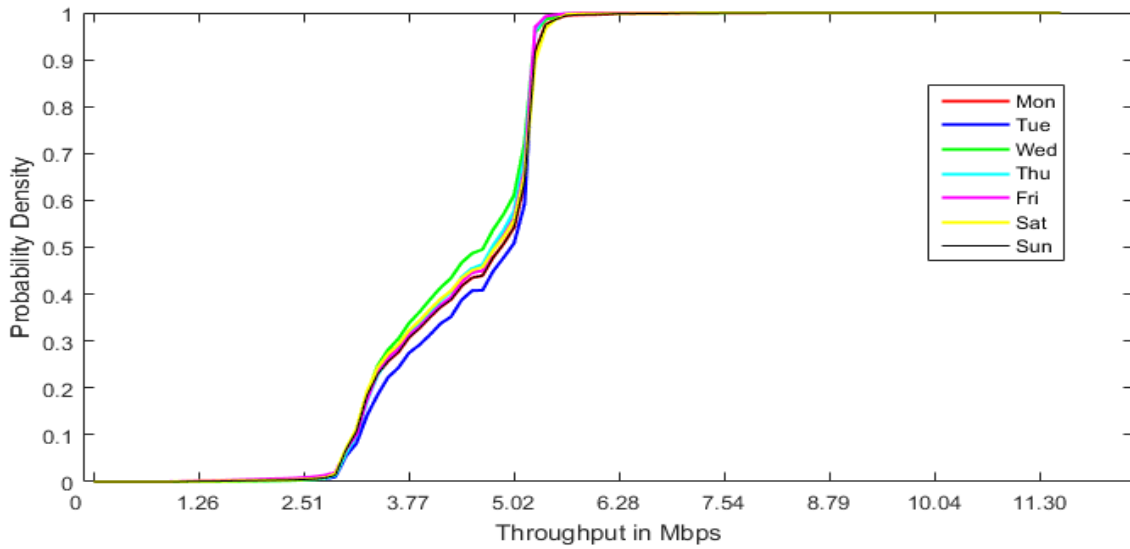


Figure D.14. RTL UE Interference CDF plot for Cell (59,35) in Zone 4

APPENDIX E  
PDF AND CDF OF RTL BS INTERFERENCE

This Appendix is a continuation of Section 4.1.3. We have the PDF and CDF plots of LTR interference for all the cells we have considered in Section 2.5.5.

### E.1 Zone 1

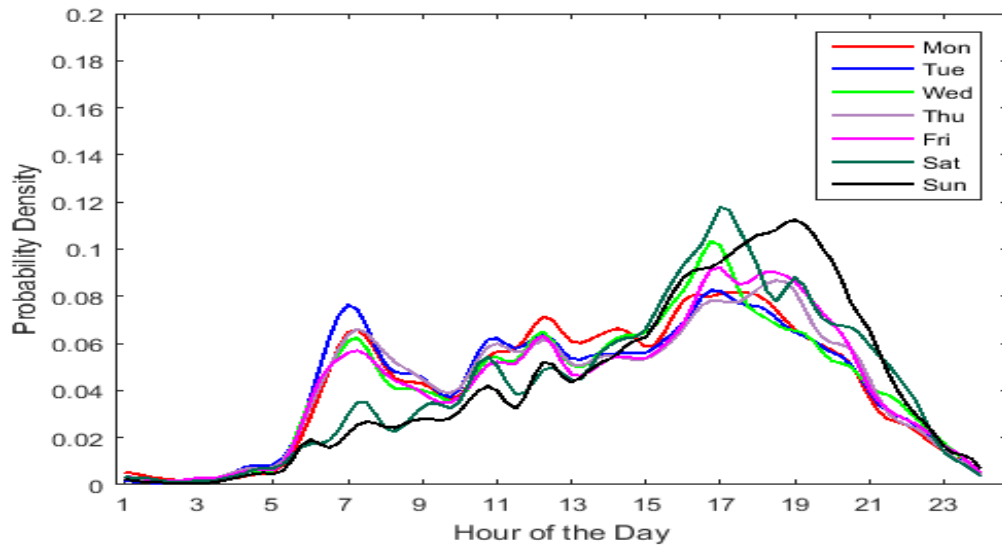


Figure E.1. RTL BS Interference PDF plot for Cell (65,23) in Zone 1

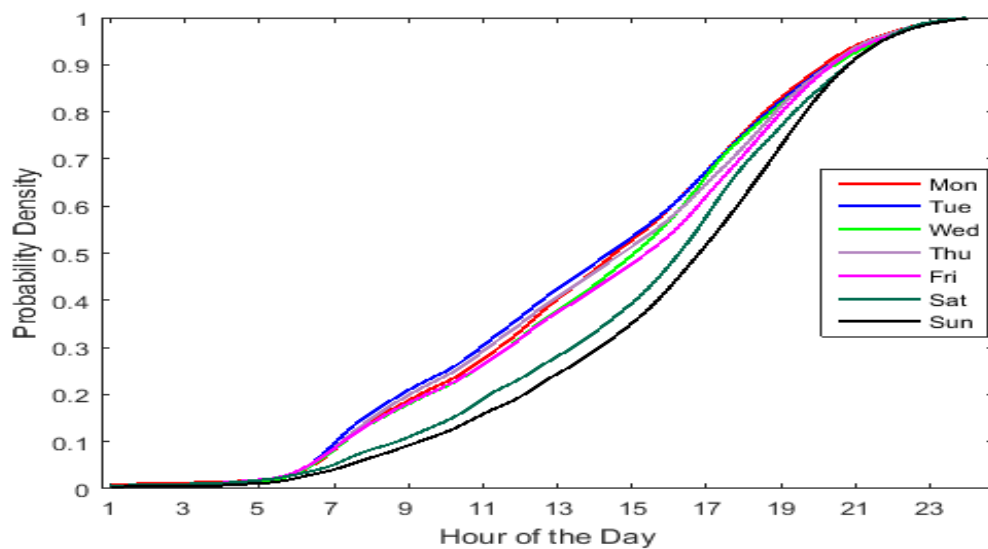


Figure E.2. RTL BS Interference CDF plot for Cell (65,23) in Zone 1

## E.2 Zone 2

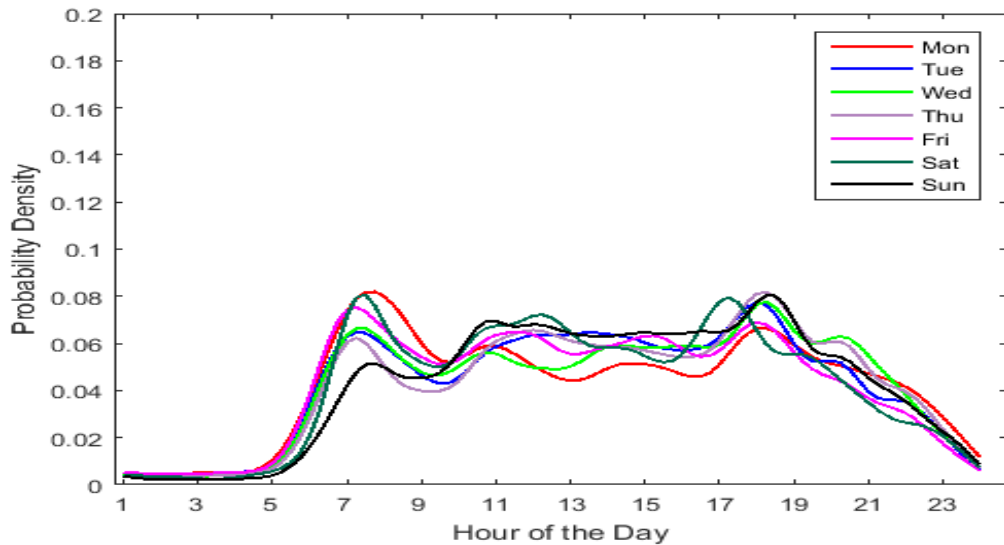


Figure E.3. RTL BS Interference PDF plot for Cell (61,4) in Zone 2

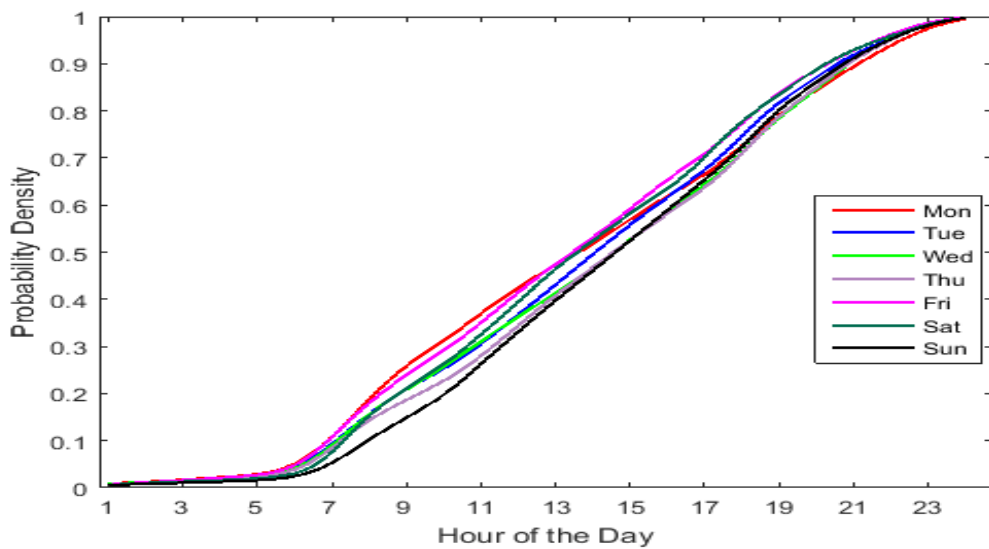


Figure E.4. RTL BS Interference CDF plot for Cell (61,4) in Zone 2

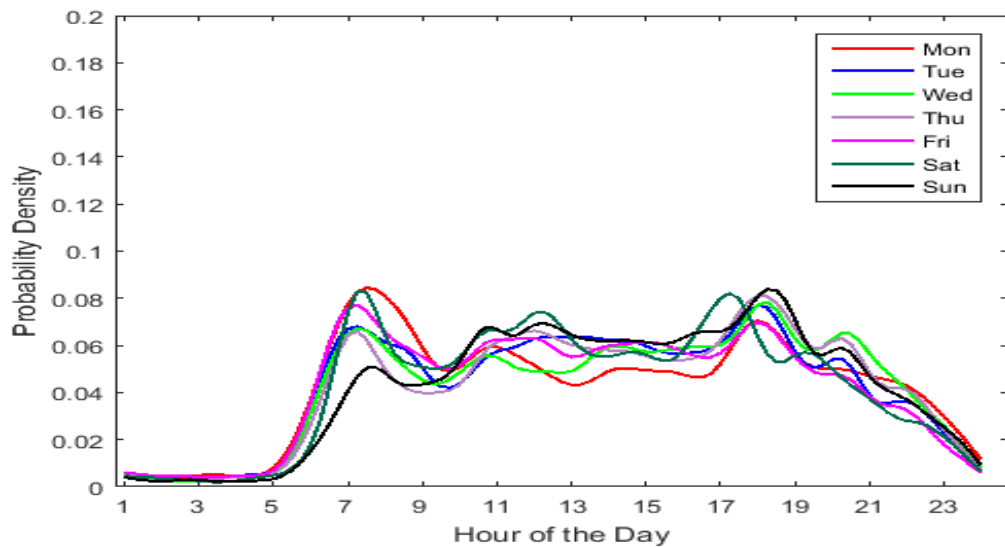


Figure E.5. RTL BS Interference PDF plot for Cell (61,7) in Zone 2

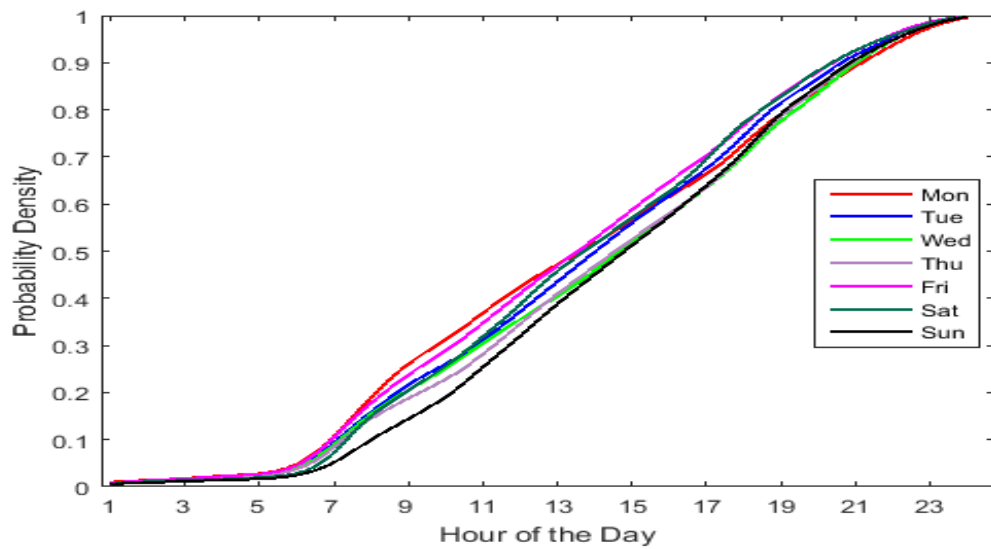


Figure E.6. RTL BS Interference CDF plot for Cell (61,7) in Zone 2

### E.3 Zone 3

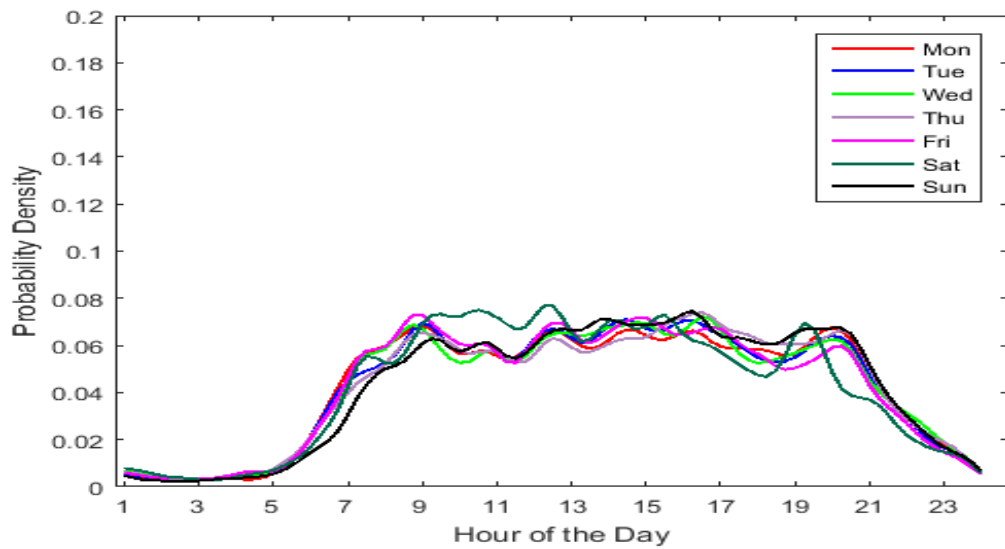


Figure E.7. RTL BS Interference PDF plot for Cell (12,16) in Zone 3

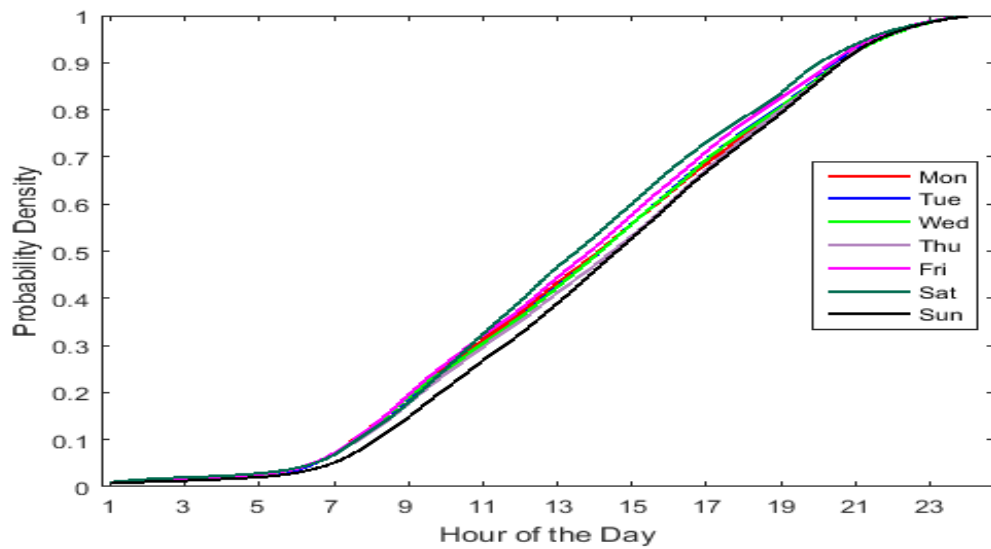


Figure E.8. RTL BS Interference CDF plot for Cell (12,16) in Zone 3

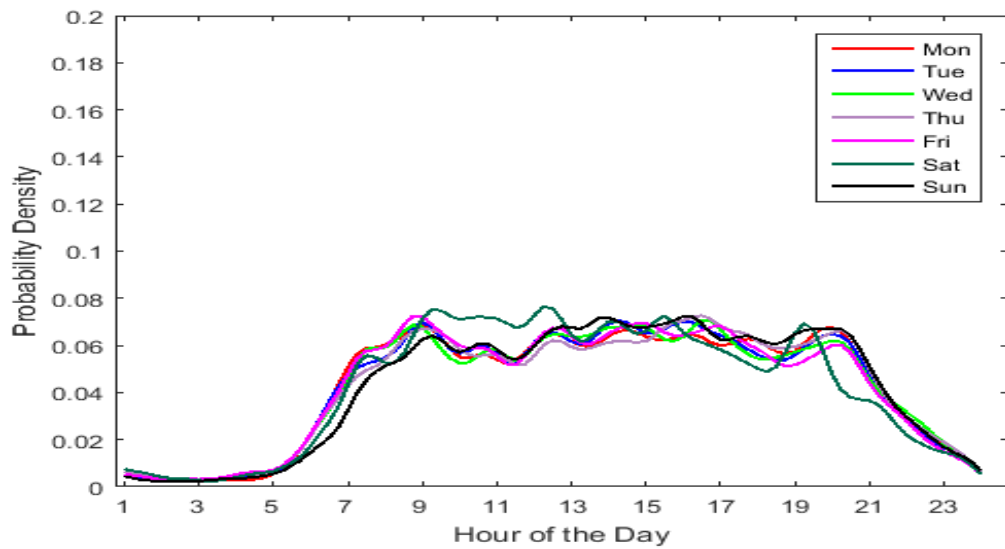


Figure E.9. RTL BS Interference PDF plot for Cell (14,15) in Zone 3

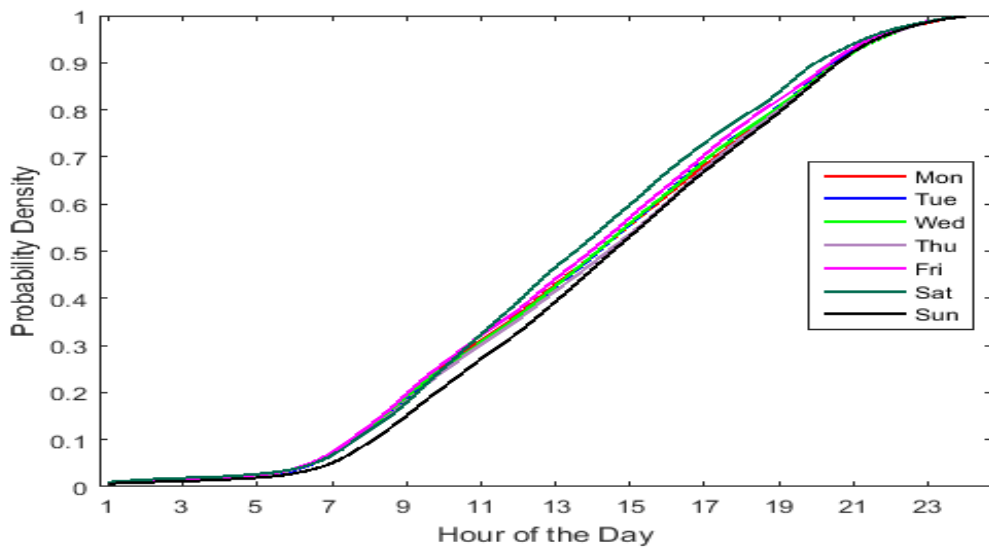


Figure E.10. RTL BS Interference CDF plot for Cell (14,15) in Zone 3

#### E.4 Zone 4

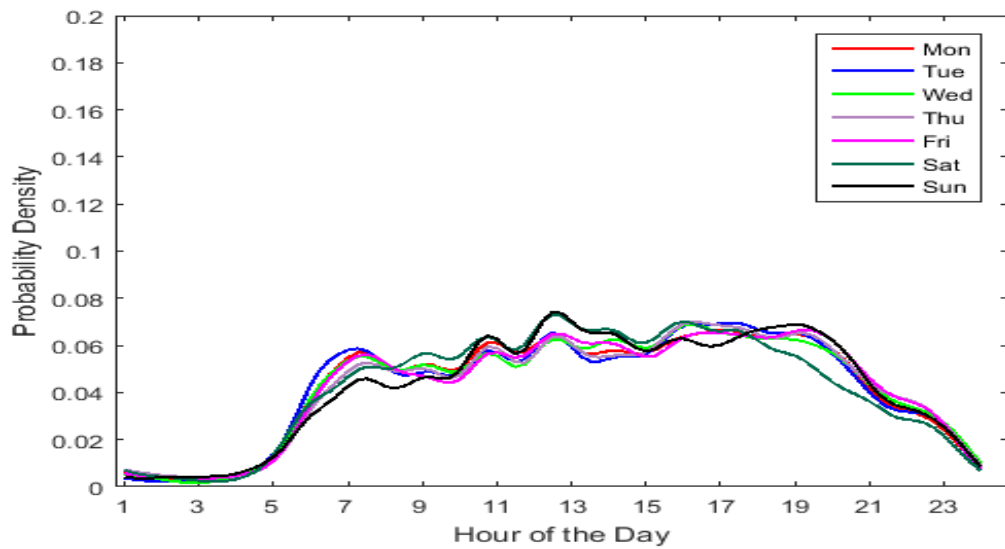


Figure E.11. RTL BS Interference PDF plot for Cell (31,38) in Zone 4

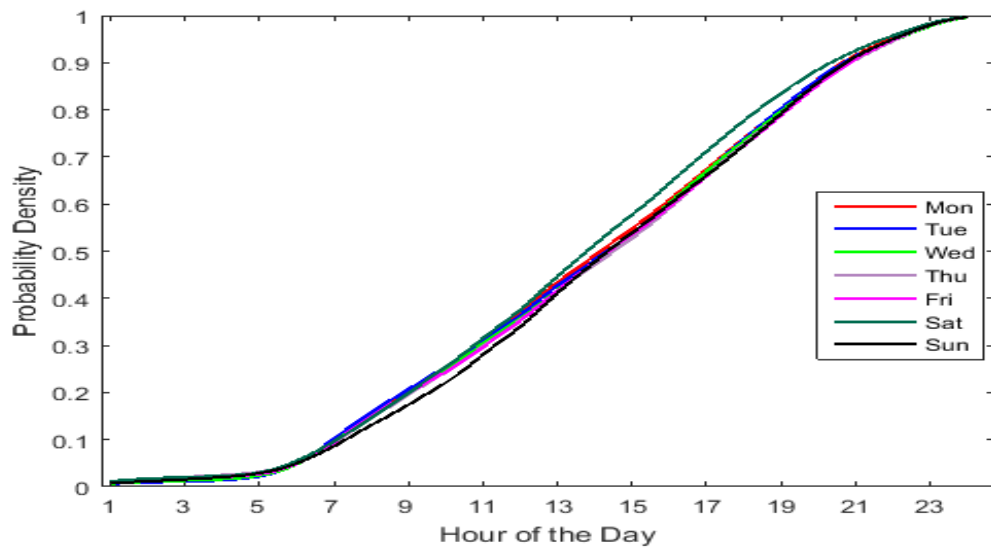


Figure E.12. RTL BS Interference CDF plot for Cell (31,38) in Zone 4

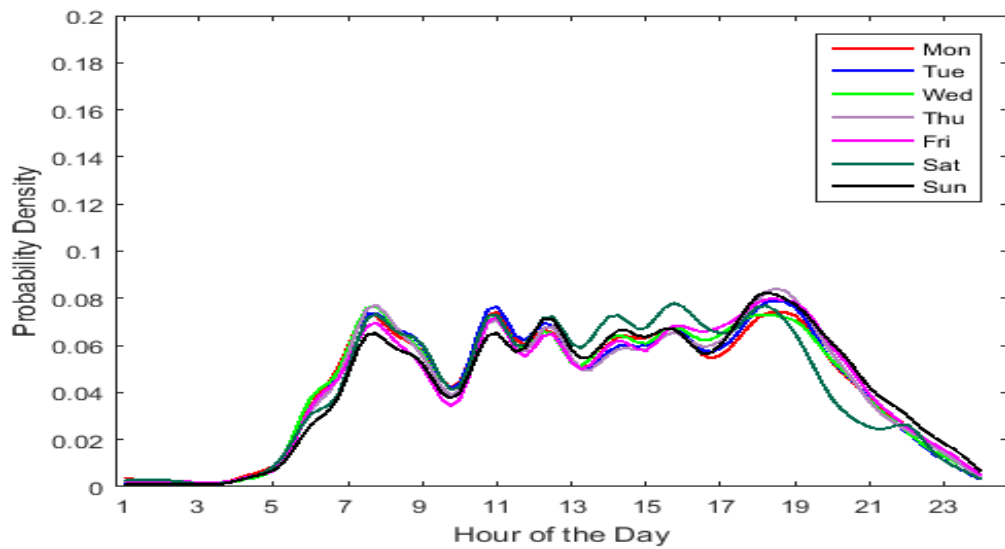


Figure E.13. RTL BS Interference PDF plot for Cell (59,35) in Zone 4

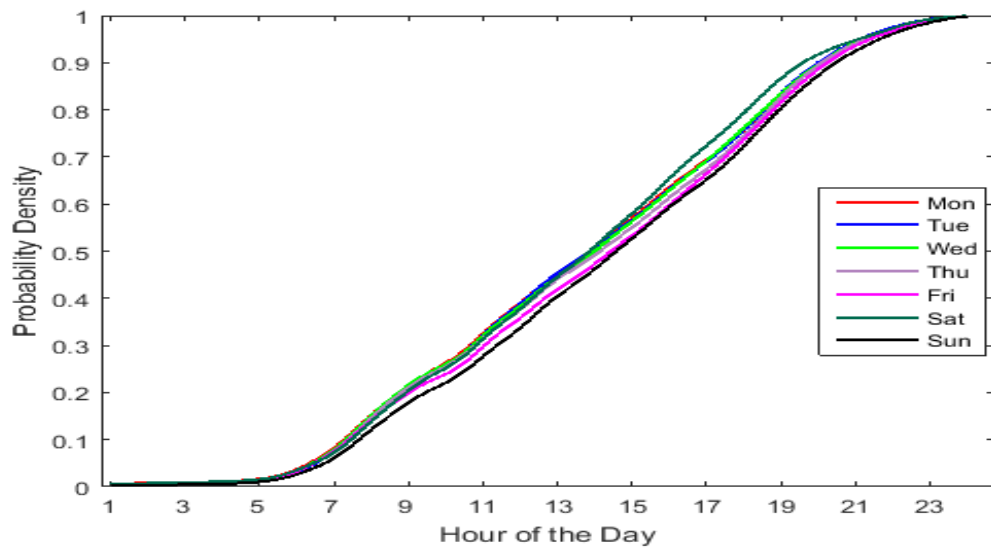


Figure E.14. RTL BS Interference CDF plot for Cell (59,35) in Zone 4

## BIBLIOGRAPHY

- [1] FCC, "Mobile Broadband: The Benefits of Additional Spectrum, Federal Communications Commission, Tech.Rep., Oct 2010.
- [2] T. Beard, G. Ford, R. Saba, and R. S. Jr, "Internet use and job search, *Telecomm. Policy*, vol. 36, no. 4, pp.260-273, May 2012.
- [3] Cisco, "VNI Global Fixed and Mobile Internet Traffic Forecasts," Cisco Visual Networking Index (VNI) Forecast, Tech.Rep., Jun. 2016. Available: <http://www.cisco.com/c/en/us/solutions/collateral/service-provider/visual-networking-index-vni/mobile-white-paper-c11-520862.html>
- [4] C. Beard, W. Stallings , " Fourth Generation Systems and LTE-Advanced" in Wireless Communication Networks and Systems, 3rd ed. Hoboken, Pearson, 2016, ch. 14, pp 451-490.
- [5] GSMA (2014, Feb) *The GSMA spectrum primer series-Introducing radio spectrum* [Online]. Available: <https://www.gsma.com/spectrum/what-is-spectrum/>
- [6] U.S. Department Of Commerce, "United States Frequency Allocations - The Radio Spectrum," National Telecommunications and Information Administration, Office of Spectrum Management, Tech.Rep., Oct 2003. Available: <https://www.ntia.doc.gov/files/ntia/publications/2003-allochrt.pdf>
- [7] FCC, "Connecting America: The National Broadband Plan, Federal Communications Commission, Tech.Rep., 2010.
- [8] M. Biggs ,USA, "Initiation of Studies Regarding Portions of the 4 200-4 400 MHz Radio Altimeter Band." In *23rd Meeting of Working Group F,Aeronautical Communications Panel (ACP)*, Cairo, Egypt September 21-27, 2010
- [9] Executive Office of the President of the USA, "Report to the president: Realizing the full potential of government-held spectrum to spur economic growth," Presidents Council of Advisors on Science and Technology, Tech.Rep., July 2012.
- [10] The White House, Office of the Press Secretary (2010, Jun.28) *Presidential Memorandum: Unleashing the Wireless Broadband Revolution* [Online]. Available: <https://obamawhitehouse.archives.gov/the-press-office/presidential-memorandum-unleashing-wireless-broadband-revolution>
- [11] A.M.Foster, M.Foster, "Spectrum Sharing," in *8th Global Symposium for Regulation, ITU*, Pattaya, Thailand, 11-13 March 2008,
- [12] E. Axell, G. Leus, E. Larsson, and H. Poor, "Spectrum sensing for cognitive radio : State-of-the-art and recent advances," *Signal Processing Magazine, IEEE*, vol. 29, no. 3, pp.101-116, May 2012.
- [13] M.A. McHenry, D. McCloskey, D.A. Roberson and J.T. MacDonald, "Spectrum Occupancy Measurements, Chicago, Illinois, November 16-18 2005," Shared Spectrum Company Report, Tech.Rep., Dec 2005.
- [14] M.A. McHenry, P.A. Tenhula, D. McCloskey, D.A. Roberson, and C.S. Hood, "Chicago Spectrum Occupancy Measurements & Analysis and a Long-term Studies Proposal,' in Proceedings of First International Workshop on Technology and Policy for Accessing Spectrum, TAPAS'06, Boston, MA, August 2006.

- [15] J. T. MacDonald and D. A. Roberson, "Spectrum Occupancy Estimation in Wireless Channels with Asymmetric Transmitter Powers," in *2nd International Conference on Cognitive Radio Oriented Wireless Networks and Communications*, Orlando, FL, USA, 2007, pp. 245-249. doi: 10.1109/CROWNCOM.2007.4549804
- [16] J. Fingas, (2017, Jun.26) *T-Mobile launches speedy LTE-U service in six cities* [Blog]. Available: <https://www.engadget.com/2017/06/26/t-mobile-launches-unlicensed-lte/>
- [17] Y. Ye, D. Wu, Z. Shu and Y. Qian, "Overview of LTE Spectrum Sharing Technologies," in *IEEE Access*, vol. 4, pp. 8105-8115, 2016. doi: 10.1109/ACCESS.2016.2626719
- [18] D. Cabric, I. O'Donnell, M.-W. Chen, and R. Brodersen, "Spectrum sharing radios," *Circuits and Systems Magazine, IEEE*, vol. 6,no. 2, pp. 30-45, 2006.
- [19] A. Ghasemi and E. Sousa, "Spectrum sensing in cognitive radio networks: requirements, challenges and design trade-offs," *Communications Magazine, IEEE*, vol. 46, no. 4, pp.32-39, April 2008.
- [20] H. T. Hayvaci and B. Tavli, "Spectrum sharing in radar and wireless communication systems: A review," in *2014 International Conference on Electromagnetics in Advanced Applications (ICEAA)*, 2014, pp. 810-813. doi: 10.1109/ICEAA.2014.6903969
- [21] F. Peng, Y. Gao, Y. Chen, K. K. Chai, and L. Cuthbert, "Using TV white space for interference mitigation in LTE femtocell networks," in *Proc. IET Int. Conf. Commun. Technol. Appl. (ICCTA)*, 2011, pp. 5-9.
- [22] R. J. Agre and D. K. Gordon (2015). *A Summary of Recent Federal Government Activities to Promote Spectrum Sharing*. [Online]. Available: <https://www.ida.org/idamedia/Corporate/Files/Publications/STPIPubs/2015/p5186final.pdf>
- [23] 5G Americas. (2015 Nov. 2). *LTE Aggregation & Unlicensed Spectrum*. [Online]. Available: [www.5gamerica.org](http://www.5gamerica.org)
- [24] M. R. Franceschini, "Overview and Applications Agenda Item 1.17", in *Future of Instrumentation & Internet Workshop*, 2015. Available: <http://waic.avsi.aero/downloads/>
- [25] M. El Amin, "Dedicated Frequency Allocation for Aircraft Onboard Wireless Systems", ICAO ACP WG-FMeeting,Nairobi,September 2007.
- [26] M. R. Bell, N. Devroye, D. Erricolo, T. Koduri, S. Rao and D. Tuninetti, "Results on spectrum sharing between a radar and a communications system," in *2014 International Conference on Electromagnetics in Advanced Applications (ICEAA)*, 2014, pp. 826-829. doi: 10.1109/ICEAA.2014.6903972
- [27] J. Taylor, Canada, "Handbook on Radio Frequency Spectrum Requirements for Civil Aviation Part I. in *28th Meeting of Working Group F,Aeronautical Communications Panel (ACP)*,Lima, Peru, 11-22 March 2013.
- [28] A. Larmo, M. Lindstrm, M. Meyer, G. Pelletier, J. Torsner and H. Wiedemann, "The LTE link-layer design," in *IEEE Communications Magazine*, vol. 47, no. 4, pp. 52-59, April 2009. doi: 10.1109/MCOM.2009.4907407

- [29] V. Pauli, J. D. Naranjo and E. Seidel, "Heterogeneous LTE Networks and Inter-Cell Interference Coordination", NomorResearch GmbH, Tech.Rep., 2010.
- [30] The Federal Aviation Administration, "Automatic Dependent Surveillance-Broadcast (ADS-B) Out Performance Requirements To Support Air Traffic Control (ATC) Service", 14 CFR Part 91., Feb. 2010. Available: <https://www.federalregister.gov/documents/2015/02/09/2015-02579/automatic-dependent-surveillance-broadcast-ads-b-out-performance-requirements-to-support-air-traffic>
- [31] Wikipedia, (2017 Jun.30) *Airspace class (United States)* [Online]. Available: [https://en.wikipedia.org/wiki/Airspace\\_class\\_\(United\\_States\)](https://en.wikipedia.org/wiki/Airspace_class_(United_States))
- [32] G. Guy, "An Air-Traffic Upgrade to Improve Travel by Plane," The New York Times, Tech.Rep., Nov. 2009. Available: <http://www.nytimes.com/2009/11/17/science/17air.html>
- [33] J. Cramer, "Development of ITU-R Recommendation on Radio Altimeters. in *28th Meeting of Working Group F, Aeronautical Communications Panel (ACP)*, Lima, Peru, 11-22 March. 2013.
- [34] A. Roy, "Preliminary Study into Radio Altimeter Adjacent Band Compatibility," in *30th Meeting of Working Group F, Aeronautical Communications Panel (ACP)*, Pattaya, Thailand 13-19 March. 2014.
- [35] J. Mettrop, "Radio Altimeters, in *30th Meeting of Working Group F, Aeronautical Communications Panel (ACP)*, Cairo, Egypt February 18-24, 2015.
- [36] M.T. Dao, D.H. Shin, Y.T. Im, and S.O. Park, "A two sweeping VCO source for heterodyne FMCW radar, *IEEE Trans. Instrument. Meas.*, vol. 62, no. 1, pp. 230-239, Jan. 2013.
- [37] M. Skolnik, "CW and Frequency-Modulated Radar" in Introduction to Radar Systems, 2nd ed. Singapore, McGraw Hill Book Company, 1962, ch. 3, pp. 68-98.
- [38] Weather Forecast Office, (Dec. 2016) *Winter Storm December 11-12, 2016* [Online] Available: <http://www.weather.gov/dtx/WinterStormDecember11-12>
- [39] M. Vidmar, "A Landing Radio Altimeter for Small Aircraft," in *12th International Power Electronics and Motion Control Conference*, Portoroz, pp. 2020-2024, 2006. doi: 10.1109/EPEPEMC.2006.4778703
- [40] R. Singh, R. Peterson, A. Riaz, C. Hood, R. Bacchus and D. Roberson, "A method for evaluating coexistence of LTE and radar altimeters in the 4.24.4 GHz band," 2017 Wireless Telecommunications Symposium (WTS), Chicago, IL, USA, 2017, pp. 1-9. doi: 10.1109/WTS.2017.7943543
- [41] CEPT, Electronic Communication Committee ECC, "Lab measurement results of 800 MHz band LTE UE unwanted emissions," Orange, Doc. SE21(13)29, June 2013.
- [42] T.S. Rappaport, "Mobile radio Propagation: Large-Scale path Loss" in *Wireless Communication Principles and Practice*, 2nd ed. Delhi, Pearson, 2010, ch.4., ISBN 978-81-317-3186-4.

- [43] ITU, "Reference radiation patterns of omnidirectional, sectoral and other antennas for the fixed and mobile services for use in sharing studies in the frequency range from 400 MHz to about 70 GHz" Recommendation ITU-R, F.1336-4, Tech.Rep., Feb 2014
- [44] J.Donovan, (2014 May. 28) "Cells, Sectors and Antenna Beamforming," [Blog] Available:<http://www.commscope.com/Blog/Cells-Sectors-and-Antenna-Beamforming/>
- [45] R. Bacchus, T. Taher, K. Zdunek, D. Roberson, "Spectrum Utilization Study in Support of Dynamic Spectrum Access for Public Safety," in *2010 Conference on Dynamic Spectrum Access*, DYSPAN, April 2010.
- [46] "Operational and technical characteristics and protection criteria of radio altimeters utilizing the band 4200-4400 MHz," Rec. ITU-R M.2059-0, Tech.Rep., Feb. 2014. Available: <http://www.itu.int/rec/R-REC-M.2059-0-201402-I>
- [47] Commerce Spectrum Management Advisory Committee, "Final Report, Working Group 1, 1695-1710 MHz Meteorological Satellite," Rev. 1, Tech.Rep., Jul. 2013. Available: [http://apps.fcc.gov/edocs\\_public/attachmatch/FCC-14-31A1.pdf](http://apps.fcc.gov/edocs_public/attachmatch/FCC-14-31A1.pdf)
- [48] MathWorks, "Simulate, analyze, and test the physical layer of LTE and LTE-Advanced wireless communications systems." [Online]. Available: <http://www.mathworks.com/products/lte-system/>
- [49] 3rd Generation Partnership Project, "Technical Specification Group Radio Access Network; Evolved Universal Terrestrial Radio Access (E-UTRA); User Equipment (UE) radio transmission and reception, 3GPP TS 36.101 Version 10.3.0 Release 10, Tech.Rep., June 2011. Available: [www.qtc.jp/3GPP/Specs/36101-800.pdf](http://www.qtc.jp/3GPP/Specs/36101-800.pdf)
- [50] 3rd Generation Partnership Project, "LTE: Evolved Universal Terrestrial Radio Access (E-UTRA); Base Station (BS) radio transmission and reception, 3GPP TS 36.104 version 10.2.0 Release 10, Tech.Rep., May 2011.
- [51] C.Cox, "LTE Basics: An Introduction to LTE: LTE, LTE-Advanced, SAE and 4G Mobile Communications, 2nd ed, Wiley, ISBN: 978-1-118-81803-9
- [52] "Reference Radiation Patterns of Omnidirectional, Sectoral and Other Antennas for the Fixed and Mobile Services for Use in Sharing Studies in the Frequency Range from 400 MHz to about 70 GHz, Recommendation ITU-R F.1336-4, Tech.Rep., 2014.
- [53] R. OConnor, "Understanding Televisions Grade A and Grade B Service Contours, *Broadcasting, IEEE Transactions*, vol. 47, no. 3, pp. 309314, Sep 2001.
- [54] FCC and NTIA, "Coordination Procedures in the 1695-1710 MHz and 1755-1780 MHz bands (FCC 13-185), July 2014.
- [55] "Propagation Data Required for the Evaluation of Coordination Distances in the Frequency Range 0.85-60 GHz (Rec. ITU-R P.620-3), Federal Communications Commission, Tech. Rep., Jul 2014.
- [56] A. B. Owen, "Empirical Likelihood for Linear Models," *The Annals of Statistic*, vol. 19, no.4, pp.1725-1747, 1991.
- [57] MathWorks, "Kernel Distribution," R2017a. [Online]. Available: <https://www.mathworks.com/help/stats/kernel-distribution.html>